

**Stijfheid van glas/ionomeerlaminaten in constructieve toepassingen**

**Stiffness of Glass/Ionomer Laminates in Structural Applications**

**Dieter Callewaert**

Promotoren: prof. dr. ir.-architect J. Belis, prof. dr. ir. R. Van Impe  
Proefschrift ingediend tot het behalen van de graad van  
Doctor in de Ingenieurswetenschappen: Bouwkunde

Vakgroep Bouwkundige Constructies

Voorzitter: prof. dr. ir. L. Taerwe

Faculteit Ingenieurswetenschappen en Architectuur

Academiejaar 2011 - 2012





Stijfheid van glas/ionomeerlaminaten in constructieve toepassingen

Stiffness of Glass/Ionomer Laminates in Structural Applications

Dieter Callewaert

Promotoren: prof. dr. ir. -architect J. Belis, prof. dr. ir. R. Van Impe  
Proefschrift ingediend tot het behalen van de graad van  
Doctor in de Ingenieurswetenschappen: Bouwkunde

Vakgroep Bouwkundige Constructies  
Voorzitter: prof. dr. ir. L. Taerwe  
Faculteit Ingenieurswetenschappen en Architectuur  
Academiejaar 2011 - 2012



ISBN 978-90-8578-469-2  
NUR 955, 956  
Wettelijk depot: D/2011/10.500/72

### **Supervisors:**

prof. dr. ir.-architect Jan Belis  
prof. dr. ir. Rudy Van Impe

### **Examination Committee:**

prof. dr. ir.-architect Jan Belis  
prof. dr. ir. Geert De Schutter (secretary)  
dr. ir. Christian Louter

Prof. Dr.-Ing. Jens Schneider  
Prof. Dr.-Ing. Geralt Siebert

prof. dr. ir. Luc Taerwe (chairman)  
prof. dr. ir. Rudy Van Impe  
prof. dr. ir. Patricia Verleysen

Ghent University  
Ghent University  
Ecole polytechnique fédérale de  
Lausanne  
Technische Universität Darmstadt  
Universität der Bundeswehr München  
/ Ingenieurbüro Dr. Siebert  
Ghent University  
Ghent University  
Ghent University

Laboratory for Research on Structural Models  
Department of Structural Engineering  
Faculty of Engineering and Architecture  
Ghent University  
Technologiepark 904  
B-9052 Ghent (Zwijnaarde)  
Belgium





voor Jivannah...





# Acknowledgements

---

Although this is the first full sentence in this book, this page is written at the very end of my PhD. With this last mile, which does not feel the longest one, I would like to express my gratitude to those who helped me realising all this.

I am indebted to my supervisors, prof. Jan Belis and prof. Rudy Van Impe, for realising the framework in which I could develop my research, for the freedom they allowed me to find my own way, for restricting it when necessary, and for their valuable support and suggestions. Jan in particular, for launching me in his large international network, for smoothing the glass-research-pave, and for encouraging me to finalize the last phase. Thanks a lot!

I am grateful to FWO-Flanders for funding the research project and giving me the opportunity to do my research at Ghent University. I also thank Lerobel, for partially providing the laminated glass and allowing me to delay the lamination process with my intensive thickness measurements, and Permasteelisa Group, for providing software to perform some instructive thermal simulations.

Special thanks to prof. Luc Taerwe, prof. Geralt Siebert, dr. ir. Christian Louter, prof. Jens Schneider, prof. Patricia Verleysen, prof. Geert De Schutter, prof. Rudy Van Impe en prof. Jan Belis because they accepted to be members of the exam committee in the midst of all their activities. Thank you also for all the insightful conversations and valuable comments.

For the pleasant atmosphere at the lab: thank you Guy, Rik, Matthieu, Kali, Wesley, Delphine, Didier, Marc, Arno, Freek, Jonas, Francine, Christel, Bart, Dennis and Eric.

I acknowledge my master students, some of them for directly contributing to my research, others for allowing me to explore some unknown fields within the glass research. Jeffrey, Pieter, Yannick, Kenneth, Jonathan, Koen, Steven, Sofie, Jonas, Lies, Davy, Thomas, Joris and Warren, thanks for all your efforts.

Furthermore, I would like to express my sincere gratitude to my family and friends, for their unconditional support and encouragements.

And finally, thank you Jivannah. Simply for everything...

Dieter  
December 2011, Ghent



# Abbreviations and symbols

---

## Abbreviations

<i>CST</i>	compression shear test
<i>DMA</i>	dynamic mechanical analysis
<i>EVA</i>	ethylene vinyl acetate
<i>FE</i>	finite element
<i>IR</i>	infrared
<i>LVDT</i>	linear variable differential transformer
<i>PET</i>	polyethylene terephthalate
<i>PVB</i>	polyvinyl butyral
<i>SG</i>	SentryGlas®
<i>SGP</i>	SentryGlas® Plus
<i>SGP2000</i>	SentryGlas® Plus 2000 (out-of-date version)
<i>SGP5000</i>	SentryGlas® Plus 5000 (recent version)
<i>TRS</i>	thermorheologically simple
<i>UV</i>	ultraviolet
<i>WLF</i>	Williams-Landel-Ferry

## Symbols

$\bar{B}_S$	substitute bending stiffness
$C_1, C_2$	WLF time shift constants
$E$	Young's modulus
$f$	factor of increase
$F$	point load
$G$	Shear modulus
$I$	moment of inertia
$J$	creep function
$k$	factor
$L$	length
$M$	moment
$N$	amount of glass plies in a laminate
$t$	thickness
<i>time</i>	load duration
$T$	temperature
$w$	deflection
$W$	width
$a_T$	shift factor
$\epsilon$	strain
$\eta$	viscosity
$\theta$	angle of twist
$\nu$	Poisson's ratio
$\sigma$	stress
$\tau$	relaxation time
$\omega$	shear transfer coefficient

## Subscripts

<i>0</i>	instantaneous
<i>1/2</i>	ply 1/2
$\infty$	infinite
<i>b</i>	bending
<i>d</i>	damper
<i>eq</i>	equivalent
<i>g</i>	glass transition
<i>exp</i>	experimental
<i>glass</i>	glass
<i>i/j</i>	ply <i>i/j</i>
<i>int</i>	interlayer
<i>lower</i>	lower limit without shear interaction
<i>m</i>	distance between the centre of the ply and the centre of the laminate
<i>max</i>	maximum
<i>mean</i>	mean
<i>min</i>	minimum
<i>nom</i>	nominal
<i>PVB</i>	polyvinyl butyral
<i>ref</i>	reference
<i>SG</i>	SentryGlas®
<i>span</i>	distance between supports
<i>s</i>	spring
<i>t</i>	torsion
<i>total</i>	total
<i>upper</i>	upper limit with full shear interaction
<i>w</i>	for bending deformations
$\theta$	for torsional deformations
$\sigma$	for bending stresses

## Units

-	dimensionless
%	percentage
°C	degree Celsius
<i>GPa</i>	gigapascal
<i>h</i>	hour
<i>K</i>	Kelvin
<i>kg</i>	kilogram
<i>m</i>	meter
<i>mm</i>	millimetre
<i>min</i>	minute
<i>MPa</i>	megapascal
<i>N</i>	Newton
<i>sec</i>	second
<i>Watt</i>	watt

# Summary

---

## 1 Context

In order to increase the post-failure behaviour of load-bearing, glass elements, almost always laminated glass is used. During the 1990's, SentryGlas® (SG) was developed as a stiffer and stronger alternative for the existing and most frequently used interlayer material Polyvinyl Butyral (PVB). Because SG is a relatively complex time and temperature dependent material, there exists only little knowledge of its exact material properties. This PhD-research tries to improve this through a combined experimental, theoretical and numerical analysis.

## 2 Experimental research

For this research, an extensive experimental programme was planned. Based on existing research in literature, firstly, a test programme was put together. A combination of torsion and bending experiments on laminated samples with relatively large dimensions was preferred. The main advantages of this test programme are:

- *Directly visible influence of the material properties of the interlayer on the overall mechanical behaviour of a laminate*
- *Direct correlation between bending and torsional stiffness with identical load duration and temperature*
- *Incorporation of the possible influence of the lamination cycle on the properties of the polymer interlayer material*
- *Possible edge effects are proportional to those in realistic building components due to a comparable edge to surface ratio*

All experiments were executed in a chamber in which temperature and air humidity could be controlled. Through this, the environmental conditions were certainly stable throughout the entire sample, even for a load duration of multiple days.

At first, preliminary test series were carried out on laminated samples with an unknown load history. Even though these samples were not laminated with the latest version of SG, the results gave already a qualitatively good insight in the behaviour of the laminates under different loading conditions. These tests clearly indicated that the stiffness of a laminate cannot be related directly to a certain shear transfer value which is only function of time and temperature. At identical

environmental conditions a laminate can behave almost monolithically, while it has already reached the lower limit for an other loading situation.

This also has a direct influence on the importance of the test setup selection for experimental investigations. If a sample already reaches the lowest possible stiffness limit after a relatively short load duration, a longer test is useless because the stiffness can no longer change. However, this steadying of the overall stiffness does not mean that the lower limit of the interlayer material properties is already reached. The preliminary bending experiments on the larger samples clearly demonstrated this.

Subsequently, the test setups were adapted to this insight. Based on theoretical models, the proportional stiffness was predicted in function of the shear modulus of the interlayer material of glass laminates. By doing so, three different complementary test setups were chosen.

- Torsion creep and relaxation experiments on 360 mm x 1100 mm laminated samples with two 6 mm fully tempered glass panes and a 1.52 mm thick SG interlayer.
- Bending creep experiments on samples – with two 8 mm annealed glass layers and 1.52 mm SG – measuring 120 mm and 180 mm x 1100 mm.
- Bending creep and relaxation experiments on 360 mm wide and 3000 mm long laminated samples with two 8 mm fully tempered glass panes and a 1.52 mm SG layer.

In Fig. 1, the theoretical stiffness in proportion to the stiffness of a monolithic glass sheet with the same overall thickness, is presented in function of the shear modulus of the interlayer material. A relatively fast stiffness reduction is expected for the torsionally loaded 360 mm wide specimen (black line). Yet, at the moment that this proportional stiffness starts to reach its lower value, the proportional bending stiffness of the test setup with a span of almost 3 m is significantly influenced by the shear modulus of the interlayer (upper dark gray curve).

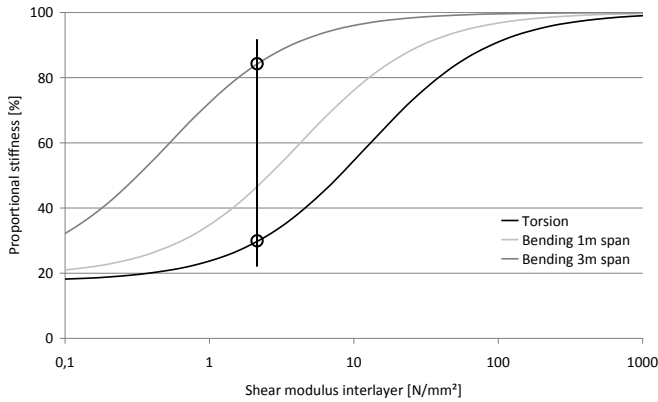


**Figure 1: Theoretical proportional stiffness in function of the interlayer shear modulus for the three chosen test configurations.**

### 3 Theoretical and numerical analysis

As a first step of the analysis, the function between time and temperature was determined. A Williams-Landel-Ferry time shift with the constants  $C_1 = 135$  and  $C_2 = 760$  °C for the reference temperature  $T_{ref}$  of 20 °C resulted in a smooth transition between the curves from experiments at different temperatures.

To enable a comparison between the results of the different test series, the experimental outcome was reduced to a proportional stiffness. This way, the results are directly rendered in proportion to the upper stiffness limit. Fig. 2 summarises all results performed at five different temperature levels between 5 °C and 65 °C with a reduced time for the reference temperature of 20 °C.

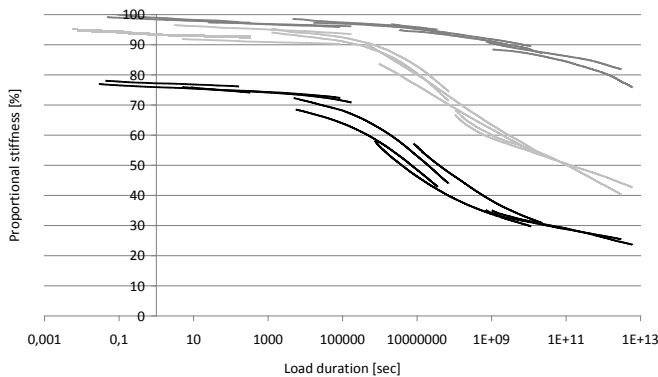


**Figure 2: Experimental proportional stiffness in function of the load duration at  $T_{ref} = 20$  °C: torsion experiments (black curves); bending experiments with a span of 2950 mm (dark grey curves); bending experiments with a span of 1050 mm (light grey curves)**

These curves prove that it is impossible to generalise a simple correlation between the proportional stiffness of the laminate and the load duration at a certain temperature. Although the two ultimate limits exist for all possible loading conditions, the type of loading, the temperature, the load duration, as well as the geometry of the element can determine whether a laminate with certain material properties leans towards the upper limit, or towards the lower one.

For this reason, the results were also analysed based on the theory of equivalent thickness<sup>1</sup>, which is suggested in [prEN 13474-3] for the calculation of the laminate stiffness. The resulting equivalent thicknesses are recapitulated in Fig. 3.

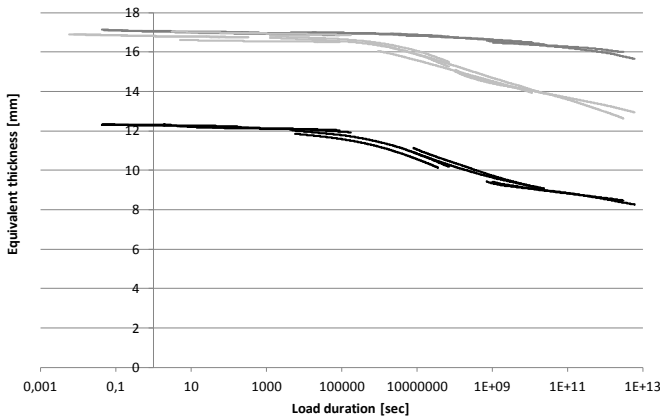


**Figure 3: Equivalent thickness in function of the load duration at  $T_{ref} = 20\text{ }^{\circ}\text{C}$ : torsion experiments (black markers); bending experiments with a span of 2950 mm (dark grey markers); bending experiments with a span of 1050 mm (light grey markers)**

Because the torsion experiments were executed on samples with two 6 mm glass panes and 1.52 mm SG, while the bending experiments were performed on samples with two glass panes of 8 mm glass and a similar interlayer thickness, the maximum equivalent thickness was obviously smaller. Nevertheless, at longer load durations, the equivalent thickness is not equal for the two bending test setups with identical thickness composition too. Its is therefore expectedly that the dimensionless  $\omega$ -factor, represented in Fig. 4, does not overlap.

---

<sup>1</sup> In literature, this method is referred to as the ‘effective thickness method’, but this might be confusing with the actual thickness of a sheet, which is also sometimes called *effective thickness*



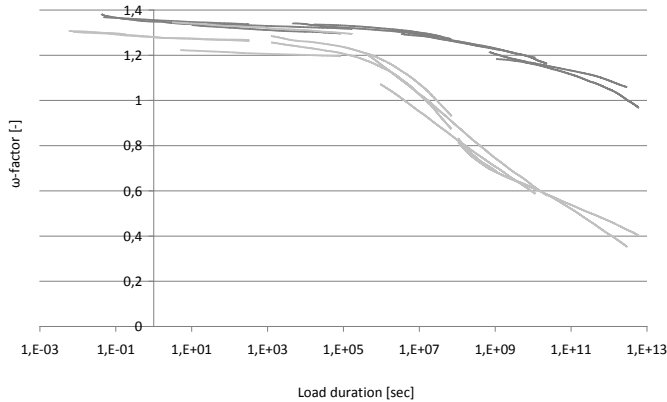


**Figure 4:  $\omega$ -factor in function of the load duration at  $T_{ref} = 20\text{ }^{\circ}\text{C}$ : bending experiments with a span of 2950 mm (dark grey markers); bending experiments with a span of 1050 mm (light grey markers)**

Although this dimensionless factor does change by varying the loading conditions and is therefore not directly usable for other loading configurations than the tested ones, it is important to notice that it also well exceeds the suggested maximum of 1 which could be expected at full interaction. The neglected interlayer thickness and a rather conservative young's modulus for the glass of 70 GPa provoke these high values at short loading durations and low temperatures for the investigated stiff interlayer.

Consequently, it seemed to make little sense to express a generalised statement concerning the overall stiffness of laminates. Accordingly, the results were transferred towards a material property of the interlayer, namely the shear modulus  $G_{SG}$ , which should be interchangeable for different loading situations.

In literature, a theoretical model exists to calculate the torsional stiffness as well as the bending stiffness of a laminated element. By introducing the material properties and the element geometry in the theory of Scarpino [Scarpino 2005], the torsional stiffness can be evaluated. This model was applied in a reversed way to determine the only unknown input, namely the shear modulus of the interlayer. Similarly, the theory of Wölfel [Wölfel 1987] was reversely used for the bending experiments. The results are represented in Fig. 5.

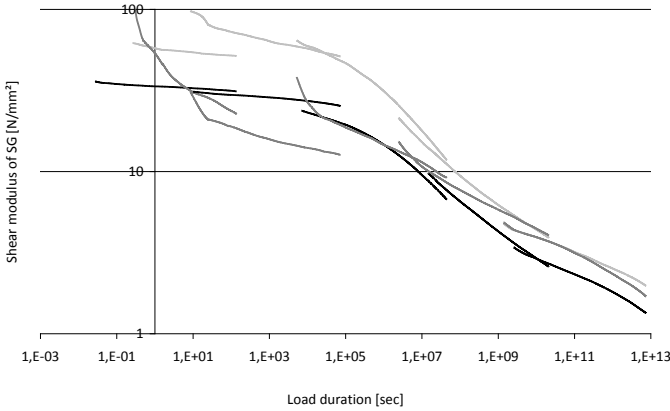


**Figure 5:  $G_{SG}$  based on theoretical models in function of the load duration at  $T_{ref} = 20\text{ °C}$ : torsion experiments (black markers); bending experiments with a span of 2950 mm (dark grey markers); bending experiments with a span of 1050 mm (light grey markers)**

The curves prove that the material property of the interlayer is almost autonomous from the test setup, contrary to the proportional stiffness or the equivalent thickness. In general, the shear modulus derived from the torsion experiments seems only slightly lower than the values distracted from the bending experiments. Therefore, and also because the theoretical models do not take into account small imperfections of the test setup, the results were also analysed numerically.

Finite element models were built up, approximating the actual test setups as closely as possible and from these, for different values of the interlayer shear modulus  $G_{intr}$  the overall laminate stiffness was deduced. By comparing the experimental stiffness with this numerical stiffness, the SG shear modulus  $G_{SG}$  was recalculated. Based on these outcomes, represented in Fig. 6, the material model was built.

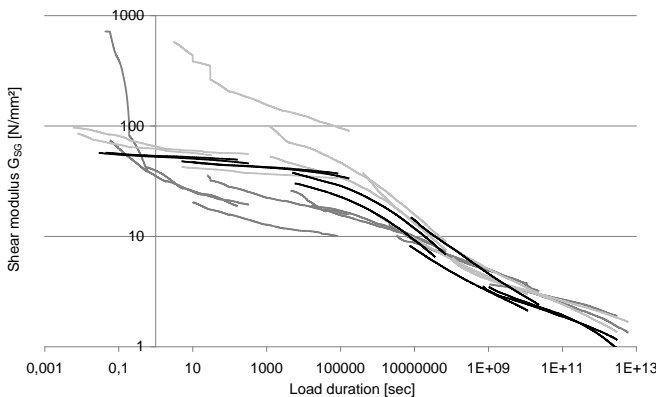


**Figure 6:  $G_{SG}$  based on numerical simulations in function of the load duration at  $T_{ref} = 20\text{ °C}$ : torsion experiments (black curves); bending experiments with a span of 2950 mm (dark grey curves); bending experiments with a span of 1050 mm (light grey curves)**

## 4 Material model for SentryGlas®

After averaging the shear modulus from the different test setups at each tested temperature, a single function was deduced which could be approximated by a linear visco-elastic Maxwell series. These five curves are represented by the red lines in Fig. 7 and were fluently approximated by a limited number of values (black markers) which could be used as manageable input to calculate the values of a Maxwell series describing the material behaviour. When recalculating the shear modulus with the derived model, the blue curve appears.

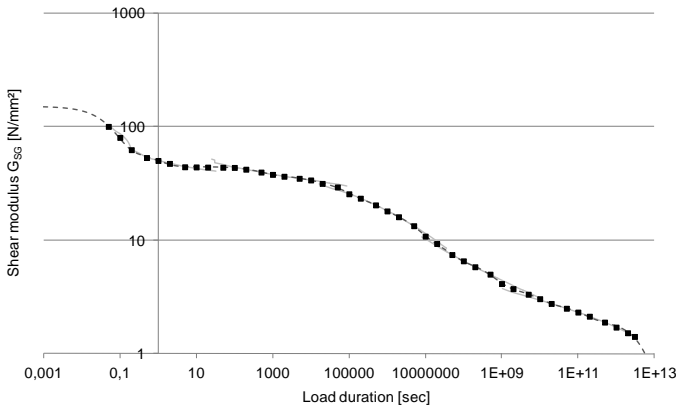


**Figure 7:  $G_{SG}$  in function of reduced load duration at  $T_{ref} = 20$  °C: averaged results based on numerical simulations (light grey curves); fluent approximation of the results (square markers); calculated properties from Maxwell series (dark gray dashed curve)**

For this, also an assumption had to be made for both the instantaneous SG shear modulus  $G_{SG,0}$  and the long term value  $G_{SG,\infty}$ . By recalculating the material properties for different values and comparing these with the input values, a safe and well-founded supposition was made. Nevertheless, the model is hereby expected not to overestimate the actual material properties outside the tested range: the model should not be used when values above 100 N/mm<sup>2</sup> or beneath 1.4 N/mm<sup>2</sup> are appearing. Moreover, polymers can behave totally different above a certain temperature. The model is therefore only applicable up to a maximum temperature of 65 °C, as no experiments were executed at a higher temperature.

Finally, the model is validated by performing visco-elastic numerical simulations of the executed experiments. In Fig. 8, the results show a good similarity with the experimental proportional stiffness from Fig. 2. Also elastic simulations and theoretical calculations with an instantaneous shear modulus extracted from the Maxwell series have a good agreement with the experiments. The latter emphasizes that the stiffness of a laminate under relatively simple loading conditions can be well approximated by using existing theoretical models.

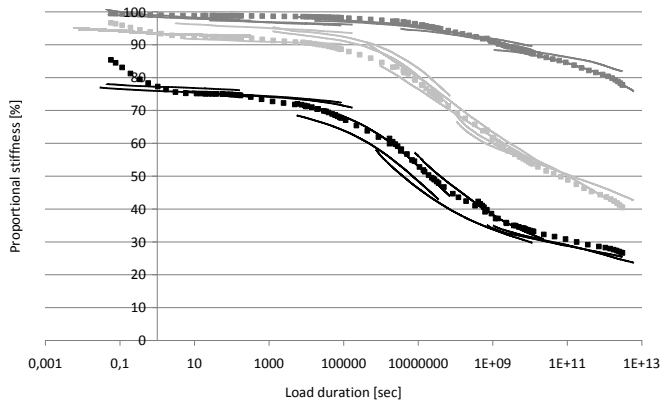


**Figure 8:** Simulated proportional stiffness in function of the load duration at  $T_{ref} = 20 \text{ }^\circ\text{C}$  compared to the test results presented in Fig. 2: torsion experiments (black); bending experiments with a span of 2950 mm (dark grey); bending experiments with a span of 1050 mm (light grey)

# Samenvatting

---

## 1 Context

Om de postdestructieve veiligheid van glazen elementen in constructieve toepassingen te verhogen wordt bijna uitsluitend gelamineerd glas gebruikt. In de jaren 1990 werd SentryGlas® (SG) ontwikkeld als een stijver en sterker alternatief voor het bestaande en vaak gebruikte tussenlaagmateriaal Polyvinyl Butyral (PVB). Doordat SG een relatief complex tijds- en temperatuursafhankelijk gedrag vertoont, bestaat er slechts een beperkte kennis over de exacte materiaaleigenschappen. Dit doctoraatsonderzoek probeert dit te verbeteren met behulp van een gecombineerde experimentele, theoretisch en numerieke analyse.

## 2 Experimenteel onderzoek

Voor dit onderzoek werd een uitgebreid experimenteel proefprogramma gepland. Op basis van bestaand onderzoek beschreven in de literatuur, werd eerst een testprogramma samengesteld. De voorkeur ging uit naar een combinatie van torsie- en buigexperimenten op gelamineerde proefstukken met relatief grote afmetingen. De belangrijkste voordelen van dit testprogramma zijn:

- De invloed van de materiaaleigenschappen van de tussenlaag op het globale mechanische gedrag van het laminaat is direct zichtbaar
- Onmiddellijke correlatie tussen de experimentele buig- en torsiestijfheid met identieke belastingsduur en omgevingstemperatuur
- Opname van de eventuele invloed van het laminatieproces op de eigenschappen van de polymeer tussenlaag
- De mogelijke invloed van randeffecten is proportioneel tot de randeffecten die kunnen optreden in realistische bouwcomponenten door een gelijkwaardige verhouding tussen rand en oppervlakte.

Alle proeven werden uitgevoerd in een klimaatruimte waarbinnen zowel de temperatuur als de relatieve luchtvochtigheid geregeld wordt. Dit zorgde ervoor dat de omstandigheden zeker constant bleven gedurende de volledige belastingsduur van meerdere dagen en doorheen het volledige proefstuk.

In het begin werden enkele voorbereidende proefreeksen uitgevoerd op gelamineerde proefstukken met een ongekende voorgeschiedenis. Los van het feit dat deze proefstukken niet met de meest recente versie van SG gelamineerd waren, verhoogden de resultaten toch het kwalitatief inzicht in het gedrag van

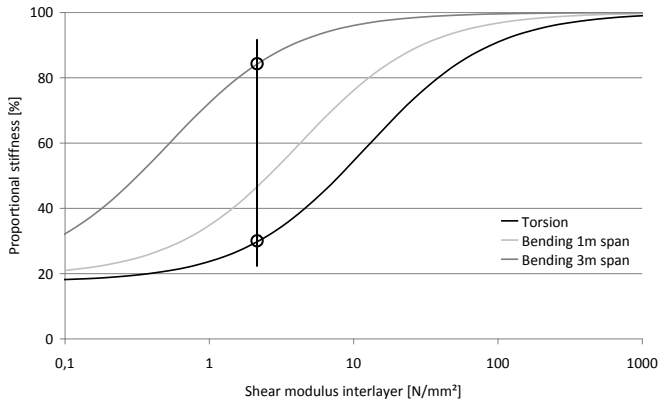
laminaten onder verschillende belastingstoestanden. De testen toonden duidelijk aan dat de stijfheid van een laminaat niet rechtstreeks gerelateerd is aan een afschuifconstante die enkel functie is van temperatuur en belastingsduur. Bij dezelfde omgevingsfactoren kan een laminaat zich quasi monolithische gedragen, terwijl de ondergrens benaderd wordt bij een gewijzigde belastingsconfiguratie.

Dit toont ook rechtstreeks het belang van een gefundeerde selectie voor een testopstelling bij experimenteel onderzoek. Als een proefmonster al de laagst mogelijke stijfheid benadert na een relatief korte duur belasting, is een langere test nutteloos omdat de stijfheid dan niet meer kan veranderen. De stabilisering van de totale stijfheid betekent echter niet dat de ondergrens van de tussenlaag materiaaleigenschappen al bereikt is. De buigstijfheid van de grotere buigproeven tonen dit duidelijk aan.

Vervolgens werden de proefopstellingen met deze kennis aangepast. Op basis van theoretische modellen werd de proportionele stijfheid voorspeld in functie van de glijdingsmodulus van de tussenlaag in gelamineerd glas. Hierdoor werden drie verschillende, complementaire testopstellingen gekozen.

- Kruip en relaxatie torsieproeven op 360 mm x 1100 mm gelamineerde proefstukken met een samenstelling van 2x 6 mm gehard glas met een 1.52 mm dikke SG tussenlaag.
- Kruip buigproeven op gelamineerd glas met een lengte van 1100 mm, een breedte van 120 mm en 180 mm en samenstelling 2x 8 mm uitgegloeid glas en 1.52 mm SG.
- Kruip en relaxatie buigproeven op 360 mm x 3000 mm gelamineerde proefstukken met samenstelling 2x 8 mm gehard glas en 1.52 mm SG.

In Fig. 1 is de theoretische stijfheid in verhouding tot de stijfheid van een monolithische glasplaat met dezelfde totale dikte bij deze proefconfiguraties weergegeven in functie van de glijdingsmodulus van de tussenlaag. Hierop is te zien dat een relatief snelle stijfheidsreductie te verwachten is bij de onder torsie belaste 360 mm brede proefstukken (zwarte lijn). Op het ogenblik dat deze proportionele stijfheid zijn ondergrens benadert, wordt de proportionele buigstijfheid van de proeven met een overspanning van 2.95 m dan weer sterk beïnvloed door een verdere afname van de stijfheid van de tussenlaag (bovenste donkergrijze curve).

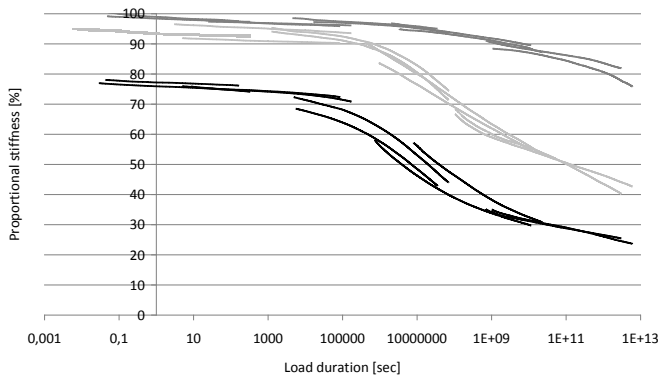


**Figuur 1: Theoretische proportionele stijfheid in functie van de glijdingsmodulus van de tussenlaag voor de drie gekozen testconfiguraties.**

### 3 Theoretische en numerieke analyse

Als eerste stap in de analyse werd de functie tussen belastingsduur en temperatuur bepaald. Een Williams-Landel-Ferry verschuivingsfunctie met constanten  $C_1 = 135$  en  $C_2 = 760$  °C bij een referentie temperatuur  $T_{ref}$  van 20 °C resulteerde in een vloeiende overgang tussen de curves van de experimentele resultaten uitgevoerd bij verschillende temperatuurniveaus.

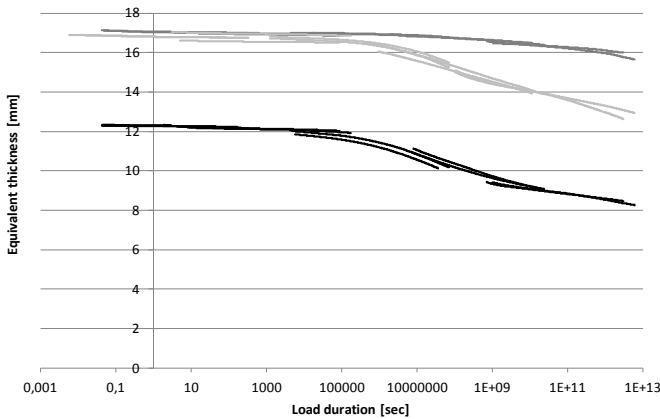
Om een vergelijking tussen de resultaten van de verschillende testseries mogelijk te maken, werden alle resultaten omgevormd tot een proportionele stijfheid. Op deze manier worden alle resultaten uitgezet in verhouding tot de bovenste limiet. Fig. 2 vat alle resultaten samen van de experimenten uitgevoerd bij vijf verschillende temperaturen tussen 5 °C en 65 °C verschoven naar  $T_{ref} = 20$  °C.



**Figuur 2: Experimentele proportionele stijfheid in functie van de belastingsduur bij  $T_{ref} = 20$  °C: torsieproeven (zwarte curves); buigproeven met een overspanning van 2950 mm (donkergrijze curves); buigproeven met een overspanning van 1050 mm (lichtgrijze curves)**

Deze curves bewijzen dat een eenvoudige correlatie tussen de proportionele stijfheid van het laminaat en de belastingsduur bij een bepaalde temperatuur niet bestaat. Hoewel de uiterste limieten van de stijfheid zelf eenvoudig te bepalen zijn, is zowel het belastingstype, de temperatuur, de belastingsduur als de geometrie van het element bepalend voor de situering van de globale stijfheid van het laminaat ten opzichte van deze limieten.

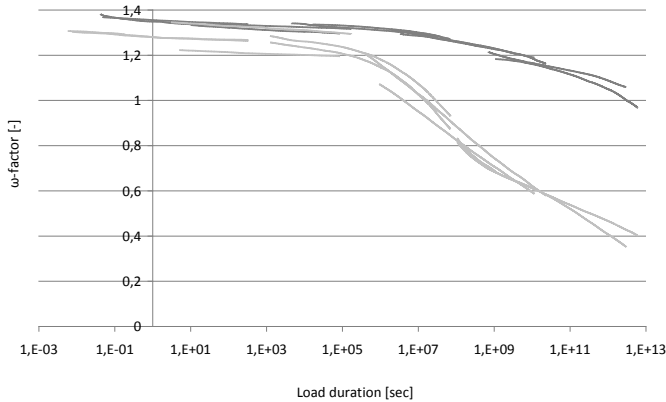
Om deze reden werden de resultaten ook verwerkt op basis van de theorie van de equivalente dikte, die voorgesteld wordt in [prEN 13474-3] voor de berekening van de stijfheid van een glaslaminaat. Fig.3 toont de berekende equivalente diktes van de uitgevoerde experimenten.



**Figuur 3: Equivalente dikte in functie van de belastingsduur bij  $T_{ref} = 20 \text{ }^{\circ}\text{C}$ : torsieproeven (zwarte curves); buigproeven met een overspanning van 2950 mm (donkergrijze curves); buigproeven met een overspanning van 1050 mm (lichtgrijze curves)**

Omdat de torsieproeven uitgevoerd werden op laminaten met een andere dikte dan de buigproeven, was de maximale equivalente dikte uiteraard kleiner. Bij langere belastingsduur is de equivalente dikte bij de buigproeven waarbij enkel de overspanning afwijkt echter ook niet gelijk. Het lijkt dan ook logisch dat de dimensieloze  $\omega$ -factor, berekend voor beide buigproefopstellingen zoals weergegeven in Fig. 4, niet overeenstemmen.



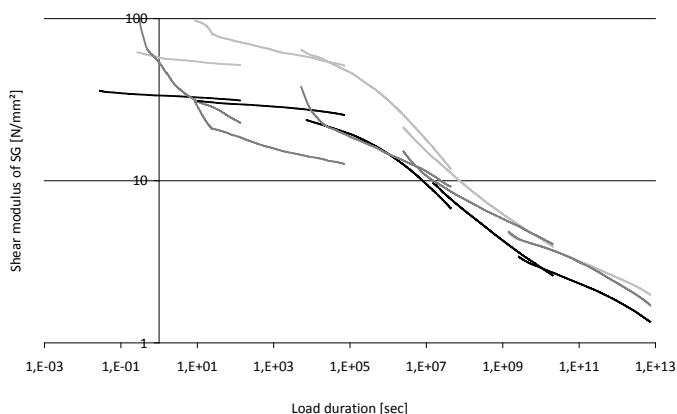


**Figuur 4:  $\omega$ -factor in functie van de belastingsduur bij  $T_{ref} = 20\text{ }^{\circ}\text{C}$ : buigproeven met een overspanning van 2950 mm (donkergrijze curves); buigproeven met een overspanning van 1050 mm (lichtgrijze curves)**

Hoewel deze dimensieloze factor verandert door het variëren van de belastingsvoorwaarden en dus niet direct bruikbaar is voor andere configuraties dan de geteste, is het toch belangrijk op te merken dat  $\omega$  de waarde 1 overstijgt, welke normaal te verwachten is bij de bovenste stijfheidslimiet. De verwaarloosde dikte van de tussenlaag en een nogal conservatieve elasticiteitsmodulus voor het glas van 70 GPa veroorzaken deze hoge waarden bij korte belastingsduur en lage temperaturen voor de onderzochte stijve tussenlaag.

Bijgevolg is het weinig zinvol om een algemene uitspraak te doen met betrekking tot de globale stijfheid van laminaten. Daarom werden de resultaten omgevormd naar een materiaal eigenschap van de tussenlaag, namelijk de glijdingsmodulus  $G_{SG}$ , die onafhankelijk zou moeten zijn van de belastingssituatie.

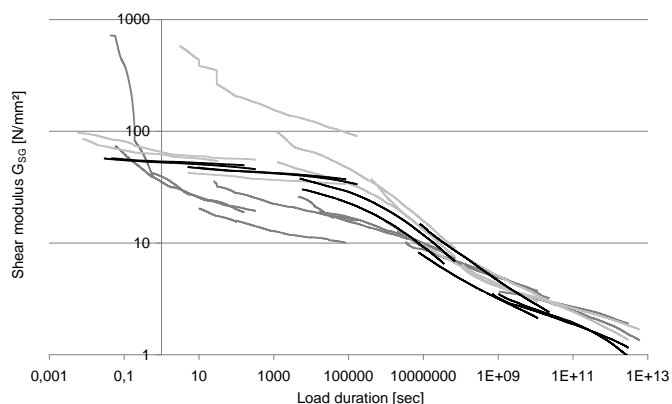
In de literatuur is zowel een theoretisch model te vinden om de torsiestijfheid en de buigstijfheid van laminaten te berekenen met behulp van de materiaaleigenschappen van de onderdelen en de geometrie van het element. De theorie van Scarpino [Scarpino 2005] werd op een omgekeerde manier gebruikt om  $G_{SG}$  te bepalen uit de experimentele torsiestijfheid. Met de experimentele buigstijfheid werd hetzelfde gedaan met behulp van de theorie van Wölfel [Wölfel 1987]. De resultaten zijn voorgesteld in Fig. 5.



**Figuur 5:  $G_{SG}$  gebaseerd op theoretische modellen in functie van de belastingsduur bij  $T_{ref} = 20 \text{ }^\circ\text{C}$ : torsieproeven (zwarte curves); buigproeven met een overspanning van 2950 mm (donkergrijze curves); buigproeven met een overspanning van 1050 mm (lichtgrijze curves)**

De curves tonen aan dat de materiaaleigenschappen van de tussenlaag quasi onafhankelijk zijn van de testopbouw, in tegenstelling tot de proportionele stijfheid of de equivalente dikte. De glijdingsmodulus van de torsieproeven lijkt in het algemeen echter iets lager dan de waardes bekomen uit de buigproeven. Daarom, en ook omdat de theoretische modellen kleine imperfecties van de proefopstelling niet in rekening kunnen brengen, werden de experimenten ook numeriek geanalyseerd.

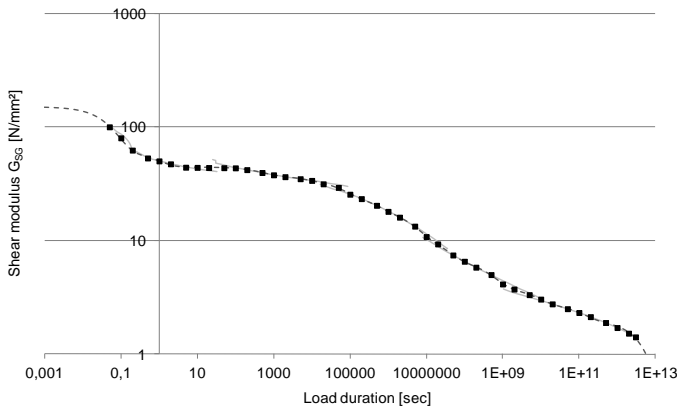
Er werden eindige elementen modellen opgebouwd die de test opstelling zo veel mogelijk benaderden, waarmee de algemene stijfheid bepaald werd voor verschillende waarden van  $G_{int}$ . Door deze te vergelijken met de experimentele stijfheden, kon  $G_{SG}$  ook numeriek bepaald worden. Op basis van deze resultaten, weergegeven in Fig. 6, werd een materiaalmodel opgebouwd.



**Figuur 6:  $G_{SG}$  gebaseerd op numerieke modellen in functie van de belastingsduur bij  $T_{ref} = 20 \text{ }^\circ\text{C}$ : torsieproeven (zwarte curves); buigproeven met een overspanning van 2950 mm (donkergrijze curves); buigproeven met een overspanning van 1050 mm (lichtgrijze curves)**

## 4 Materiaalmodel voor SentryGlas®

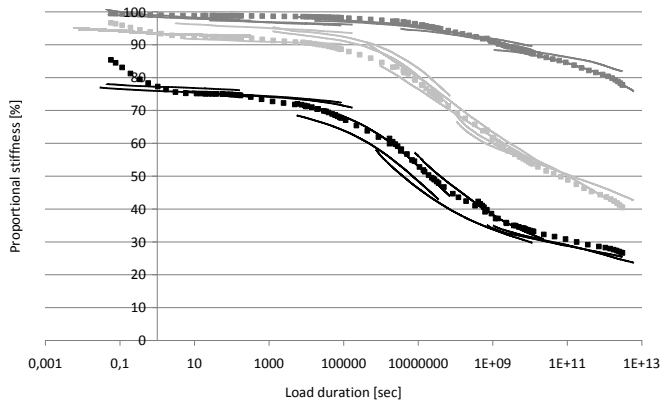
Na uitmiddeling van de experimentele  $G_{SG}$  per testtemperatuur, konden alle resultaten benaderd worden met één lineair visco-elastisch Maxwell model. De vijf gemiddelde curves zijn in rood weergegeven in Fig. 7 en werden vloeiend benaderd met een beperkt aantal waardes (zwarte punten) die als bruikbare basis dienden voor de bepaling van een Maxwell serie. De blauwe curve geeft een herberekening van  $G_{SG}$  op basis van dit model.



**Figuur 7:**  $G_{SG}$  in functie van de belastingsduur bij  $T_{ref} = 20$  °C: gemiddelde resultaten op basis van numerieke analyse (lichtgrijze curves); vereenvoudigde benadering (zwarte punten); herberekening op basis van Maxwell model (donkergrijze gestreepte curve)

Voor dit model moest ook een aanname worden gemaakt voor zowel de ogenblikkelijke glijdingsmodulus van SG  $G_{SG,0}$  als de lange duur waarde  $G_{SG,\infty}$ . Via herberekening van de materiaaleigenschappen met Maxwell series die gebaseerd werden op verschillende schattingen, werden veilige en goed onderbouwde waardes gekozen. Maar ondanks dat dit model waarschijnlijk ook niet buiten het geteste gebied de werkelijke eigenschappen overschat, is het niet aangewezen het te gebruiken wanneer een glijdingsmodulus boven  $100$  N/mm<sup>2</sup> en onder  $1.4$  N/mm<sup>2</sup> bekomen wordt. Bovendien kunnen polymeren zich vanaf een bepaalde temperatuur totaal anders gedragen. Het model is dan ook slechts bruikbaar tot een temperatuur van maximaal  $65$  °C, want hierboven werden geen experimenten uitgevoerd.

Tot slot, werd het model gevalideerd met behulp van visco-elastische numerieke simulaties van de uitgevoerde testen. In Fig. 8 tonen deze resultaten een goede overeenkomst met de experimentele proportionele stijfheid uit Fig. 2. Ook elastische numerieke simulaties en theoretische berekeningen met ogenblikkelijke glijdingsmodulus geëxtraheerd uit het Maxwell model, leverden een goede gelijkenis met de testresultaten. Dit laatste benadrukt nogmaals dat de stijfheid van een laminaat onder relatief eenvoudige belastingssituaties goed benaderd kan worden met behulp van bestaande theoretische modellen.



**Figuur 8: Numeriek bepaalde proportionele stijfheid in functie van de belastingsduur bij  $T_{ref} = 20\text{ }^{\circ}\text{C}$  in vergelijking met de testresultaten uit Fig. 2: torsieproeven (zwarte curves); buigproeven met een overspanning van 2950 mm (donkergrijze curves); buigproeven met een overspanning van 1050 mm (lichtgrijze curves)**

# Contents

---

<b>Chapter I: Introduction</b>	<b>1</b>
I.1 Situation	1
I.2 Problem definition	2
<i>I.2.1 Laminated glass – limiting cases</i>	2
<i>I.2.2 Visco-elastic material behaviour</i>	3
<i>I.2.3 Objectives of the research</i>	3
I.3 Method	3
I.4 Structure of the thesis	4
<b>Chapter II: Materials</b>	<b>7</b>
II.1 Glass	7
<i>II.1.1 Short history</i>	7
<i>II.1.2 Main material properties</i>	8
II.1.2.1 Stiffness	9
II.1.2.2 Strength	9
II.2 Interlayer materials	10
<i>II.2.1 Short history</i>	10
<i>II.2.2 Main material properties</i>	12
II.3 Lamination	16
<i>II.3.1 Autoclave lamination</i>	16
<i>II.3.2 Vacuum lamination</i>	17
<b>Chapter III: Experimental stiffness of glass/ionomer laminates</b>	<b>19</b>
III.1 State of the art	19
<i>III.1.1 Material scale</i>	19
<i>III.1.2 Intermediate scale</i>	22
<i>III.1.3 Full scale</i>	25
III.2 Experimental test programme	27
<i>III.2.1 Combination of experimental test series</i>	27
<i>III.2.2 Temperature control</i>	28
III.3 Preliminary experiments	29
<i>III.3.1 Bending experiments with IR-heating</i>	30
III.3.1.1 Materials & methods	30
III.3.1.2 Results	30
III.3.1.3 Discussion	31
<i>III.3.2 Torsion tests in climatic chamber</i>	31
III.3.2.1 Materials & methods	31
III.3.2.2 Results	32
<i>III.3.3 Bending tests in climatic chamber</i>	33
III.3.3.1 Materials & methods	33
III.3.3.2 Results	34
<i>III.3.4 Discussion and conclusions</i>	36

III.4	Torsion	38
III.4.1	<i>Samples</i>	38
III.4.2	<i>Experimental setup</i>	39
III.4.3	<i>Experimental procedure</i>	40
III.4.4	<i>Results</i>	41
III.5	Bending	42
III.5.1	<i>Samples</i>	42
III.5.2	<i>Experimental setup</i>	43
III.5.3	<i>Procedure</i>	45
III.5.4	<i>Results</i>	45
III.6	Discussion	47
<b>Chapter IV: Analytical and numerical analysis</b>		<b>51</b>
IV.1	Theoretical analysis	51
IV.1.1	<i>Williams-Landel-Ferry time-shift</i>	52
IV.1.2	<i>Effective thickness method</i>	57
IV.1.3	<i>Theoretical models</i>	64
IV.1.3.1	Torsional stiffness by Scarpino	65
IV.1.3.2	Bending stiffness by Wölfel	67
IV.1.3.3	Combined results	72
IV.2	Numerical analysis	73
IV.2.1	<i>Finite element models</i>	73
IV.2.1.1	Torsion model	73
IV.2.1.2	Bending model	74
IV.2.2	<i>Theoretical versus numerical stiffness</i>	75
IV.2.3	<i>Numerically deduced interlayer stiffness</i>	77
IV.3	Discussion	81
<b>Chapter V: SentryGlas® material model</b>		<b>83</b>
V.1	Material model	83
V.1.1	<i>Rheology</i>	83
V.1.2	<i>SG material model</i>	86
V.2	Comparison with existing material models	91
V.3	Recalculation with proposed material model	94
V.3.1	<i>Numerical simulations with visco-elastic material model</i>	95
V.3.2	<i>Numerical simulations with elastic material behaviour</i>	97
V.3.3	<i>Theoretical calculations with elastic material behaviour</i>	99
V.4	Discussion	100
<b>Chapter VI: Conclusions</b>		<b>103</b>
VI.1	Conclusions	103
VI.2	Further research	104
<b>References</b>		<b>107</b>
<b>Appendices</b>		<b>117</b>

# Chapter I: Introduction

---

## 1 Situation

After serving for many centuries as a transparent infill panel for openings in buildings, it was discovered that glass was strong enough to carry a significant load. By transferring important building loads through glass elements - to fulfil the increasing architectural wish for transparency - the concept of *Structural glass* was born. Bearing floors, beams and columns in glass became possible through enhanced production processes with belonging quality inspections, an increasing knowledge of the material behaviour and innovative safety concepts.



**Figure I.1: Structural glass applications: staircase with four-sided supported glass treads (left); high-end full-glass structure (Apple store, Bohlin Cywinski Jackson architects, 2010, Shanghai) (right)**

The most applied technique to increase the post-failure behaviour of the brittle glass is to laminate multiple glass sheets together with a soft interlayer material. This way, a certain plastic mechanical behaviour is added to the component. In case of an impact on the element, the interlayer can partially absorb the impact energy, which will hopefully limit failure to only one glass sheet. Additionally, the glass fragments remain attached to the interlayer, so the probability that people get injured is drastically reduced.

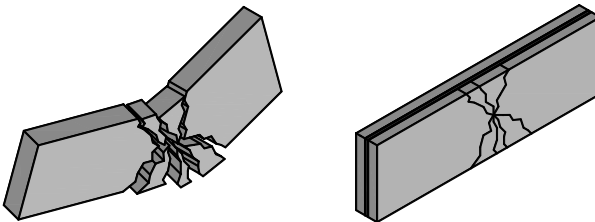


**Figure I.2: Post-failure behaviour after impact: monolithic glass (left); laminated glass (right)**

## 2 Problem definition

### 2.1 Laminated glass – limiting cases

Independent of the choice of interlayer material (resin, polymer, polycarbonate, etc.), the structural properties of a laminated element are always situated between two limiting cases. For laminated glass, the upper limit corresponds to a monolithic glass plate (normally the stiffest material of the composed element) with a thickness equal to the total thickness of the laminate. On the other hand, the lower limit corresponds to the sum of the individual glass plies. In the latter case, the mechanical properties of the interlayer materials, as well as their contribution to the interaction between the different glass sheets, are totally neglected.

The most conservative way to calculate the mechanical behaviour of laminated glass is to use the lower limit. Doing so, the load is proportionally distributed among the different glass sheets in such a way that the deformation of all plies is identical. A thicker glass layer in a laminate will thus take more load than a thinner one and the highest stresses can be expected in the thickest pane.

On the other hand, the upper limit is the easiest calculation method because only one monolithic plate has to be taken into account, resulting in a more standard calculation. Unfortunately, this state is generally a significant overestimation of the actual strength and stiffness of the element, possibly causing dangerous situations. To avoid this, it may seem interesting to always use the lower limit, which is also relatively easy to calculate for a structural engineer and it always results in an underestimation of the stiffness, which is in most cases a safe assumption.

However, it can certainly be rewarding to take into account the interaction between the different plies of the laminate because the difference between the two ultimate states can be highly significant. For instance, for a two sided supported laminate with two glass sheets with equal thickness, the upper limit can carry double the load, while the deflections of the laminate with this double load remain half of those which can be expected for the lower limit, as illustrated in Fig. 1.3. However, an adequate technique must be applied, when the shear transfer between the different glass panes in a laminate is taken into account.

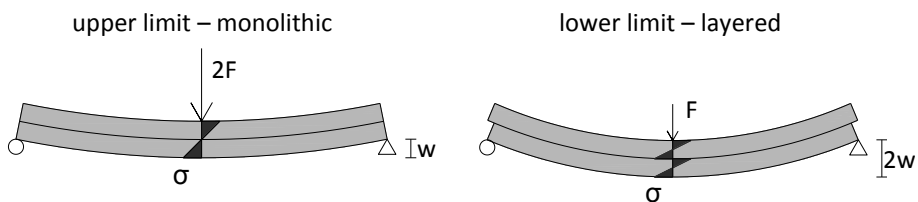


**Figure 1.3: Ultimate limit states for the mechanical behaviour of laminated glass: upper limit with full shear interaction (left); lower limit without shear interaction (right)**



Glass/Polyvinyl Butyral (PVB) laminates were developed for the automotive sector, where the windshields need to keep their integrity during a car crash. Unfortunately, a PVB interlayer is relatively soft, and therefore it is not ideal for structural glass. For the latter, usually the laminate must be as stiff as possible to restrict deflections. The ionomer interlayer material SentryGlas<sup>®</sup>, or shortly SG (formerly known as SentryGlas<sup>®</sup> Plus, or briefly SGP), is an example of a much stiffer interlayer material which can reduce deformations and bending stresses in laminated components.

## 2.2 Visco-elastic material behaviour

Contrary to monolithic glass, which behaves fully elastically until it breaks, a glass/polymer laminate usually behaves visco-elastically. This means that the stiffness of the laminate depends on the load duration and the temperature of the interlayer: a glass laminate will creep under a constant load and relaxation will occur under enforced constant deformation. These phenomena will also speed up at increased temperature. When applied in structural applications, it is therefore important to know the mechanical behaviour accurately to be able to design a safe, but economic structure.

For normal building applications, the shear modulus of the interlayer varies generally between 0.01 MPa and 100 MPa. Although this highest value is already 300 times smaller than the shear modulus of glass, this range may cause a highly significant difference for the laminated building component.

## 2.3 Objectives of the research

Consequently, the main objectives of this research are:

- Improvement of the understanding of the mechanical behaviour of laminated glass with a stiff interlayer under different loading conditions
- Determination of the visco-elastic material properties of SG
- Verification of the applied analysing techniques

## 3 Method

The problem is approached from a structural point of view. To incorporate the possible influence of the lamination process (a process with high pressure and an elevated temperature-cycle) on the properties of the polymer interlayer, most tests were performed on laminated glass. This is in contrast to e.g. standardised dynamic mechanical analysis (DMA), which are carried out on samples of the interlayer material only [ASTM D4065-06] [NBN EN ISO 6721].

Furthermore, as a consequence of the variety of realistic loading conditions for structural glass elements, the test programme is subdivided into two

complementary simplified loading conditions: three-point bending about the weak axis and torsion about the longitudinal axis. Afterwards, a combination of these two conditions can be used to describe other situations.

Subsequently, the experimental results are analysed both theoretically and numerically. The experimental outcome is evaluated, leading towards a material model which describes the visco-elastic behaviour of laminated glass with SG well. Finally, existing calculation methods are also used to validate the model.

## 4 Structure of the thesis

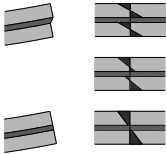
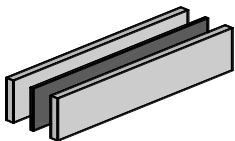
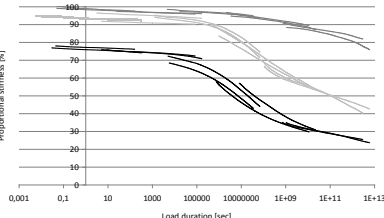
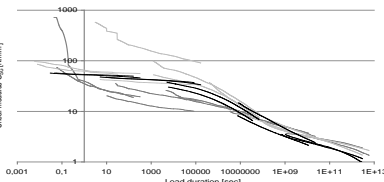
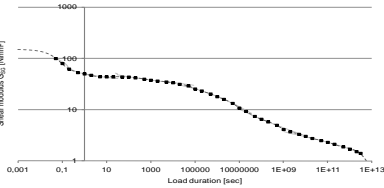
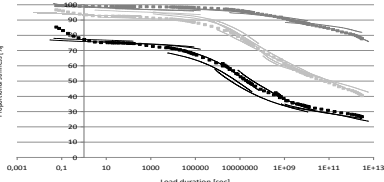
Following this introduction, the basics about laminated glass and its components are explained in [chapter II](#). A short history of the development of glass and its main material properties are summarised. Then, this is also provided for the most common visco-elastic polymer interlayer materials. Finally, the chapter finishes with a brief description of two common lamination techniques.

[Chapter III](#) treats the experimental campaign. It begins with a limited overview of existing research concerning the stiffness of interlayer materials, divided in three categories determined by the scale of the test specimen: 1) the material scale for which experiments are executed on small samples of the interlayer material; 2) the intermediate scale for which the relatively small test samples are extracted from larger laminated elements; and 3) the large scale which contains experiments executed on samples with dimensions relatively comparable to normal structural laminated components. Based on the advantages and disadvantages of each test method, a test programme with complementary test series is proposed with an adequate temperature control. In the third section of this chapter III, some preliminary experimental series are summarised which form an informative study for the actual torsion and bending test series, described in the next two chapters. The samples, the experimental test setup and the accompanying procedure are presented and the results of all tests are converted into proportional stiffness in order to accomplish a simplified representation.

In [chapter IV](#), the results from the experimental research are further analysed. First, the temperature dependent behaviour is described by a Williams-Landel-Ferry time-shift function, so the results performed at different temperatures can be represented as tests with reduced load duration at one single reference temperature. Then, these shifted resulting stiffness are approached by the equivalent thickness method, presented in a European draft standard for the calculation of laminated glass stiffness [prEN 13474-3]. Because the resulting equivalent thickness is not directly applicable to predict different loading conditions, the experimental results are also transferred into values of the shear modulus of the interlayer based on an inversed application of existing theoretical models. Finally, a similar analysis is also based on numerical simulations of the test setups.

Next, the resulting shear modulus of SG is approximated by a linear visco-elastic material model in chapter V. A Maxwell series, which describes the time- and temperature dependent mechanical behaviour of the interlayer, is set up based on a simplified representation of the averaged results from all different test setups. In the second paragraph, this model is compared to three different models provided by the producer of the material. As a last step, the model is also used to recalculate the stiffness of laminated elements in order to verify both the model as the applied calculation methods.

Finally in chapter VI, the conclusions of the research are presented. The approach and the outcomes are evaluated. The chapter ends with a proposition for future interesting research concerning pre-failure behaviour of laminated glass.

I	Introduction	<p>I.1 Use of glass in structural applications</p> <p>I.2 Problem definition: mechanical behaviour of laminated glass</p> <p>I.3 Method: experimental approach from structural point of view</p> <p>I.4 Structure of the thesis</p>	
II	Materials	<p>II.1 Glass: history and main material properties</p> <p>II.2 Interlayer materials: history and visco-elastic properties</p> <p>II.3 Lamination techniques</p>	
III	Experiments	<p>III.1 Overview of existing experimental research</p> <p>III.2 Composition of the test programme: torsion &amp; bending</p> <p>III.3 Preliminary torsion and bending experiments</p> <p>III.4 Torsion experiments on glass/SG laminates</p> <p>III.5 Bending experiments on glass/SG laminates</p> <p>III.6 Discussion</p>	
IV	Analysis	<p>IV.1 Analysis based on the theoretical models</p> <p>IV.2 Analysis based on numerical simulations</p> <p>IV.3 Discussion</p>	
V	Model	<p>V.1 Determination of visco-elastic SG material model</p> <p>V.2 Comparison of proposed model with existing models</p> <p>V.3 Validation</p> <p>V.4 Discussion</p>	
VI	Conclusion	<p>VI.1 Conclusions</p> <p>VI.2 Suggested further research</p>	

# Chapter II: Materials

---

The basics about laminated glass are presented in this chapter. It begins with a short history about the material glass, and its main mechanical properties. Then, a short introduction is also given for the most popular interlayer materials for laminated glass. Finally, the chapter ends with a short introduction to most common lamination techniques.

## 1 Glass

### 1.1 Short history

Glass is, from a chemical point of view, an inorganic amorphous solid. The amorphous structure can be obtained by melt quenching, a rapid cooling of the liquid material which prevents crystallisation during solidifying [Haldimann et al. 2008].

The latter specific phase transition can also occur naturally, for example at some volcanoes, which already in the stone age lead to the first applications with glass. Pieces of natural obsidian were manually processed into sharp and hard utensils. The first objects made of self-produced glass, for which the basic raw materials were combined and molten together, were found in graves from about 3500 BC. Hereafter, it lasted till the first century BC until the molten material was given shape with a blowpipe.

Derived from the glassblowing, the first flat glass for the use in buildings was produced around the year 1300 AD with the Crown glass process. To obtain a flat disk, an opened glass bulb was whirled around. Because of the weight of the material, only relatively small glass plates could be made. The maximal producible size was a little bit increased with the later developed cylinder blown sheets method, but the true revolution in the flat glass production came at the beginning of the 20th century with the industrial revolution. In 1904 large glass plates were pulled out of a molten glass bath with the Fourcault-process [Austin 1984]. During a period of 50 years the process was gradually refined until Pilkington developed in 1959 the float glass process. For the latter production method, the melted glass mass is poured on a tin bath which results in an extremely smooth glass surface [Amston 1997].

Currently, the majority of the flat glass is still produced with the float production process. For practical reasons, the continuous glass sheet coming from the float process is normally cut into manageable standardised glass plates of (4500, 5100

or) 6000 mm long and 3210 mm wide<sup>1</sup> [NBN EN 572-2]. These basic plates are further cut, coated, treated, laminated, etc. into all kinds of current end user glass products for the building industry.

## 1.2 Main material properties

The chemical composition of glass has an important influence on the physical properties of the material. Fused quartz for instance, one of the most simple glass materials which contains almost purely silicon dioxide<sup>2</sup>, has a high thermal stability and chemical resistance which is crucial for particular laboratory equipment. Due to the high processing temperature, however, it is practically unusable for most of the applications. Therefore, other materials, such as sodium oxide and calcium oxide are added to the glass material so it becomes more workable. As a consequence, different compositions have been commercialised for various specific applications. In buildings, almost exclusively soda lime silica glass is used because of the relatively low production cost for a type of glass which satisfies most demands.

In Table II.1, the chemical composition of soda lime silica glass according to the European standard EN 572-1 is presented.

**Table II.1: Chemical composition of soda lime silica glass [NBN EN 572-1]**

component	mass amount [%]
silicon dioxide (SiO <sub>2</sub> )	69 - 74
calcium oxide (CaO)	5 - 14
sodium oxide (Na <sub>2</sub> O)	10 - 16
magnesium oxide (MgO)	0 - 6
aluminium oxide (Al <sub>2</sub> O <sub>3</sub> )	0 - 3
others	0 - 5

In Table II.2, some important material properties of fused quartz and soda lime glass are summarised. Because the strength and stiffness of the material are more complex and of major importance for structural applications, these mechanical properties are separately discussed in the next paragraphs.

**Table II.2: Main material properties of fused quartz and soda lime glass**

property	fused quartz	soda lime silica glass	unit
Density	2200	2500	kg/m <sup>3</sup>
Coefficient of thermal expansion	0.55	9	10 <sup>-6</sup> K <sup>-1</sup>
Glass transition temperature	1100	550	°C

<sup>1</sup> As an exception, some companies produce larger plates. At moment of writing, the largest processed flat glass plate measured 25 m by 4.2 m [clfg 2011] and the largest insulated glass unit was 18 m long by 3.3 m wide [Henze-Glas 2010].

<sup>2</sup> Some small impurities are inevitable.

### 1.2.1 Stiffness

At ambient temperature, glass has an almost perfect isotropic linear elastic behaviour, which means that it does not yield and it breaks in a brittle manner. The stiffness is therefore fully determined by Young's modulus and Poisson's ratio.

*Table II.3: Stiffness properties of soda lime silica glass*

Reference	Young's modulus [GPa]	Poisson's ratio [-]
[NBN EN 572-1]	70	0.2
[DIN 1249-10]	70-73	0.23

In literature, also small inelastic deformations have been observed at ambient temperature [Schneider & Wörner 2006], but these are limited compared to the overall linear deformations. Therefore, they are not further taken into account for the presented research.

### 1.2.2 Strength

The strength of a glass element is ambiguous, because it is not an actual material property. This is caused by the difference between on the one hand side the theoretical strength, which is determined by the strength at molecular level, and at the other the actual strength, which is dominated by flaws on the surface. In literature exists quite some research exclusively dealing with different aspects of glass strength [Norville & Minor 1985], [Haldimann 2006], [Lindqvist et al. 2011], [Vandebroek et al. 2011], [Veer & Rodichev 2011]. Nevertheless this research focuses only on the pre-breakage effects of laminated glass and therefore, only the most important basic ideas are summarised below.

Every glass sheet contains surface flaws, which already inevitably appear during the production of flat glass sheets and which further increase due to processing, transportation, installation, cleaning, etc. For tensile stresses, typically occurring at one side of a bended glass plate, these tiny flaws act as stress concentrators. At the tip of the crack, the local stresses reach very high values which can cause brittle fracture of the entire element. Under compression, these micro-cracks are squeezed together without causing high tension peaks. Therefore, the actual tensile strength is much lower than the compressive strength.

This also forms the basis of thermal and chemical strengthening of glass which theoretically increases the surface tensile strength. With a thermal or chemical process, internal prestresses are introduced. By doing so, compression stresses are implemented at the outer surface of the glass pane, while tension occurs at the internal zone of the sheet, where no flaws appear which can cause stress peaks. When a strengthened plate bears structural loads, the applied stresses can be superimposed to the prestresses. So, higher structural bending stresses can be taken until the element breaks.

An important consequence of the glass strengthening is the high amount of energy released at failure, which results in a changing breakage pattern. When the

prestress level is increased, the size of glass fragments reduces. This is of major importance to predict the post-failure behaviour. Fig. II.1 depicts the fracture pattern of a laminated element with fully tempered glass sheets (left) and annealed glass sheets (right) after a torsional overload.

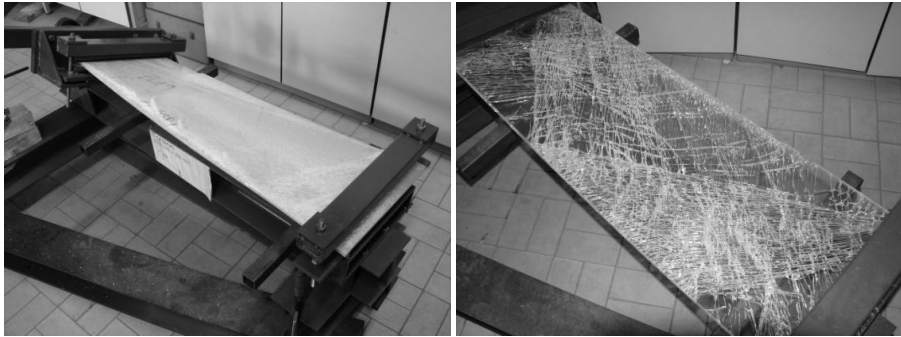


**Figure II.1: Fracture pattern of a laminated element after torsional overload fully tempered glass (left); annealed glass (right)**

In [ASTM C1048-04], the required surface compressive stress is determined for both heat-strengthened glass as for fully tempered glass (see Table II.4). In [NBN EN 12150-1], the fragment size and amount of particles of a standardised fracture test are determined for which glass meets the requirements of thermally toughened soda lime silicate safety glass.

**Table II.4: Amount of surface compression according to [ASTM C1048-04]**

	Surface compression	Unit
Heat-strengthened glass	24 - 52	N/mm <sup>2</sup>
Fully tempered glass	>69	N/mm <sup>2</sup>

## 2 Interlayer materials

### 2.1 Short history

In 1909, Edouard Benedictus became the owner of the first successful patent for what he called safety glass. He was a chemist who, according to the legend, accidentally discovered the post-breakage advantages of the combination of glass with plastic materials by dropping a glass flacon containing cellulose nitrate [Trimm 2005]. Instead of shattering into pieces, the bottle remained relatively intact because the liquid formed a thin plastic film which kept the glass fragments together. His patent also led to the first important wide-scale application of glass/polymer combined elements in gas masks during World War I.



## **PVB**

Then around 1930, Polyvinyl Butyral (PVB) was developed as the interlayer material for larger laminated glass sheets. Its main application scope was the increase of the post-failure behaviour of car windshields. The automobile market boomed at that period and therefore the safety of the driver and passenger became a priority [Hinckley 2005]. During a car crash, it had to be prevented that a passenger could fly through the broken windshield, while the screen still had to be soft enough to absorb striking energy at a head impact reducing the risk of life-threatening injuries. For this application, the PVB interlayer material was specifically developed. Although the basic constituent is a rather hard copolymer resin, the material is customised with plasticizers to meet the necessary requirements.

After the success of laminated glass in the automotive sector, it also gradually found its way into the building industry. For the last 40 years, the laminated glass market is still dominated by the PVB composition with an almost unchanged chemical composition, but additionally, different variants were redesigned to meet new application-specific requirements [Pardos 2004]. This resulted for instance in PVB materials with enhanced acoustic performance or coloured and printable architectural interlayers. These interlayers are produced on rolls with different widths and a thickness which is normally a multitude of 0.38 mm (15 milli-inch).

## **EVA**

Apart from these PVB variants, also more recent materials were employed for laminated glass, for instance ethylene vinyl acetate copolymer (EVA). The major advantage of EVA is the reduced complexity of the lamination technique compared to PVB and the high flexibility and clarity, which are very satisfactory to e.g. the solar industry [Weller et al. 2005].

## **SG(P)**

During the 1990's the ionomer interlayer material SentryGlas® (SG) was specifically developed by DuPont de Nemours<sup>3</sup> for the improvement of the hurricane resistance of facades in the USA<sup>4</sup>. Through the years, SG has also been on the market as a bomb blast resistant interlayer material – especially after 9/11 – and is now presented as a structural interlayer with enhanced edge stability. During this period, also changes have been implemented to the material itself as a response to some delamination problems which occurred especially at low temperatures and

---

<sup>3</sup> In [Bennison 2008a] it is stated that this product is actually produced by the company AGP Plastics under the name Noviflex®. DuPont de Nemours, as one of the world leaders in the production of interlayer materials for laminated glass, markets their product as SentryGlas®.

<sup>4</sup> This material may not be mistaken with SentryGlas® Expressions, which is a printable PVB material.

the name evolved from SentryGlas® through SentryGlas® Plus (SGP), SentryGlas® Plus 2000 (SGP2000), SentryGlas® Plus 5000 (SGP5000) back to SentryGlas® (SG) in 2008.

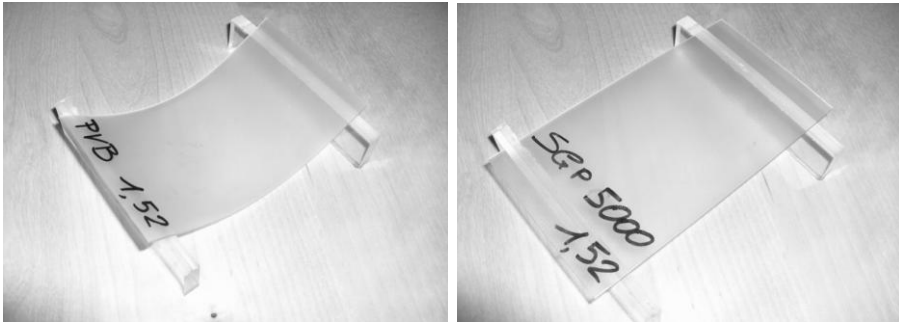


**Figure II.2: Qualitative stiffness comparison at room temperature of PVB and SG with equal thickness**

SG is also characterised as an ionoplast, which DuPont defined more closely as “A stiff sheet (Young’s Modulus greater than 100 MPa at temperatures up to 50 °C) comprised of ethylene / methacrylic acid copolymers containing small amounts of metal salts, that may be permanently bonded to glass.” [Stelzer et al. 2008]. In 2010, they also refer to SentryGlas® as an ionomer material [Stelzer 2010], a more generally accepted chemical group of materials to which the material was already referred to in literature.

In addition to these three shortly discussed interlayer materials, also others are used to reduce the brittleness of a glass component. Polycarbonate plates for bullet resistant glass, adhesive polyethylene terephthalate (PET)-films, and curing acrylic resins are some examples.

## 2.2 Main material properties

The three sheet interlayer materials mentioned above are polymer materials, which are characterised by their temperature dependent mechanical behaviour. In general, a polymer can behave elastic, visco-elastic or viscous depending on its temperature. In the *normal* temperature range for building applications (from -20 °C up to +80 °C), most interlayer materials behave visco-elastic. This means that their mechanical properties vary in function of time and temperature: creep and relaxation occur at increasing load durations and these phenomena accelerate at higher temperatures. Because of the complex behaviour, all experimentally determined properties have to be evaluated with proper attention.

The glass transition temperature  $T_G$  (of which a definition is presented in Fig. II.3), generally characterises whether the polymer situates in the elastic glassy state, the visco-elastic transition region, or the rubbery state at a certain temperature level. Practically, the glass transition is not a fixed value but a wider temperature region which can depend e.g. on the cooling rate of the interlayer or on the applied

definition. Fig. II.4 schematically represents the behaviour of amorphous and slightly cross-linked polymers over a wider temperature range.

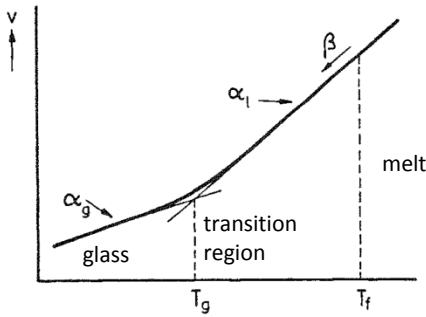


**Figure II.3: Definition of glass transition temperature, based on specific volume in function of temperature [Schwarzl 1990]**

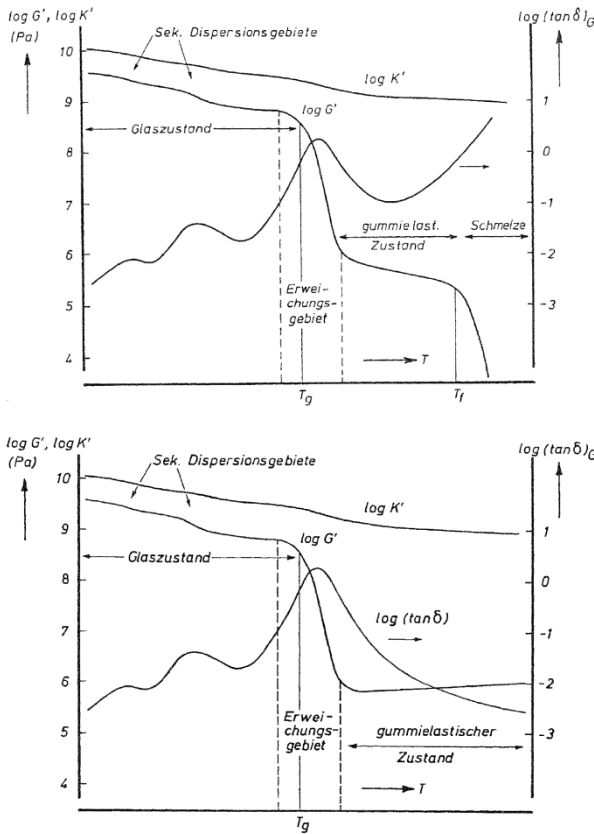


**Figure II.4: Schematic dynamic properties at 1 Hz of polymers in function of temperature: amorphous polymer (upper); lightly cross-linked polymer (lower) [Schwarzl 1990]**

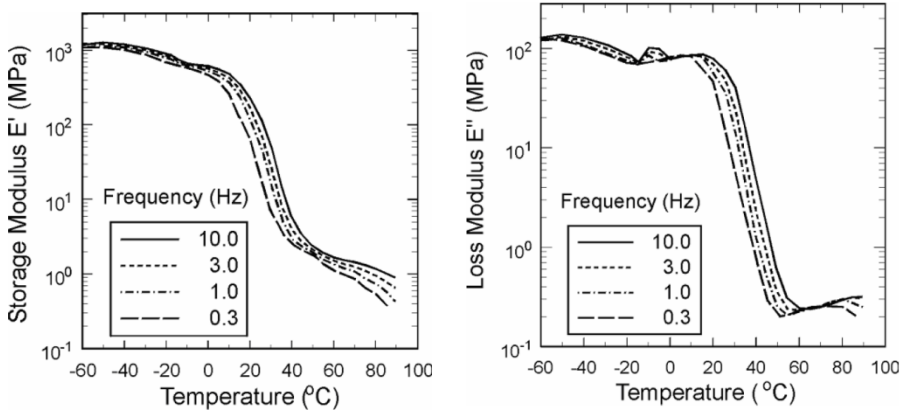


**Figure II.5: Storage and Loss modulus for PVB in function of temperature. Dynamical mechanical analysis (DMA) test results at different frequencies [Bennison & Gizzi 2007]**

In Fig. II.5, the dynamic properties of PVB are presented in function of the temperature. With this, the glass transition temperature  $T_G$  of PVB can be situated around 20 °C. For SG,  $T_G$  is about 55 °C, which both falls within *normal* temperatures. The  $T_G$  of EVA situates around -25 °C and -15 °C, but this relatively soft interlayer material is mainly used in applications where the shear transfer in a laminated element is not take into account.

The determination of the time and temperature dependent mechanical behaviour of SG is the main objective of this research. However, some material models for polymer interlayers are already described in literature. In Fig. II.6 for instance, two linear visco-elastic models for PVB are presented. Because the shear modulus is important for the calculation of the stiffness of the laminated glass, this property is usually reported in function of the load duration and the temperature level.

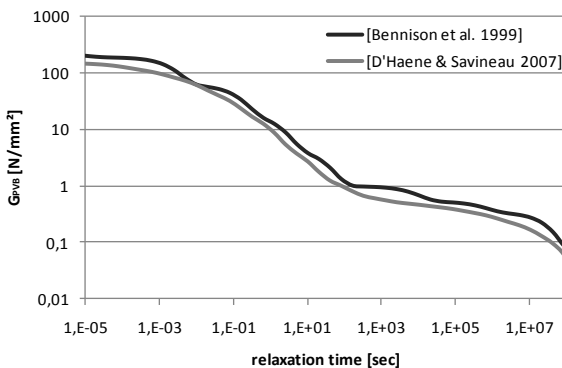


**Figure II.6: Visco-elastic material properties for PVB [Bennison et al. 1999], [D'Haene & Savineau 2007] at reference temperature  $T_{ref} = 20$  °C**

Three different material models for SG composed by the manufacturer have also been presented so far [Belis 2005] [Bennison & Gizzi 2007] [Bennison et al. 2008], for which the last is depicted in Fig. II.7.

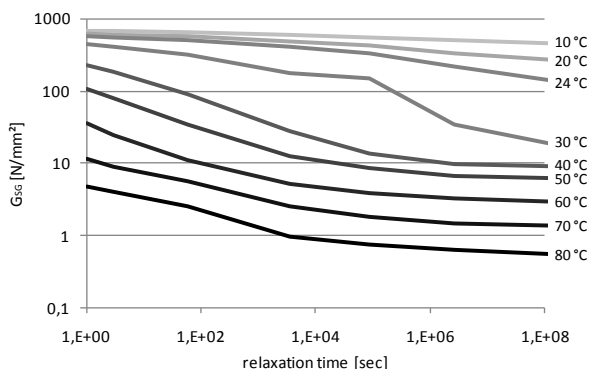


**Figure II.7: Visco-elastic material properties for SG [Bennison et al. 2008]**

Although the latter describes the mechanical behaviour for a wide application range, there are some drawbacks to these models. Firstly, they are only formulated and validated by the producer of the material themselves. Secondly, it is stated that the models are derived from dynamic mechanical analysis (DMA) according to [ASTM D4065-06] in combination with creep tests, but the actual test results and the exact method how the model have been derived from it, were never presented. Finally, there exists also some lack of clarity for some abnormalities in the models, like the fluctuation of the first two models the way the PVB models does in Fig. II.6 or the twist in the stiffness-curve for 30 °C at a load duration of 1 day in Fig. II.7 (30 °C). For these reasons, it was decided to perform an independent experimental research, which is presented in detail further on.

In Table II.5, an overview of some other important material properties of EVA, PVB and SG is provided.

**Table II.5: Main properties of the interlayer materials EVA, PVB and SG at ambient temperature. Properties might slightly differ depending on the specific type and/or the producer.**

property	PVB	EVA	SG	unit
Density	1070	930	950	kg/m <sup>3</sup>
Tensile strength	>20	10-25	34.5	N/mm <sup>2</sup>
Maximal elongation	>250	>500	400	%
Coefficient of thermal expansion	468	90	100-150	10 <sup>-6</sup> K <sup>-1</sup>
Glass transition temperature	20	-20	55	°C

## 3 Lamination

### 3.1 Autoclave lamination

After cutting the standard glass sheets to size, treating the edges<sup>5</sup>, making optional holes or other cut-outs and implementing the desired pre-stress, the lamination process can start. Because the adhesion of the interlayer material to the glass surface is very dependent on the cleanliness of the components and the humidity of the interlayer, the glass sheets are washed before they enter a clean room. The latter provides a controlled environment in which the interlayer can be manipulated safely. In this room, the different layers are stacked onto each other.

For the first step of the actual lamination, namely the pre-compound of the entity, two different production techniques are available [Van Russelt 1997]: a nip roller process and a vacuum-bag process. Both processes intend to 1) remove the air between the different layers as much as possible and 2) hold everything together for the final lamination in the autoclave.

In the nip roller process, the component is heated up with IR-heaters (Fig. II.8) and the edges are sealed by an upper and a lower compression roller [Greenyer 2009]. With the vacuum bag process, the components are placed in a plastic bag, which can be either sealed under vacuum or a vacuum can be created during the entire second step of the lamination.

The final adhesion of the interlayer sheets to the glass panes over their entire surface occurs during the second phase of the lamination, which takes place inside the autoclave. In this cycle, which usually takes about 2 to 3 hours, the elements are heated up to a temperature of 130 °C to 150 °C under an atmosphere pressure of about 13 bar<sup>6</sup>.

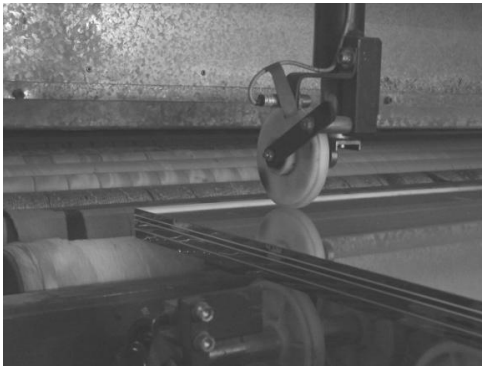


**Figure II.8: Nip roll lamination process**

---

<sup>5</sup> Annealed float glass can be processed after lamination as well

<sup>6</sup> These values can slightly differ, depending on the different interlayer materials

During the production cycles, often 300 mm by 300 mm plates are laminated for quality testing. On these samples, pummel tests, boiling tests, haze tests and/or compressive shear tests are executed in order to check the quality of the entire lamination cycle [Van Russelt 1997].

### **3.2 Vacuum lamination**

EVA is usually bonded to glass sheets during a process called vacuum lamination: the EVA sheets are adhered to the glass surface in a vacuum at temperatures between 140 °C and 155 °C. The major difference with the vacuum bag process in the autoclave lamination technique of § II.3.1, is that the high external atmospheric pressures are no longer required during this process. An autoclave is thus no longer required, which can significantly reduce the production costs.

Recently, this vacuum lamination method is also applied with other interlayer materials, such as PVB and SG, for applications with limited dimensions.





# Chapter III: Experimental stiffness of glass/ionomer laminates

---

As a first step in this research, the stiffness of laminated glass with a SentryGlas® interlayer was determined experimentally. In this chapter, these results are presented concisely. In the first paragraph, the presented experimental research is situated in the current context documented in literature. Then the reasons and fundamentals behind the chosen test programme are explained. Subsequently, two different methods to control the temperature environment of the tests are described. Then, the results of some preliminary tests are discussed and finally, the core test programme with torsion and bending experiments is presented.

## 1 State of the art

Ever since laminated glass is used in load bearing elements, the strength and stiffness of the component is an important issue for which experimental research is inevitable. Owing to this, there is already quite some research documented in literature, mainly focussing on glass/PVB laminates, which is an older and more common interlayer material than SG.

Generally, three categories of experimental research can be distinguished. In the first category, tests are performed on small samples of the interlayer material only. For the second category, small-scale laminated glass/interlayer samples are used. The third and last category contains experiments performed on laminated samples with realistic dimensions compared to building applications. In the next paragraphs, an inexhaustive overview of existing research is presented for each category, each having its own specific advantages and disadvantages.

### 1.1 Material scale

Most experiments of this first category are based on standardised tests for plastics. Examples of frequently used standards for the characterisation of the mechanical properties of interlayer materials in this category are ISO 527 [NBN EN ISO 527], ISO 899 [NBN EN ISO 899] and ISO 6721 [NBN EN ISO 6721] or their ASTM equivalents D638 [ASTM D638-10], D2990 [ASTM D2990-09] and D4065 [ASTM D4065-06].

With uniaxial tensile tests on dogbone-shaped specimens according to e.g. ISO 527, nominal stress strain curves can be drawn up from which Young's modulus and Poisson's ratio can be determined. In literature, results are available for both PVB and SG [Bucak & Meißner 2005], [Kott & Vogel 2006], [Belis et al. 2009]. Figs. III.1 and III.2 represent some exemplary results.

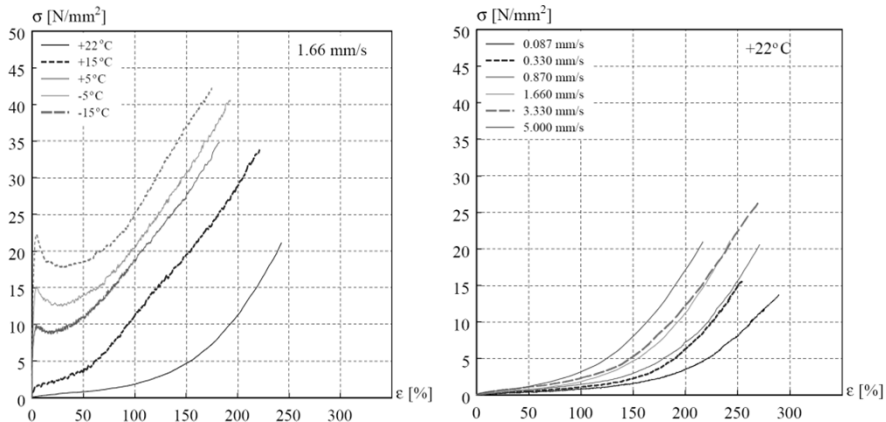


**Figure III.1: Average stress/deformation curves from uniaxial tensile tests on series of four not artificially aged PVB specimens according to [Kott & Vogel 2006]; with a deformation rate of 100 mm/min at five temperature levels (left); with six different deformation rates at a temperature of 22 °C (right)**

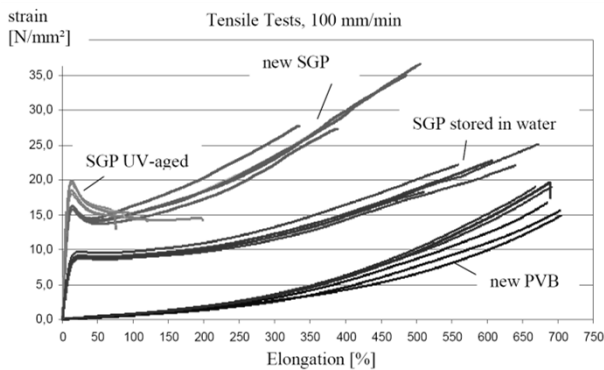


**Figure III.2: Stress/deformation curves from uniaxial tensile tests on six not artificially aged PVB samples, five unaltered and two times five artificially altered SG specimens with a deformation rate of 100 mm/min at a temperature of 23 +/- 2 °C according to [Bucak & Meißner 2005]**

These graphs demonstrate that, although the test procedure is precisely laid down in standards, the results yield non-negligible differences. While e.g. the PVB specimens in the first graph results in a total strain of about 240 % and an according maximal stress of 21 N/mm<sup>2</sup> with a deformation rate of 100 mm/min (1,66 mm/sec) at 22 °C, the failure stress is about 15 % lower in Fig. III.2. This indicates that not all PVB interlayers behave with the same characteristics and consequently, the results must always be handled with care.

The graphs in Fig. III.1 for instance also emphasize the important influence of time and temperature on this kind of visco-elastic polymer materials. Not only does the maximal stress and deformation alter in function of the test procedure; also the shape of the curves changes significantly. Where the tests on PVB specimen at low

temperatures develop an outline comparable to the results of SG samples at ambient temperature, the tests at higher temperatures do not exhibit any linear-elastic behaviour at small deformations. This may be explained by the test temperature: if the latter is below the glass transition temperature  $T_g$ , the tests will usually yield a linear elastic results at the beginning of the experiment. However, the results presented in Fig. III.3, demonstrate that this is not exclusively caused by the test temperature but also by the deformation rate.

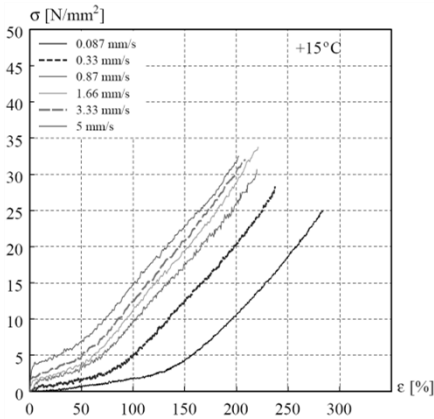


**Figure III.3: Average stress deformation curves for series of four not artificially aged PVB specimens with six different deformation rates at a temperature of 15 °C [Kott & Vogel 2006]**

It must be emphasised that the plastic behaviour of SG in Fig. III.2 starts at relatively large deformations. Generally, the deformations of interlayer materials in pre-failure state of the laminated element, remain small enough to avoid plastic behaviour. Consequently, the large strain visco-elasto-plastic deformations of interlayers become important only near cracks in a post-failure state [Delincé et al. 2010].

Based on dynamic mechanical analysis (DMA) measurements following ISO 6721 or ASTM D4065, the visco-elastic properties of an interlayer material can be measured. Dynamic deformations with varying frequencies are enforced to small samples of the interlayer material at different temperature levels. Dependent on the chosen part of the standard, torsion, bending or shear experiments are performed. The principles of a dynamic shear test are presented in Fig. III.4. Fig. III.5 depicts the dynamically determined stiffness comparison between PVB and SG as a function of temperature, provided by DuPont [Bennison et al. 2008].

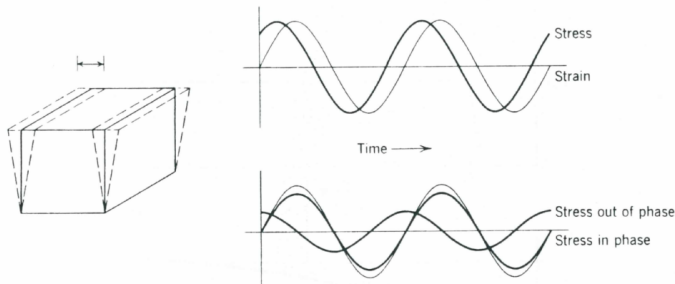


**Figure III.4: Principle of dynamic test with enforced sinusoidally varying shear [Ferry 1980]**

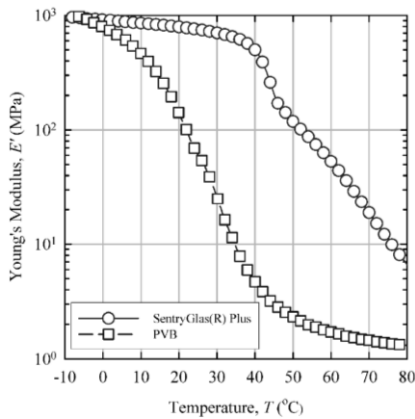


**Figure III.5: Comparison of the Young's modulus  $E'$  of PVB and SG as a function of temperature. The load duration has not been specified [Bennison et al. 2008]**

This kind of dynamic experiments, performed with many frequencies of the oscillations at many different temperatures, are often used by producers of interlayer materials to build up the visco-elastic material models presented in Fig. II.6 [D'Haene & Savineau 2007], [Van Duser et al. 1999], [Bennison et al. 2008]. The main advantage of these tests is that a relatively complete predictive model for static loading can be provided in a fast and relatively easy way.

Unfortunately, a comparison of test results obtained by uniaxial tensile tests according to ISO 527 point out that with small scale experiments, very different outcomes may be expected. This is possibly caused by the delicate preparation of small samples of interlayer material with minor geometry imperfections, humidity levels, shape effects, etc.

## 1.2 Intermediate scale

In order to incorporate the possible effects of the lamination cycle and to investigate the actual stiffness of the interlayer material between the glass layers, often small samples are extracted from laminated elements. These experiments are generally not based on existing standards, but are specifically developed to investigate specific characteristic mechanical properties of laminated glass.

One of such tests is the compression shear test (CST, see Fig. III.6) which was designed to measure the adhesion strength between the interlayer material and the glass surface. In the experiments, small laminated samples are loaded in compression and shear at a specific angle to the loading direction (45°). This method was many times applied and adjusted in literature [Jagota et al. 2000], [Parmentier et al. 2007], [Froli & Lani 2010], [Trosifol 2011].

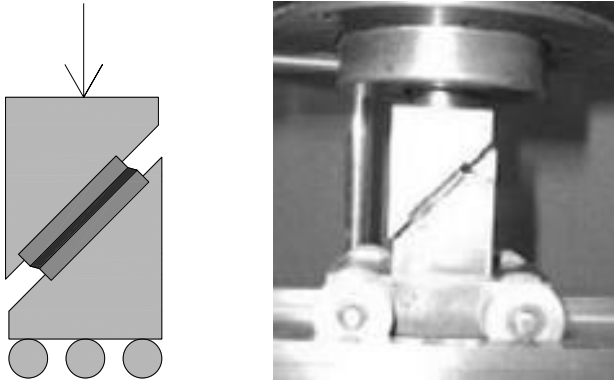


**Figure III.6: Compressive shear test [Trosifol 2011]**

Sobek et al. used a variant on this test method to define the viscoelastic mechanical properties of PVB [Sobek et al. 1999]. Fig. III.7 depicts the basic test principle and a visualisation of the simplified material model deduced from the experimental results. Similar tests were performed at the Belgian Building Research Institute on both PVB and SGP2000 samples. The results, presented in Fig. III.8 demonstrate that SGP2000 not only behaves stiffer than PVB but yields also a higher adhesion strength, although multiple samples already delaminated entirely during the water-cooled drilling of the test specimen out of laminated plates [Parmentier et al. 2007]. This extraction method of the test samples might also be an explanation for the higher dispersion of the results.

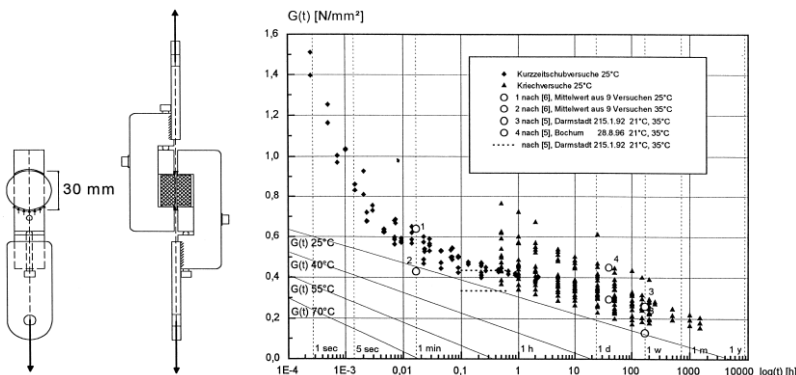


**Figure III.7: Tensile shear test [Sobek et al. 1999]**

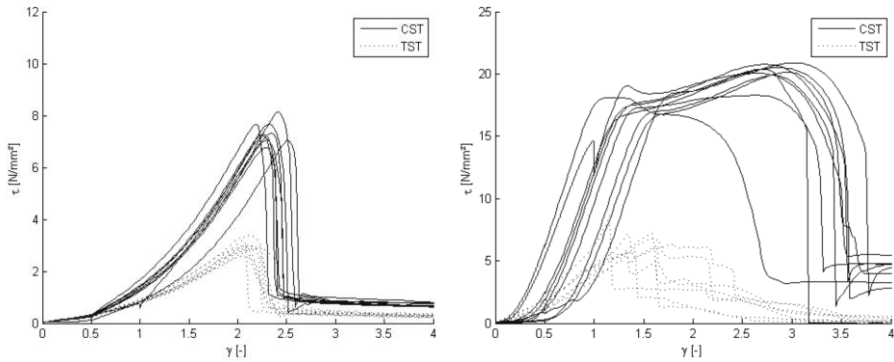


**Figure III.8: Shear stress in function of shear deformation angle during compression shear tests at an angle of 45° (CST) and tensile shear tests (TST): laminated samples with PVB (left); laminated samples with SG (right) [Parmentier et al. 2007]**

A second example of an intermediate scale test is the tensile shear test, which was also adapted by Schuler, who avoided the possibility of a high humidity influence by dry cutting rectangular specimens out of laminated beams [Schuler 2003]. By further applying one crack in both glass layers according to Fig. III.9 a well defined area is subjected to shear during testing. In 2005, similar tests were executed on new and artificially aged laminated specimen with both PVB and SG interlayers [Bucak & Meißner 2005]. The results, summarised in Table III.1, indicate the sensitivity of the interlayer stiffness to UV and humidity aging.

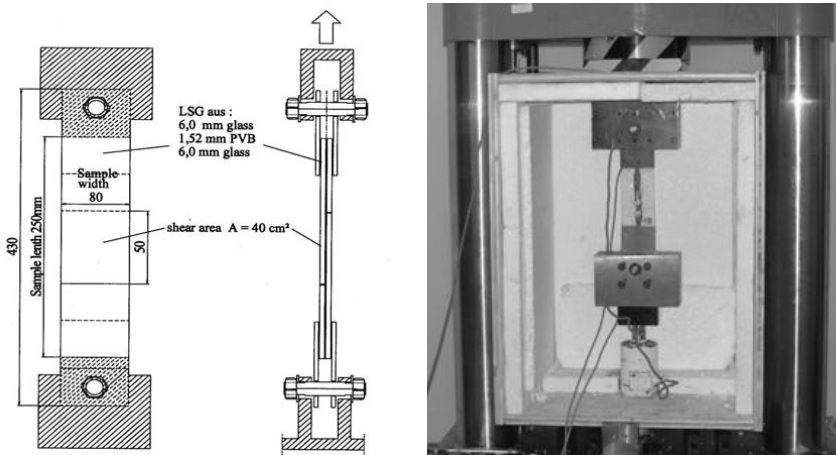


**Figure III.9: Shear tests [Schuler 2003]**

**Table III.1: Shear modulus after a load duration of 5 sec on small new and artificially aged laminated samples with PVB and SG interlayer [Meißner & Sackmann 2006]**

sample	20 °C	40°C	60°C
SG (new)	74.7 N/mm <sup>2</sup>	19.2 N/mm <sup>2</sup>	19.9 N/mm <sup>2</sup>
SG (UV ageing)	48.7 N/mm <sup>2</sup>	39.6 N/mm <sup>2</sup>	21.6 N/mm <sup>2</sup>
SG (humidity aging)	43.5 N/mm <sup>2</sup>	21.0 N/mm <sup>2</sup>	14.3 N/mm <sup>2</sup>
PVB (new)	2.5 N/mm <sup>2</sup>	0.4 N/mm <sup>2</sup>	0.2 N/mm <sup>2</sup>
PVB (UV aged)	2.3 N/mm <sup>2</sup>	0.4 N/mm <sup>2</sup>	0.4 N/mm <sup>2</sup>
PVB (humidity aged)	0.9 N/mm <sup>2</sup>	0.3 N/mm <sup>2</sup>	0.2 N/mm <sup>2</sup>

The effect of high moisture at an elevated temperature level on the shear strength of small glass to metal bonded samples was also investigated in [Belis et al. 2011]. The most striking result of the tests on the SG samples was the important influence of the overlap length of the test samples. While the strength of the samples with an overlap zone measuring 10 mm x 25 mm significantly reduced by increasing the moisture exposure, this was not noticed for the 25 mm x 25 mm overlap zones. This emphasises the importance of the sample size on the usefulness of test results.

Generally, the main advantage of this kind of intermediate scale testing compared to full scale testing is the ease to produce a large amount of laminated samples. Unfortunately, because of their small size, there might appear important edge effects due to the high edge-surface ratio which can barely be taken into account for the analysis of the results. Also imprecise handling or limited imperfections might lead to unforeseen inaccuracies. Therefore, the representativeness of the smaller samples compared to the mechanical behaviour of full-size laminated elements in structural applications might become questionable.

### 1.3 Full scale

The third and final category contains experiments on samples with a scale comparable to typical laminated glass elements used in building practice. However, no standards exist to investigate the visco-elastic behaviour of the interlayer material. Therefore, most existing full scale experiments are derivatives from standardised tests to investigate the strength of glass in which always a certain region has to be subjected to a constant bending moment. E.g. the coaxial double ring test [NBN EN 1288-2] or the four point bending tests [NBN EN 1288-3] are the most applied [Schuler 2003], [Bucak & Meißner 2005], [Parmentier et al. 2007], [Bricolli Bati et al. 2010].

Fig. III.10 depicts the dimensions of the standardised four point bending experiment and an exemplary test. In Fig. III.11, the results of this kind of experiments on both PVB and SG laminated plates is represented as a bending stiffness factor which represents the ratio of the experimentally measured bending stiffness to the bending stiffness of a monolithic glass plate with similar nominal thickness.

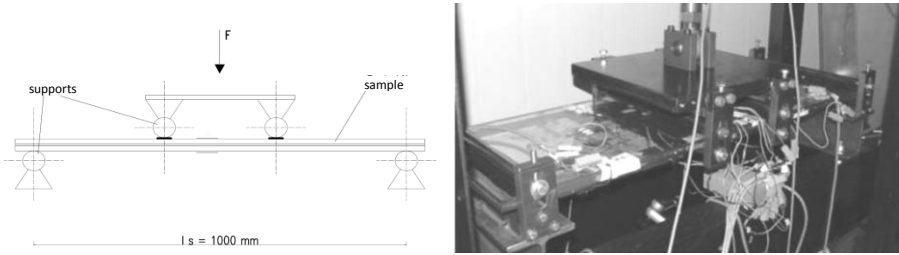


**Figure III.10: Four point bending test according to ISO 1288-3 [Bucak et al. 2006]**

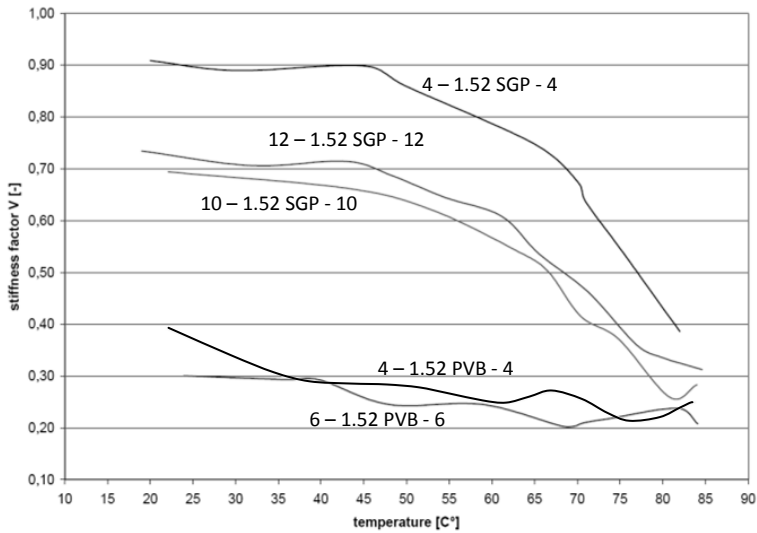


**Figure III.11: Bending stiffness factor of PVB and SG laminated samples [Meißner & Sackmann 2006]**

In 2005, Kasper took the dimensions of this standardised four point bending test as a starting point for the investigation of the torsional stiffness of glass/PVB laminates [Kasper 2005]. Fig. III.12 depicts the derived test setup in which one side of the laminates sample is clamped to a fixed support, while the other side is clamped in a support which can rotate. With these tests, the influence of the interlayer stiffness on the lateral torsional buckling of laminated beams was investigated. Based on the experimental torsional stiffness, also the visco-elastic shear modulus of the PVB interlayer was calculated for a load duration of up to 1000 seconds.



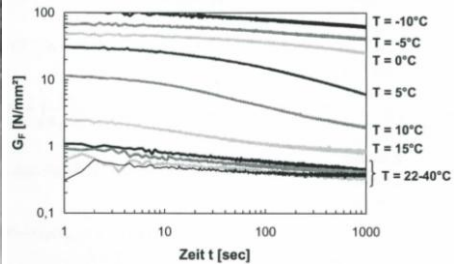


Figure III.12: Torsion test setup and results of glass/PVB laminates by Kasper [Kasper 2005]

## 2 Experimental test programme

Building further on the existing experimental research, a complementary test programme was first selected. In a second step, two possible temperature control methods were evaluated.

### 2.1 Combination of experimental test series

To incorporate the influence of the lamination process on the characteristic properties of the interlayer material, tests on laminated specimens are preferred rather than tests on pure interlayer samples. This way, the interlayer material is also encapsulated by glass sheets so the processed material is almost entirely cut off from humidity influences which can importantly alter the material stiffness.

Because the main goal of the research is not only to define the material properties of SG, but also to increase the insight in the structural behaviour of real components, the choice was made to perform tests on specimens with realistic building dimensions. This way, possible edge effects are not scaled up to improbable proportions, but remain in proportion to reality.

Furthermore, the intention was to cover the variety of realistic loading conditions of structural glass with a complementary test programme with different loading conditions. Based on common building practice, it seems obvious that bending over the weak axis has to be investigated. However, contrary to the existing research, in which bending tests are generally a direct copy from the four-point bending tests of [NBN EN 1288-3], three-point bending experiments on 3000 mm long plates were chosen. The first reason to deviate from common practice is the technically higher complexity of the loading system of four-point bending compared to three-point bending. When the glass strength is investigated, it is important that a certain area is subjected to uniform stresses, due to the statistically complexity of this property, but this unnecessarily complicates a stiffness investigation. Additionally, the increase of the length of the specimen, originated from the research history of our laboratory at UGent, at which the

lateral torsional buckling of laminated beams was already investigated by buckling tests on 3000 mm long beams [Belis 2005]. The remaining unbroken test samples of this previous research were directly available to perform some preliminary bending test series. Furthermore, it seems highly interesting to verify whether the overall bending behaviour of the large samples matches the bending stiffness results on 1100 mm long glass/SG specimen available in literature.

Complementary, torsion tests have been executed. In general, only little knowledge exists about the torsional stiffness of laminated glass and especially of laminated glass with a stiff interlayer.

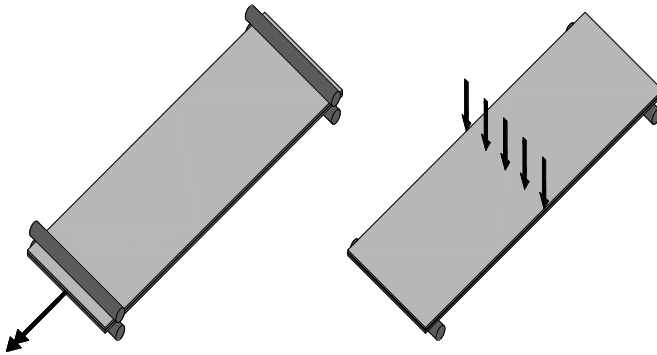


**Figure III.13: Basic principle of the experimental test setup: torsion setup (left); bending setup (right)**

The results from the aforementioned tests can be used to explore more realistic situations. Consider for example a beam loaded in bending. On the one hand, it is well known that the stiffness of a laminated beam that is subjected to bending about the strong axis, depends mainly on the elastic bending stiffness of the individual glass sheets. However, on the other hand, the lateral torsional buckling load should be determined by taking into account the visco-elastic bending and torsional behaviour of the laminate [Belis 2005].

## **2.2 Temperature control**

Because the stiffness of the interlayer is known to be extremely dependent on its temperature, the environment must be well-controlled and stable during the entire duration of the experiments. Already in 1955, William et al. described how the influence of the temperature on this kind of polymer visco-elastic material can be taken into account [Williams et al. 1955]. With a so-called Williams-Landel-Ferry (WLF) equation, an equivalent load duration can be calculated for different temperatures. With this kind of time-shift functions, it is possible to predict the long-term behaviour of the material at room temperature by conducting test series at elevated temperature.

First, a technique with IR-heaters as depicted in Fig. III.14 (left) was examined. The latter enabled to heat up the entire surface of the tested element. Therefore, this seemed an ideal solution to develop a test procedure which could easily be reproduced elsewhere. It is a flexible heat-control method which makes it also suitable for custom-made large test setups. For safety reasons, this heating method could be used only under constant supervision, so load durations were limited to about 10 hours.



**Figure III.14: Bending experiment with IR-heaters (left); chamber with temperature and humidity controlled environment (right)**

Additionally, a climatic chamber has been built in order to be able to perform experiments also below room temperature and with longer load durations. The room internally measures 3.9 m by 3 m and is 2.4 m high, so it can easily contain the entire bending and torsion setup (Fig. III.14 right). Inside, the temperature can be regulated between 5 °C and 65 °C and the relative humidity between 30 % and 70 %.

### **3 Preliminary experiments**

Prior to the core experimental programme of this research, three series of preliminary exploratory tests on a relative small number of samples have been performed to investigate potential test setups and methods. Firstly, three-point bending experiments on 3 m long samples were performed, using the IR heaters to raise and control the temperature level [Vander Beken 2006], [Depaepe 2008].

Under the controlled environment inside the climatic chamber, two additional series of preliminary experiments were carried out in order to fine-tune the experimental procedures [De Vogel 2008], [Depaepe 2008], [Callewaert et al. 2008]. Based on these preliminary results, the main test programme was composed.

### 3.1 Bending experiments with IR-heating

#### 3.1.1 Materials & methods

For the preliminary bending experiments, eight 3 m long and 150 mm or 200 mm wide specimen with the composition 2x 6 mm glass and 1.52 mm SGP2000 were available. To increase the experimental temperature level, longitudinal IR heaters were chosen to heat up these samples. In detail, a combination of two 500 Watt and one 1500 Watt *Comfortinfra* heaters from *Frico* were used.

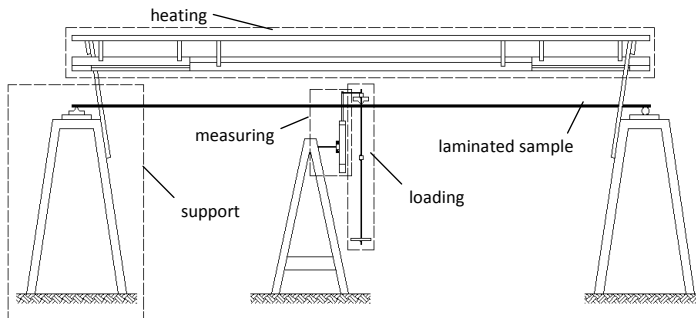


**Figure III.15: Experimental test setup for preliminary bending experiments with IR-heaters [Vander Beken 2006]**

At the beginning of the experiment, the sample was laid on two supports with a span of 2950 mm and the element was heated up to 55 °C, which took about 20 minutes. Subsequently, the heaters were dimmed to obtain a rather constant temperature level. When the latter was achieved, a line load was applied in the centre of the plate and the creep deformations were measured continuously during several hours. Also the temperature at the top and the bottom of the laminated element was registered with two thermocouples.

#### 3.1.2 Results

A typical result is presented in Fig. III.16. During the first 400 seconds, an increasing upwards deformation is noticeable, which can be attributed to the raising temperature difference between the upper and the lower glass plate. For the next 800 sec, this thermal difference and the corresponding deformation remain almost constant, while this diminishes again after the heaters are dimmed.

After about 1600 sec in total, the temperature level was stabilised and the central load was applied. Then, the creep deformations were noticeable for 2000 sec after which the heaters were turned of. The latter led to an increase of the deformations due to a decrease of the thermal differences inside the element. Finally, the load was removed from the specimen.

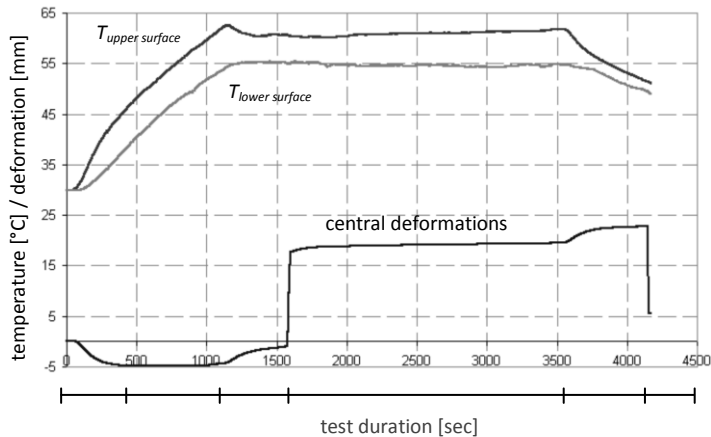


**Figure III.16: Measured temperature and deformations during a bending experiment with IR-heaters on 3 m long and 150 mm wide laminated elements with a central load of 70 N [Belis et al. 2007]**

### 3.1.3 Discussion

Using the described heating method, Vander Beken also performed lateral torsional buckling tests on laminated beams at elevated temperatures [Vander Beken 2006]. Similar 3 m long specimens were heated in a much larger test setup used by Belis [Belis 2005], which demonstrated the flexibility of the IR-heaters.

Unfortunately, during the first bending tests also multiple drawbacks of the heating system were detected. The main difficulties were 1) the impossibility of two-sided heating of the element due to the presence of the loading and measuring devices which caused a temperature difference between the two glass plates and thus also a thermal deflection of the tested element, 2) to keep a uniform temperature over the entire specimen, 3) the impossibility to directly measure the temperature of the interlayer, 4) the complexity of regulating the electric capacity of the heaters for a longer period and 5) the uncertainty about the potential influence of the intense IR-radiation on the material quality of the interlayer.

Depaepe further investigated different IR configurations to optimise the uniformity of the temperature over the specimen [Depaepe 2008], but eventually, this heating method was not found accurately enough. Consequently, all further experiments were executed in the climatic chamber.

## 3.2 Torsion tests in climatic chamber

### 3.2.1 Materials & methods

In the torsion test setup illustrated in Fig. III.17, laminated plates of 100 mm x 1100 mm with 2x 4 mm fully toughened glass and a 1.52 mm thick SGP2000 interlayer were used, and tests were executed at 5, 20, 35, 50 and 65 °C. These samples were mounted in the test setup by fixing them between round bearings, positioned at a

distance of 1080 mm from each other. The samples were subjected to a torque as shown in Fig. III.13 (left).

The preliminary torsion experiments were all carried out on laminated glass plates, with the outdated SG variant SGP2000, that were available from previous research at the laboratory. Because the test history and the preservation circumstances are unknown, the results are only illustrative.

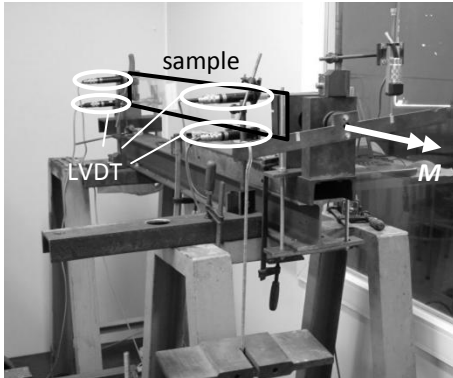


**Figure III.17: Preliminary torsion creep test setup**

A quasi-constant torque was applied to the sample by applying a weight on a lever arm. During the experiments, the creep deformations were measured with four linear variable differential transducers (LVDT's) on the glass surface (indicated with ellipses, Fig. III.17). The torsional deformation was deduced from these four measurements for which the locations were pre-determined. The measured overall thickness of the specimen, their test temperature and the accompanying load duration are summarised in Table III.2. Furthermore, all tests were also non-destructive.

**Table III.2: Details of the preliminary torsion experiments tested in the climatic chamber.  
All specimen measured 1100 mm x 100 mm**

Temperature [°C]	Overall thickness [mm]	Load duration [h]
5	9.33	16
20	9.33	18
20	9.35	27
35	9.35	26
50	9.35	20
65	9.35	18

### 3.2.2 Results

Fig. III.18 summarizes the results of the six torsion tests, realised at five different temperatures between 5 °C and 65 °C as indicated in Table III.2. The proportional torsional stiffness  $G I_t$  is calculated with Eq. (III.1). The 100 % value therefore corresponds to the torsional stiffness of a monolithic glass plate with a thickness equal to the measured overall thickness of the laminated test specimen  $t_{total}$ .

$$GI_t = \frac{GI_{t,exp}}{GI_{t,upper}} \quad (III.1)$$

$$GI_{t,exp} = \frac{M_{exp}L_{span}}{\theta_{exp}} \quad (III.2)$$

$$GI_{t,upper} = G_{glass} \frac{Wt_{total}^3}{3} \quad (III.3)$$

The torque  $M_{exp}$  and the angle of twist  $\theta_{exp}$  were measured during the experiments.  $L_{span}$  is the distance between the supports,  $W$  is the width of the laminated element and  $G_{glass}$  is the shear modulus of glass. The results are presented this way, in order to omit the test specific influences, e.g. the actual sample thickness or the length of the lever arm which slightly changes in function of the torsional deformation of the test sample. From these graphs, it is rapidly apparent whether the laminate behaves close to the upper limit (100 %) or to the lower one (about 18 % for this sample composition).

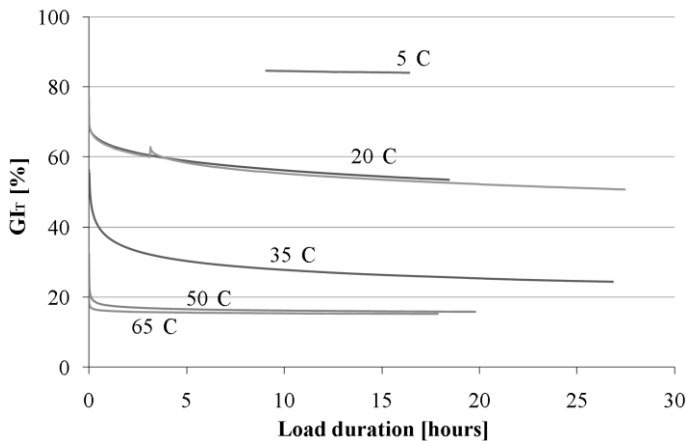


Figure III.18: Experimental proportional torsional stiffness at five different temperatures

### 3.3 Bending tests in climatic chamber

#### 3.3.1 Materials & methods

For these preliminary three-point bending tests, three of the laminated glass specimens of the first preliminary test series with the IR-heaters were reused supplemented by two additional 300 mm wide laminated samples with an unknown history. All 3 m long samples had a section of 2x 6 mm glass with 1.52 mm SGP2000 interlayer and while the glass panes of the 150 mm wide samples were heat-strengthened, the other samples were composed with fully tempered glass panes.

The bending experiments were performed similarly to the first preliminary experiments described in § III.3.1.1: the test specimens were simply laid down on two well positioned linear supports spanning 2950 mm and a line load was introduced in the middle of the span by means of a gravity loading system and weights of a known magnitude. As shown in Fig. III.19, a LVDT measured the creep deflections of the upper side of the laminate in the middle of the span. The characteristics of this series of preliminary bending tests are presented in Table III.3. Firstly, bending experiments at 20 °C were executed on the five specimens, and afterwards the same specimens were tested at 65 °C. This temperature level was controlled during the entire experiment and additionally all specimens were conditioned for at least 12 hours prior to testing.

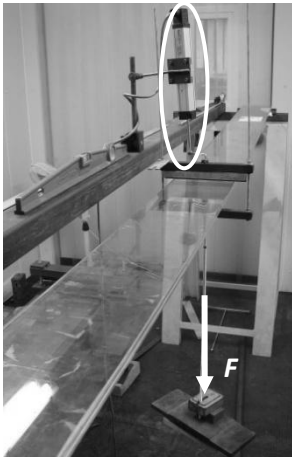


**Figure III.19: Preliminary three-point bending test setup**

**Table III.3: Details of the preliminary three-point bending experiments performed in the climatic chamber. All specimens were 3000 mm long, 2x 6 mm glass with 1.52 mm SGP2000**

Width [mm]	Overall thickness [mm]	Load duration at 20 °C [h]	Load duration at 65 °C [h]
150	13.38	17	28
150	13.33	5	139
200	13.24	21	14
300	13.45	28	27
300	13.48	70	117

### 3.3.2 Results

Fig. III.20 depicts the processed results of the five three-point bending tests executed at 20 °C and of the bending tests with the same specimens at 65 °C. The results are again only illustrative, because the total test history and the preservation circumstances of the samples are unknown.



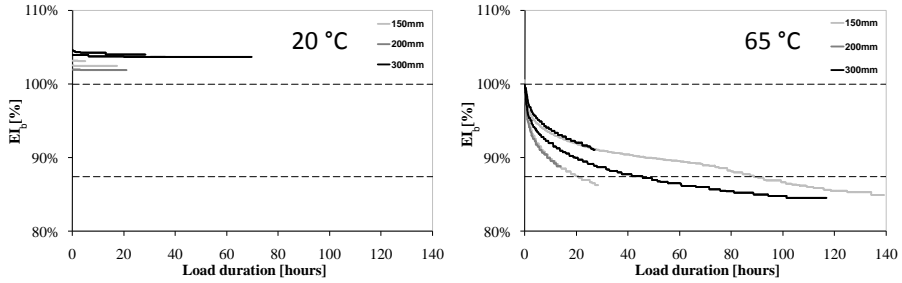


**Figure III.20: Experimental proportional bending stiffness: at 20 °C (left); at 65 °C (right)**

The experimental proportional bending stiffness  $EI_b$  is calculated according Eq. (III.4). Here, the 100 % value represents the calculated bending stiffness of a monolithic glass plate with a thickness equal to the overall thickness of the test specimens  $t_{total}$ .

$$EI_b = \frac{EI_{b,exp}}{EI_{b,upper}} \quad (III.4)$$

$$EI_{b,exp} = \frac{F_{exp}L_{span}^3}{48w} \quad (III.5)$$

$$EI_{b,upper} = E_{glass} \frac{Wt_{total}^3}{12} \quad (III.6)$$

In Eqs. (III.5) and (III.6), the load in the centre of the element is represented with  $F_{exp}$ ,  $w$  is the deflection in the middle and  $L_{span}$  is the distance between the supports. The Young's modulus of Glass is  $E_{glass}$  and the width of the sample is  $W$ .

The first important observation is that the bending stiffness at 20 °C exceeds this 100 % value. A plausible explanation could be that the assumed Young's modulus of 70 000 N/mm<sup>2</sup> for glass, as included in EN 572, is lower than the actual glass stiffness of these test specimens. In DIN 1249, a possible Young's modulus for glass of 70 000 to 73 000 N/mm<sup>2</sup> is noted. With the latter value, all results would drop below 100 %. After this was noticed, the Young's modulus of glass was determined experimentally with short term bending tests. The value of  $E_{glass} = 73$  GPa and  $G_{glass} = 30$  GPa was found to be accurate. Accordingly, this value was further used in the analysis of the experiments.

At 65 °C, a more pronounced decrease of the bending stiffness was noticed. Immediately after positioning the test specimen, the plate started to creep. Even after a loading period of more than five days, this creep was not yet finished. The tests prove that the influence of the decreasing shear modulus has a larger impact on the torsion stiffness  $GJ_T$  for this particular configuration than on the tested

bending stiffness. Between 20 °C and 35 °C, the decrease of the torsional stiffness is most significant (see Fig. III.18), while the difference between the tests at 50 °C and 65 °C is almost negligible. At these high temperatures, the torsion stiffness of the laminated glass specimens is barely higher than the torsion stiffness of the two individual glass sheets together. For identical load duration and temperature, the bending stiffness still remains above 80 % of the upper limit (see Fig. III.20).

### 3.4 Discussion and conclusions

While the bending stiffness did not yet lose 20 % of its proportional bending stiffness after testing for multiple days at 65 °C, the difference between the torsion stiffness of the laminated test specimens above 50 °C and the torsion stiffness of the same un laminated glass sheets is already negligible. This corresponds to earlier observations that the increased global stiffness, due to the use of SG instead of PVB, is less pronounced for lateral torsional buckling than it is for weak axis bending conditions [Vander Beken 2006], [Belis et al. 2008].

When comparing the proportional bending stiffness of a laminated glass plate to similar results from literature on specimens with a smaller span, e.g. [Bucak & Meißner 2005], it seems that the proportional stiffness is largely influenced by the dimensions of the samples and the loading conditions. Therefore, the theoretical model developed by Scarpino [Scarpino et al. 2004] is used to compare the proportional torsional stiffness of the preliminary test samples with the one for 1100 mm long and 360 mm wide laminated samples as used by Kasper in [Kasper 2005]. In Fig. III.21, the results are plotted as a function of the varying shear modulus.

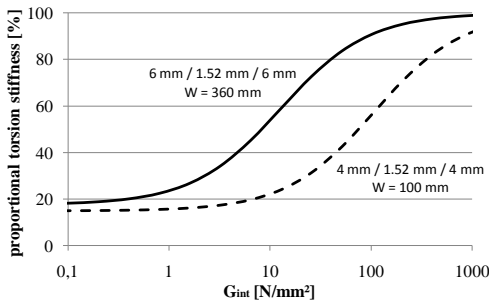


**Figure III.21: Scarpino’s proportional torsion stiffness as a function of the interlayer shear modulus**

This graph clearly indicates the influence of the width on the proportional torsion stiffness for equal shear modulus of the interlayer. When a laminated plate is subjected to a certain load duration at a specific temperature, then the proportional torsional stiffness shall increase when the width of the element becomes larger.

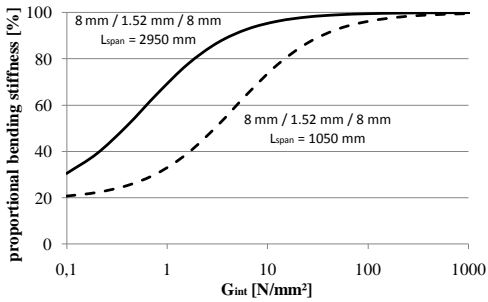


**Figure III.22: Wölfel's proportional bending stiffness as a function of the interlayer shear modulus**

When a similar calculation is made for the proportional bending stiffness with the theoretical model from Wölfel [Wölfel 1987], a similar influence of the span of the laminated element is noticed. Fig. III.22 depicts the calculated proportional bending stiffness for a laminated element spanning both 2950 mm and 1050 mm.

Additionally, the above mentioned analytical calculations clearly illustrate the importance of making the right decision about the test set-up and the selection of samples. The graphs in Figs. III.21 and III.22 indicate that some samples will yield barely any difference in some particular regions of the interlayer stiffness. Torsion tests on samples with a width of 100 mm almost reach the lower limit at an interlayer shear modulus of 2 N/mm<sup>2</sup>, while the proportional stiffness of an element with a width of 360 mm still can lower with about 10 %.

For this reason, it was decided to perform further torsion tests on laminated specimen with a width of 360 mm. For an analogous reason, it was also decided to carry out bending experiments on both 1100 mm long and 3000 mm long samples. According to Fig. III.22, the first will already exhibit a noticeable decrease of the bending stiffness at a interlayer shear modulus lower than 100 N/mm<sup>2</sup>, whereas the latter will only start to loose notable stiffness when the shear modulus drops below 10 N/mm<sup>2</sup>. This way, each experiment has a particular region in which the accuracy can be expected to be high as well as intervals where a change in the stiffness of the interlayer has almost no effect on the overall stiffness.

Therefore, a sensitivity analysis was performed for the three chosen test configurations. The influence of the glass thickness  $t_{glass}$ , the interlayer thickness  $t_{int}$ , the width  $W$ , the span  $L_{span}$ , the stiffness of glass  $E_{glass}/G_{glass}$  and the load  $P/M$  on the expected deformations is summarised in Appendix A. Because of the influence of the shear modulus on the sensitivity of a test method (see Figs. III.21 and III.22), this was calculated for three different values of the shear modulus of the interlayer, namely 1, 10 and 100 N/mm<sup>2</sup>. Additionally, the stiffness of the interlayer was recalculated with the modified results, similar to the analysis presented in § IV.1.3, to directly visualise the effect of a certain parameter. This indicates that e.g. the accuracy of the results form the bending test setups increase with a decreasing interlayer stiffness in this region, while the lowest deviations with the torsion test occur at 10 N/mm<sup>2</sup>.

## 4 Torsion

### 4.1 Samples

For these tests, twenty glass/SG and eight glass/PVB samples had been produced. In Table III.4, an overview of the main geometrical characteristics of all test samples is presented (only test series A and D are used for torsion tests). The actual specimen thickness was determined as accurately as possible, because 1) it is generally known that the effective dimensions of products differ from their nominal values and 2) the thickness is highly significant for the calculation of the torsion stiffness because it is raised to the third power. For this, the individual glass thickness  $t_{glass}$  of the test specimens was measured with a micrometer screw gauge prior to lamination and the total thickness  $t_{total}$  after lamination, prior to testing (see Appendix B). By doing so, no unfounded assumptions must be made based on the overall thickness of the laminate, which is the only thickness measurable after lamination without breaking the test specimen. The actual thickness of the interlayer  $t_{int}$  is then determined by subtracting the sum of the two average glass thicknesses from the mean total thickness for which an overview is provided in Table III.5. The following processing of the results will always take into account these effective dimensions.

**Table III.4: Nominal geometry of all test samples**

Test series	Number of samples	Type of glass	Length [mm]	W [mm]	$t_{glass}$ [mm]	$t_{int}$ [mm]
A	20	fully tempered	1100	360	2 x 6	1.52 (SG)
B	20	annealed	1100	180	2 x 8	1.52 (SG)
C	8	fully tempered	3000	360	2 x 8	1.52 (SG)
D	8	fully tempered	1100	360	2 x 6	1.52 (PVB)
E	20	annealed	1100	120	2 x 8	1.52 (SG)

**Table III.5: Average results of the measured actual geometry of the torsion test samples**

Test series	L [mm]	W [mm]	$t_{glass}$ [mm]	$t_{total}$ [mm]	$t_{int}$ [mm]
A	1100.14	360.78	5.91	13.40	1.59
D	1100.00	360.98	5.90	13.34	1.54

The first noticeable observation of the measurements is that the production process generally results, on the average, in a 0.07 mm larger thickness for the SG interlayer than the nominal value of 1.52 mm. Nevertheless, the thickness of the SG layer was also measured before the lamination and the nominal value was found to be accurate. This could indicate that the lamination process has a

significant effect on this interlayer material. A possible explanation can be found in the production process of the interlayer sheets. The basic ingredients are mixed and molten together after which the material is pulled and rolled in sheets with a fast cooling. The high temperatures during the lamination can trigger the thicker shape-memory of the polymer material.

In addition, it is worth mentioning that the individual glass thickness always varies between the nominal thickness and the minimum allowed thickness of 5.8 mm according to the European standard [NBN EN 572-2].

## 4.2 Experimental setup

Based on the experimental research reported by Kasper [Kasper 2005], a torsion test setup was built at Ghent University. Founded on the results of numerical simulations, some modifications of the test setup were implemented [Callewaert 2007], of which the most important are 1) the transposition of the rotation axis to the centre of the laminate, 2) the shape of the supports, and 3) the loading device.

In the setup, the test specimen was clamped between a fixed support and a rotating support. Both supports consisted of two round steel bars and small aluminium strips were placed between the supports and the laminated specimen to prevent direct contact. The load was introduced at the end of a cantilever arm which was linked to the rotating support. The position of the specimen and the most important dimensions are schematically shown in Fig. III.23.

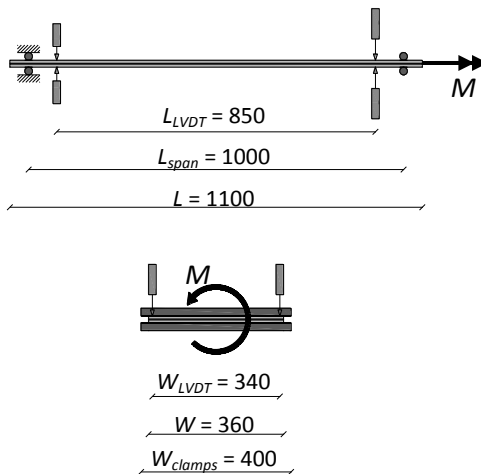


**Figure III.23: Schematic overview of torsion test setup. All dimensions are expressed in mm**

Both creep and relaxation experiments have been performed. In case of a creep test, as represented in Fig. III.24 left, the load was a fixed dead weight on the lever arm, causing a quasi constant torque. Only the small deviations in the length of the lever arm, due to the increasing torsional deformation during the experiment, caused a minor change in the torque during the test. For a relaxation test on the other hand (see Fig. III.24 right), a constant deformation was introduced with a

mechanical jackscrew. With this, a precise deformation could be enforced for a long period, in contrast to e.g. a hydraulic jack which would face a pressure loss over time. The force induced by the jackscrew was digitally measured with a load cell. To be able to calculate the effective torsion of the specimen, the vertical displacement was measured at four predetermined points on the top surface of the laminate.

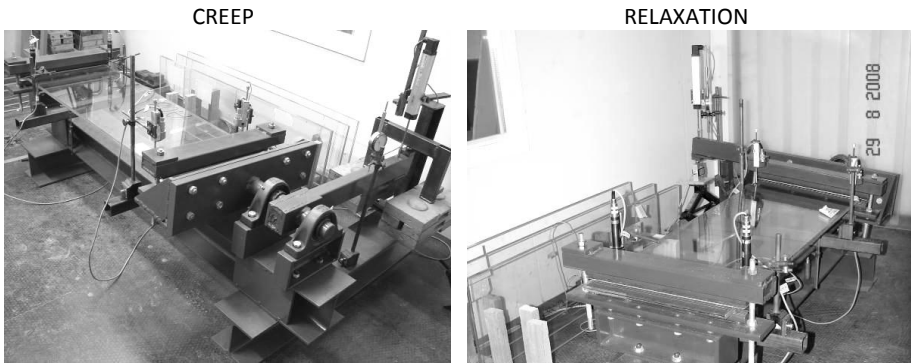


**Figure III.24: Refined torsion test setup: creep test (left); relaxation experiment (right)**

Furthermore, Fig. III.24 also depicts the storage of the torsion test specimens before testing. The glass/SG laminates are stored vertically to minimize the possible creep under self-weight. Also there is a space of about 5 cm between the specimens to optimize the temperature regulating air flow. Prior to testing, each specimen was always stored in the environmental conditions for at least 60 hours.

### 4.3 Experimental procedure

In a first testing cycle, all 20 test specimens of series A (glass/SG laminates) were subjected to a relaxation test. More specifically, four relaxation tests were executed at 5, 20, 35, 50 and 65 °C. For each test, a different specimen was carefully fixed in the test setup. Subsequently, a rather large torsional deformation of 6° was gradually enforced in a time span of about fifteen seconds. And finally, the relaxation of the specimen was continuously monitored for at least 48 hours by measuring the resulting torque at the applied constant deformation of the specimen.

In a second test cycle, the same twenty specimens were subsequently subjected to a torsion creep test. Taking into account the stiffness reduction at increased temperatures, different load levels have been applied at the five different temperatures. For the tests at 5 °C and 20 °C, a weight was applied on the cantilever, corresponding with a torque of about 360 Nm, depending on the slightly varying lever arm. At 35 °C the torque was reduced to about 300 Nm and above this temperature the applied torque was lowered to about 240 Nm in order to prevent excessive deformations. To avoid dynamic oscillation effects, this load was each time cautiously applied on the lever arm in about five seconds. Finally, for each test the creep deformation was measured during 24 hours.

In a third and fourth test cycle, the first sixteen glass/SG laminated samples were subjected to a 24 hours relaxation test similar to the first cycle. However, this time, the temperature interval between the different test series in the range between 5 °C and 65 °C was reduced from 15 °C to 5 °C. Finally, during a fifth and sixth test cycle, four glass/PVB samples were subjected to a relaxation torsion test at 5, 20 and 35 °C. In Table III.6 and Table III.7, an overview of the performed tests on each sample is recapitulated.

**Table III.6: Overview of torsion tests on glass/SG samples**

Samples	1 <sup>st</sup> cycle	2 <sup>nd</sup> cycle	3 <sup>rd</sup> cycle	4 <sup>th</sup> cycle
A01-A04	relaxation at 65 °C	creep at 5 °C	relaxation at 10 °C	relaxation at 40 °C
A05-A08	relaxation at 50 °C	creep at 20°C	relaxation at 15 °C	relaxation at 45 °C
A09-A12	relaxation at 5 °C	creep at 35 °C	relaxation at 25 °C	relaxation at 55 °C
A13-A16	relaxation at 20 °C	creep at 50 °C	relaxation at 30 °C	relaxation at 60 °C
A17-A20	relaxation at 35 °C	creep at 65 °C	n/a	n/a

**Table III.7: Overview of torsion tests on glass/PVB samples**

Samples	5 <sup>th</sup> cycle	6 <sup>th</sup> cycle
D01-D04	relaxation at 5 °C	relaxation at 20 °C
D05-D08	relaxation at 35 °C	n/a

## 4.4 Results

The calculated proportional stiffness of each group of four torsion tests are averaged and represented in the logarithmic graphs in Figs. III.25, III.26 and III.27, in which each line describes one test temperature.

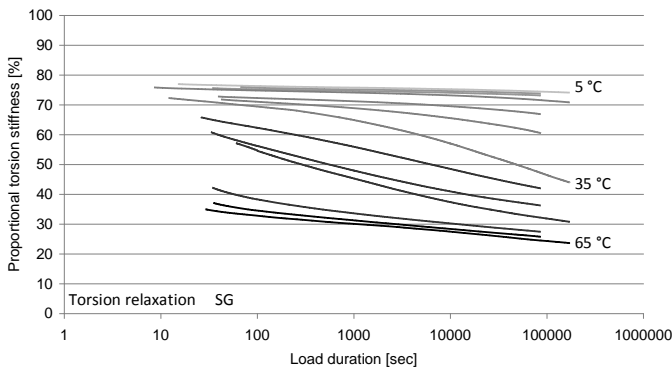


**Figure III.25: Proportional torsional stiffness during relaxation tests on glass/SG laminates of series A at 5, 10, 15, 20, 25, 30, 35, 40, 45, 50, 55, 60 and 65 °C**

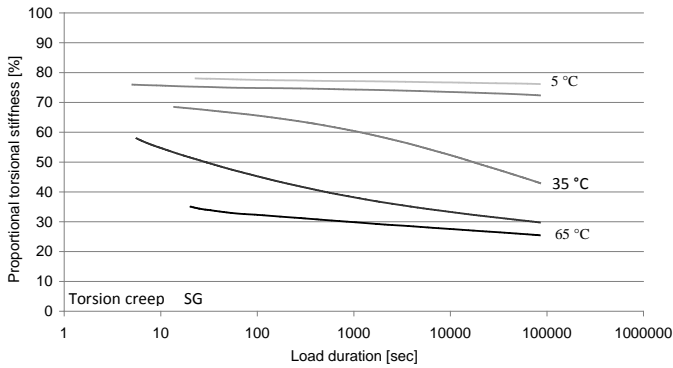


**Figure III.26: Proportional torsional stiffness during creep tests on glass/SG laminates of series A at 5, 20, 35, 50 and 65 °C**

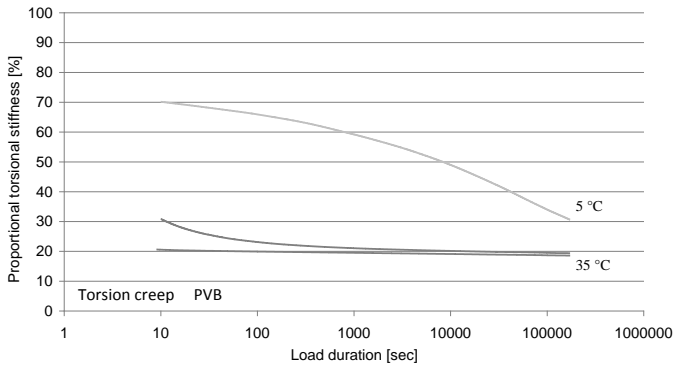


**Figure III.27: Proportional torsional stiffness during creep tests on glass/PVB laminates of series D at 5, 20 and 35 °C**

The results of the individual torsion experiments are given in detail in Appendix E, F and G.

## 5 Bending

### 5.1 Samples

Two different sample lengths have been used, because preliminary experiments indicated an important influence of the span on the proportional bending stiffness (see §III.3.4). Additionally, the tests on the specimens with the smallest span were performed on samples with two different widths (series B and E) to investigate whether a significant edge influence existed. The nominal dimensions of the sample series B, C and E for bending are reported in Table III.4. For these samples as well, all actual dimensions were determined as accurately as possible for the further processing of the results (see Table III.8). Again, a small increase of the



interlayer thickness due to the lamination was noticeable. The actual measurements are summarised in Appendix B.

**Table III.8: Average results for the measured actual geometry of the bending test samples**

Test series	$L$ [mm]	$W$ [mm]	$t_{glass}$ [mm]	$t_{total}$ [mm]	$t_{int}$ [mm]
B	1099.10	181.26	7.77	17.17	1.62
C	2999.94	360.33	7.77	17.14	1.60
E	1100.81	120.48	7.79	17.11	1.53

## 5.2 Experimental setup

For the bending experiments, one of the most simple loading conditions was chosen, namely three-point bending. However, during the preliminary tests, it was noticed that it is difficult to take into account the effect of the self weight off the specimen, which also leads to an increasing inaccuracy of the results. Therefore, an adapted bending test setup was designed with which it is possible to perform three-point bending tests about the weak axis with the specimen placed vertically for which the principle is represented in Fig. III.28. This way, the self-weight acted about the strong axis of the sample, not causing interfering deflections for the experiment. In Fig. III.29, the most significant sizes are represented.

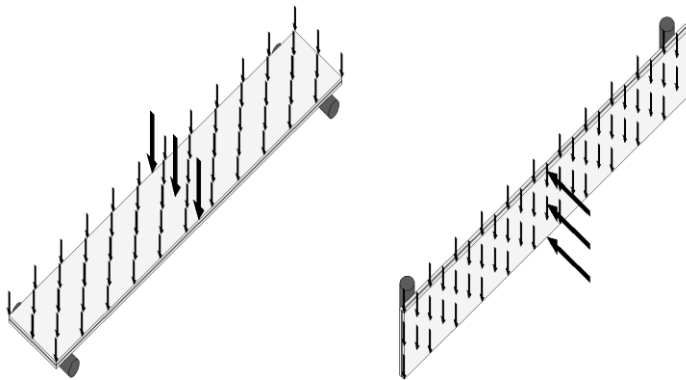


**Figure III.28: Self weight during three-point bending: acting about the weak axis of the laminate (left); acting about the strong axis of the laminate (right)**

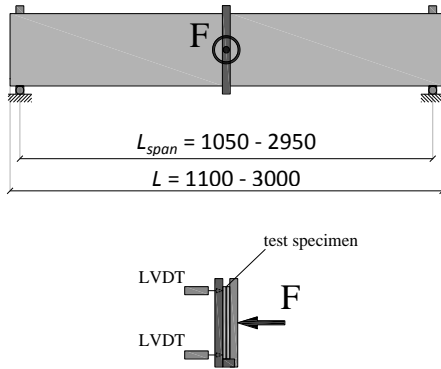


**Figure III.29: Schematic overview of bending test setup. All lengths are expressed in mm**



**Figure III.30: Bending test setup with specimen placed vertically: small creep experiment for test samples B and E with a span of 1050 mm (left); large relaxation experiment for test samples C with a span of 2950 mm (right)**

Fig. III.30 illustrates the small and large test setups on which the bending experiments have been executed. In order to carry out a creep test (Fig. III.30 left), a fixed dead weight was gently lowered so it could generate a line load in the middle of the test specimen. Because the samples were placed vertically, a specific loading system was developed to transfer the vertical load through a steel cable, over a pulley with a ball bearing to a horizontal line load on the test specimen.

In case of a relaxation test (Fig. III.30 right), a large amount of weights was lowered onto a bearing surface enforcing a constant predefined deformation to the test sample. During the relaxation of the laminate, an increasing amount of load was taken by the bearing system, while the relaxation tensile force on the steel cable was measured continuously with a load cell.

During all tests, the deformations were registered with two (small bending setup) or three (large bending setup) LVDT's mounted directly onto the back glass surface right behind the line load.

### 5.3 Procedure

Simultaneously with the first torsion test cycle, creep bending tests were executed on the samples B and the first four samples of series C at 5, 20, 35, 50 and 65 °C. The dead load on the small and large setup was 147 N and 392 N respectively.

*Table III.9: Overview of bending tests*

Samples	1 <sup>st</sup> cycle	2 <sup>nd</sup> cycle	3 <sup>rd</sup> cycle	4 <sup>th</sup> cycle
B01-B04	creep 65 °C	n/a	n/a	n/a
B05-B08	creep 5 °C	n/a	creep 10 °C	creep 40 °C
B09-B12	creep 20 °C	n/a	creep 15 °C	creep 45 °C
B13-B16	creep 35 °C	n/a	creep 25 °C	creep 55 °C
B17-B20	creep 50 °C	n/a	creep 30 °C	creep 60 °C
C01-C04	creep 5 °C	n/a	creep 10 °C	creep 40 °C
C01-C04	creep 20 °C	n/a	creep 15 °C	creep 45 °C
C01-C04	creep 35 °C	n/a	creep 25 °C	creep 55 °C
C01-C04	creep 50 °C	n/a	creep 30 °C	creep 60 °C
C01-C04	creep 65 °C	n/a	n/a	n/a
C05-C08	n/a	relaxation 5 °C	n/a	n/a
C05-C08	n/a	relaxation 20 °C	n/a	n/a
C05-C08	n/a	relaxation 35 °C	n/a	n/a
C05-C08	n/a	relaxation 50 °C	n/a	n/a
C05-C08	n/a	relaxation 65 °C	n/a	n/a
E01-E04	n/a	creep 5 °C	n/a	n/a
E05-E08	n/a	creep 35 °C	n/a	n/a
E09-E12	n/a	creep 20 °C	n/a	n/a
E13-E16	n/a	creep 50 °C	n/a	n/a
E17-E20	n/a	creep 65 °C	n/a	n/a

During the second cycle, similar creep tests were performed on the samples E with a load of 98 N (identical width/load ratio as series B), while the other four samples of series C were subjected to bending relaxation tests. Finally, also more bending creep series were performed on the last sixteen samples of series B and the first four samples of series C with a temperature interval of 5 °C parallel to the extra torsion tests. During the first cycle, the tests had a load duration of at least two days. For the other cycles, the tests lasted over 24 h.

### 5.4 Results

Similar to the results of the torsion tests, the bending test results are converted into graphs with the averaged proportional bending stiffness in function of the temperature.

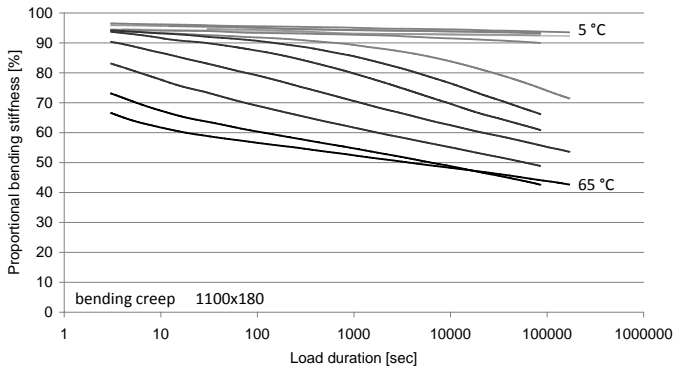


**Figure III.31: Proportional bending stiffness during creep tests on sample series B at 5, 10, 15, 20, 25, 30, 35, 40, 45, 50, 55, 60 and 65 °C**

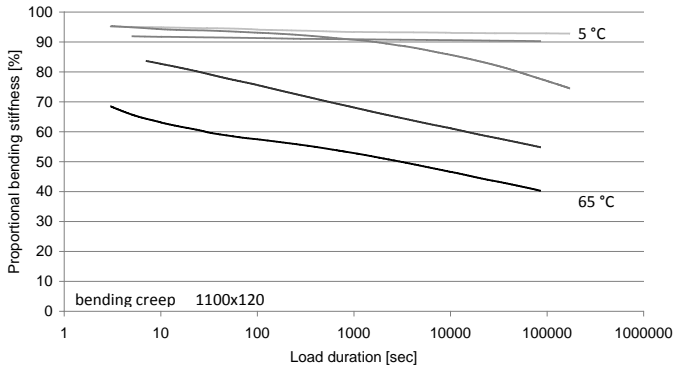


**Figure III.32: Proportional bending stiffness during creep tests on sample series E at 5, 20, 35, 50 and 65 °C**

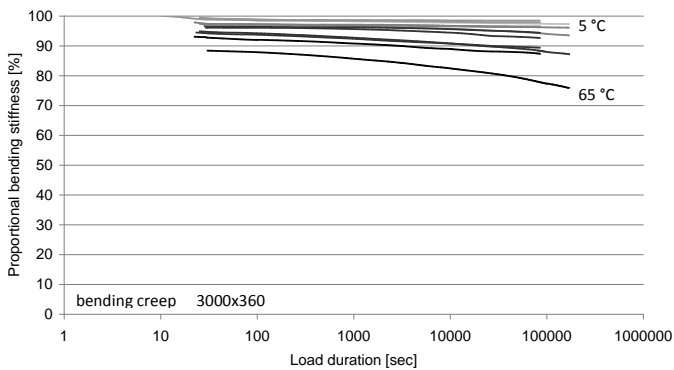


**Figure III.33: Proportional bending stiffness during creep tests on sample series C at 5, 10, 15, 20, 25, 30, 35, 40, 45, 50, 55, 60 and 65 °C**

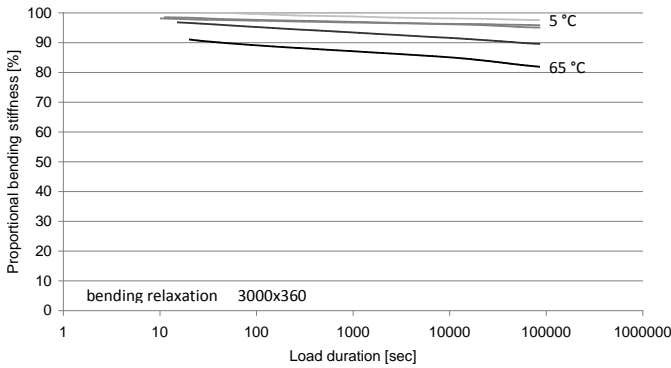


**Figure III.34: Proportional bending stiffness during relaxation tests on sample series C at 5, 20, 35, 50 and 65 °C**

The results of each individual experiment are gathered in Appendices H up to K.

## 6 Discussion

It is clear that the time and temperature dependent material properties of the visco-elastoplastic ionomer interlayer material extremely influence the overall mechanical behaviour of the laminate also before fracture of a glass plate. By increasing the temperature or the load duration, the stiffness of the interlayer decreases and the proportional stiffness of the laminate reduces significantly.

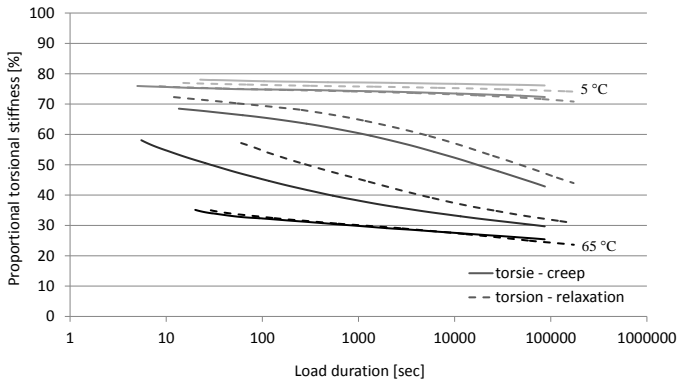


**Figure III.35: Proportional torsional stiffness during creep and relaxation tests on sample series A at 5, 20, 35, 50 and 65 °C**

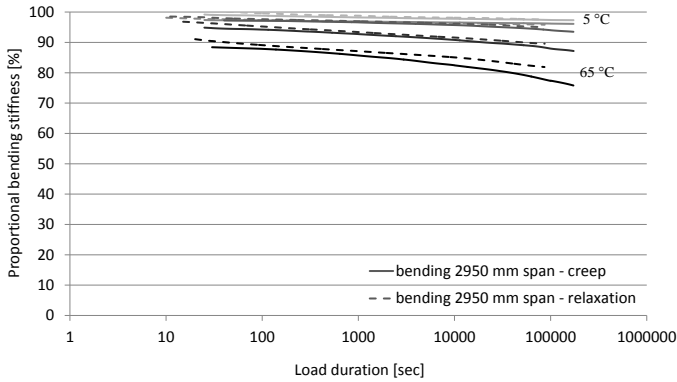


**Figure III.36: Proportional bending stiffness during creep and relaxation tests on sample series C at 5, 20, 35, 50 and 65 °C**

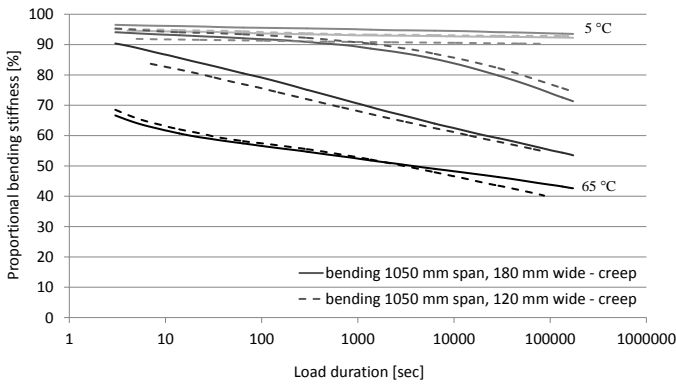


**Figure III.37: Proportional bending stiffness during creep tests on sample series B and E at 5, 20, 35, 50 and 65 °C**

When comparing the creep tests with the relaxation tests at the same temperature level as presented in Figs. III.35 and III.36, the results are almost identical, both for torsion and bending. Also for the bending creep tests on the samples of series B and E, illustrated in Fig. III.37, where only the width of the samples differ, the results yield no significant dissimilarity.

When, on the other hand, Figs. III.35, III.36 and III.37, representing the three different experimental setups (torsion, small bending and large bending), are compared with each other, a major influence of the load type (torsion versus bending) and the geometry (small bending versus large bending) becomes manifest. While the proportional torsion stiffness almost reaches the theoretically lowest possible limit at the end of the experiments (see Fig. III.35) with the highest tested temperature - comparable with the stiffness of two glass sheets with no shear transfer at all - the decrease is less pronounced for the proportional bending stiffness (see e.g. Fig. III.36).

Additionally, for the bending experiments, there is a major difference between the small and the large samples with identical temperature condition, load duration and composition of the laminate (compare Fig. III.36 with Fig. III.37).

From these experiments, it is clear that there exists no direct correlation between the mechanical properties of a visco-elastic interlayer - determined by the temperature and the load duration - and the overall proportional stiffness of the laminate. An increase of the span of a plate subjected to bending for instance, also increases the proportional stiffness.

Moreover, the difference in proportional torsion stiffness compared to the proportional bending stiffness proves that the loading condition of the laminate must always be taken into account.

These results are the basis for the subsequent analysis presented in chapter IV.





# Chapter IV: Analytical and numerical analysis

---

In this chapter, the experimental results are further processed. In the first section, the results are analysed by using analytical models. Firstly, the outcome of the experiments at different temperatures is shifted towards a reference temperature according to the time-shift equations proposed by Williams, Landel and Ferry [Williams et al. 1955]. Subsequently, the method of equivalent thickness, which is proposed in [prEN 13474-3] to be used for the calculation of the laminated glass stiffness, is used to evaluate the results of the bending experiments. Finally, all the proportional stiffness results are used to obtain the material properties of the interlayer materials, based on the theory of Scarpino [Scarpino 2002] and Wölfel [Wölfel 1987] for the torsion and bending experiments respectively.

In the second part of this chapter, the results are further investigated numerically. First, the developed finite element (FE) models are presented, and then also the shear modulus of the interlayer is recalculated based on the simulated torsion and bending stiffness. Finally, the analytical and numerical results are compared and validated by a comparison with the experimental outcome presented in chapter III.

## 1 Theoretical analysis

Analytical models are presented in literature to deal with the visco-elastic stiffness of an interlayer and to determine the structural performances of laminated materials. Already in 1955, Williams et al. developed a theory to describe the temperature dependence of the mechanical relaxation process of viscoelastic polymers [Williams et al. 1955]. With a single empirical function, the mechanical properties at a certain temperature can be time-shifted towards an other temperature level. This method is often successfully applied to describe the relation between the load duration and the temperature of visco-elastic interlayer materials around their glass transition temperature [Van Duser et al. 1999], [D'Haene & Savineau 2007] and [Bennison & Gizzi 2007]. An Arrhenius function could be used as an alternative, but temperature range in which the accuracy of this function is satisfactory is narrower than for the WLF-function [Scherer 1992]. Additionally, the Arrhenius equation is rarely used in small strain visco-elastic models for interlayer materials.

To calculate the stiffness of a laminated material, different analytical models were formulated for varying loading conditions. More specifically the structural performance of laminates can be well predicted for relatively simple loading situations, comparable to the ones in our experiments.

## 1.1 Williams-Landel-Ferry time-shift

The principle behind the WLF time-shift is that the stiffness of a polymer after a certain load duration at a particular temperature level is equal to the stiffness that corresponds with a shorter load duration at an elevated temperature level. For a linear viscoelastic polymer, the material properties can be represented by a single mastercurve at a reference temperature  $T_{ref}$ , which can be time-shifted to deduce the properties for an other temperature  $T$ . With the relaxation times  $\tau_{ref}$  at the reference temperature  $T_{ref}$  for a particular material, the relaxation times  $\tau$  at temperature  $T$  can be calculated with the shift factor  $a_T$  according to Eq. (IV.1).

$$a_T = \frac{\tau(T)}{\tau_{ref}(T_{ref})} \quad (IV.1)$$

Williams et al. proposed that the correlation between  $a_T$ ,  $T_{ref}$  and  $T$  can be represented by the mathematical equation Eq. (IV.2):

$$\log a_T = -\frac{C_1(T-T_{ref})}{C_2+(T-T_{ref})} \quad (IV.2)$$

Fig. IV.1 represents the principles of the time-temperature superposition of a thermorheologically simple material, which can be applied in the glass-rubber transition of polymer materials [Schwarzl 1990].

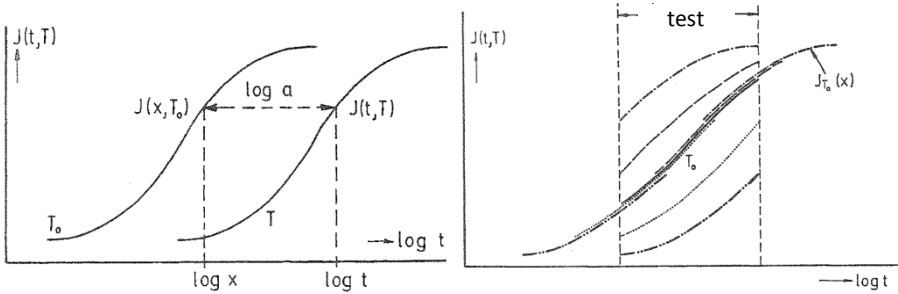


**Figure IV.1: Principle of time-temperature shift (left); Composition of a complete creep function from tests at different temperatures with a limited load duration (right) [Schwarzl 1990]**

With this time-shift principle, the results of the experiments at different temperatures can be shifted towards one reference temperature (see Fig. IV.1 right). Based on Eqs. (IV.1) and (IV.2) and the experimental results presented in chapter III, the time-shift constants  $C_1$  and  $C_2$  for SG were determined by equalling

the stiffness at the end of an experiment, i.e. for a well known load duration, to the stiffness at the beginning of the experiments at a higher temperature. Because of the limited number of tests on PVB test specimen performed for this research, the constants provided by Bennison et al. were applied for the shift of the torsion results of the tests on series D [Bennison et al. 1999]. With a reference temperature  $T_{ref}$  of 20 °C as proposed in working document WG8-N260 accompanying prEN 13474, the constants are summarised in Table IV.1 [WG8-N260E 2009].

Table IV.2 summarises the shift factors  $a_T$  for part of the tested temperatures. This provides a clearer image of the rather abstract time shift constants. The shift factor demonstrates e.g. that a test with a load duration of one hour at 50 °C correlates at 20 °C with a load duration of 134 000 hours, or more than 15 years.

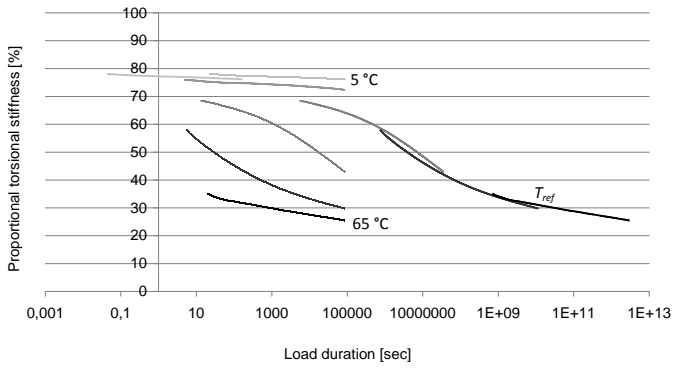
**Table IV.1: Time shift constants  $C_1$  and  $C_2$  for SG (deduced from the experimental results) and PVB (according to [Bennison et al. 1999])**

Interlayer material	$C_1$ [-]	$C_2$ [°C]
SG	135	760
PVB [Bennison et al. 1999]	20.7	91.1

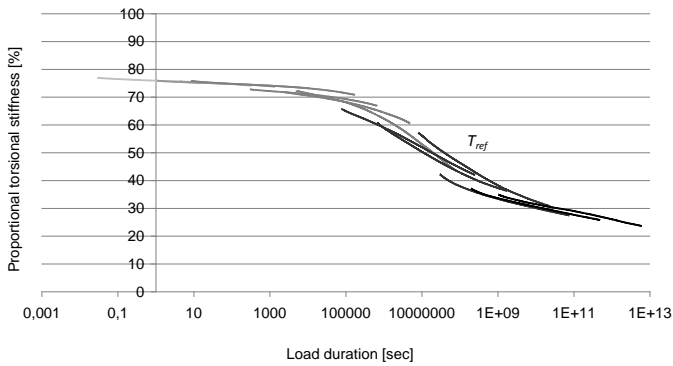
**Table IV.2: Shift factor  $a_T$  for SG (deduced from own experimental results) and PVB (following [Bennison et al. 1999])**

$T$ [°C]	$a_{T,SG}$ [-]	$a_{T,PVB}$ [-]
5	1.91E-03	8.31E-05
20	1.00E+00	1.00E+00
35	4.10E+02	8.44E+02
50	1.34E+05	1.34E+05
65	3.52E+07	6.99E+06

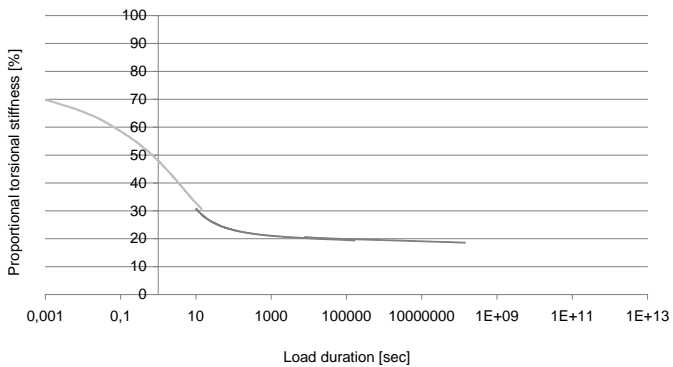
When applying these constants on the calculated proportional stiffness, the resulting curves are shifted horizontally in a graph with logarithmic time indication. This is presented in Figs. IV.2 and IV.3 for the torsion experiments on glass/SG laminates of series A and in Fig. IV.4 for the torsion creep experiments on glass/PVB laminates of series D. In Fig. IV.2, the unshifted curves are also drawn in order to visualise the actual meaning of the shifting.



**Figure IV.2: Unshifted and shifted proportional torsional stiffness during creep tests on glass/SG laminates (1100 mm x 360 mm)**



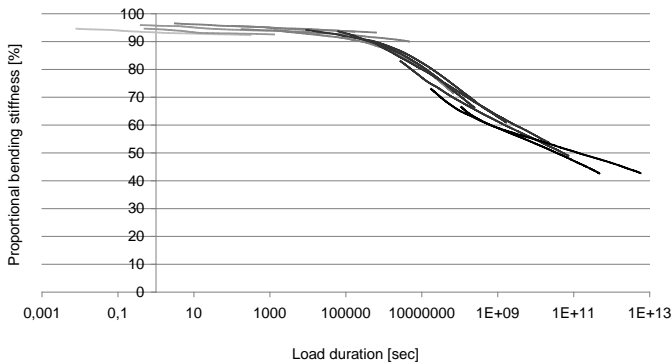
**Figure IV.3: Shifted proportional torsional stiffness during relaxation tests on glass/SG laminates (1100 mm x 360 mm)**



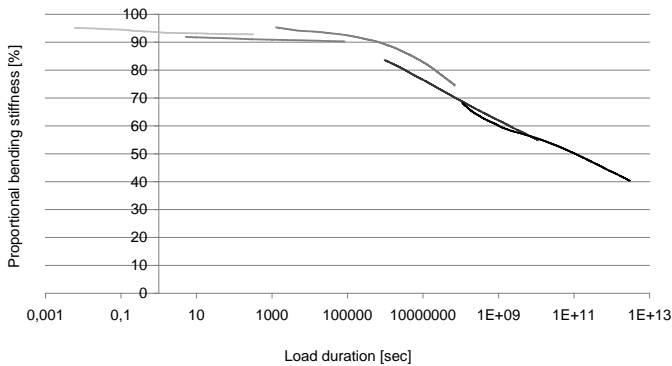
**Figure IV.4: Shifted proportional torsional stiffness during relaxation tests on glass/PVB laminates (1100 mm x 360 mm)**

Fig. IV.2 shows that the shifted curves do not all go over in each other smoothly with the calculated time-shift constants. However, the shifted curves in Fig. IV.3 indicate that a smaller temperature difference between the experiments reveal a more complete image that could be approached by a smooth mastercurve. In Fig. IV.4, a good outcome of the time-shift constants for PVB from literature is visible. A comparison between the stiffness of SG and PVB is presented in Appendix Q.

Figs. IV.5 to IV.6 represent the shifted results of the small bending experiments.



**Figure IV.5: Shifted proportional bending stiffness during creep tests on glass/SG laminates (1100 mm x 180 mm)**



**Figure IV.6: Shifted proportional bending stiffness during creep tests on glass/SG laminates (1100 mm x 120 mm)**

In Fig. IV.6, an abnormality could be detected in the shifted curve, representing the results of bending experiments with a temperature of 35 °C. The experimental stiffness appears to be too high, or the results could be shifted to far to the right. However, the shifted experimental results with a smaller temperature interval, represented in Fig. IV.5, lead to a more complete curve with a certain dispersion, indicating that this deviation in Fig. IV.5 is rather insignificant. Figs. IV.7 and IV.8 summarize the large bending test results.

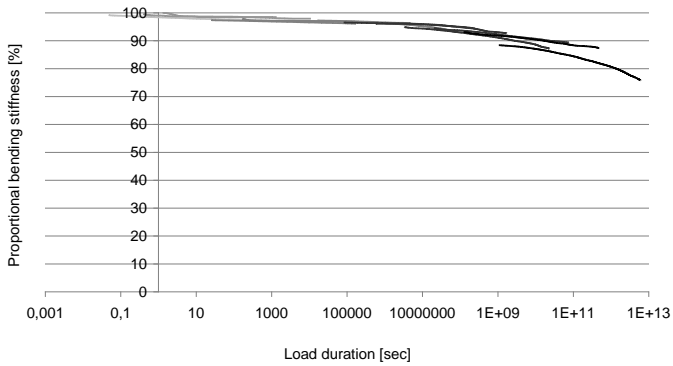


**Figure IV.7: Shifted proportional bending stiffness during creep tests on glass/SG laminates (3000 mm x 360 mm)**

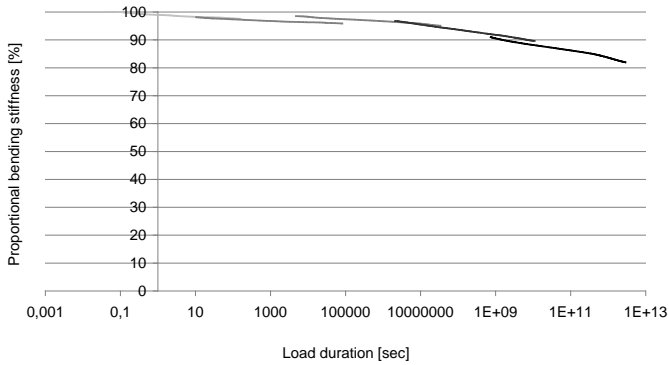


**Figure IV.8: Shifted proportional bending stiffness during relaxation tests on glass/SG laminates (3000 mm x 360 mm)**

With the empirically determined WLF time-shift function, the results of tests at different temperatures form a smooth curve at  $T_{ref}$  for the different test setups. Consequently, the results can be well approximated as a thermorheologically simple material in the tested temperature range around  $T_G$ . This matches a conclusion in [Scherer 1992] which states that “oxide glasses are thermorheologically simple over a wide range of temperatures near the glass transition. This is an approximation, albeit a good one.”<sup>1</sup> The test results confirm that glasses and the polymer material SG show similar mechanical behaviour, as generally accepted.

Compared to the results of the small bending experiments, the larger test specimen render a much higher proportional stiffness. Because the proportional stiffness of a laminate changes not only by varying the load duration or the temperature, but is also significantly affected by the load situation, these results seems not suitable for

<sup>1</sup> [Scherer 1992] p.55

the prediction of the mechanical behaviour of glass laminates in other than the tested loading conditions. Consequently, the proportional stiffness is inadequate and an alternative, standardised technique is investigated in the next paragraph.

## 1.2 Equivalent thickness method

In [prEN 13474-3], the method of equivalent thickness is proposed for the calculation of the bending stiffness and strength of laminated glass where the shear transfer between the glass layers is taken into account. This method gives equations to calculate the thickness of a monolithic plate with the same mechanical properties as a laminated plate. With this thickness, the bending deformations and stresses in the laminated material can be calculated as if it was a monolithic glass plate. In literature, this method is referred to as *effective thickness* method, but this appellation might be confused with the actual thickness of an element. It is therefore called *equivalent thickness* throughout this work.

Although the basic concept behind this method seems rather simple, the application of the method is more complex. For instance, the equivalent thickness must be calculated separately for strength and stiffness because its definition is different. To determine the deformations Eq. (IV.3) must be used, while Eqs. (IV.4) and (IV.5) should be applied for the determination of the maximal stresses in the glass.

$$t_{eq,w} = \sqrt[3]{(1 - \omega) \sum (t_{glass,i}^3) + \omega (\sum t_{glass,i})^3} \quad (IV.3)$$

$$t_{eq,\sigma,j} = \sqrt{\frac{t_{eq,w}^3}{t_{glass,j} + 2\omega t_{m,j}}} \quad (IV.4)$$

$$t_{eq,\sigma} = \min(t_{eq,\sigma,j}) \quad (IV.5)$$

With:

$t_{eq,w}$	Equivalent glass thickness for the calculation of the bending deformations
$\omega$	Dimensionless shear factor varying between 0 (no shear transfer) and 1 (full shear transfer)
$t_{glass,i/j}$	Thickness of the individual glass plies
$t_{eq,\sigma,j}$	Equivalent glass thickness for the calculation of the bending stresses in glass ply $j$
$t_{m,j}$	Distance between the centre of glass ply $j$ and the centre of the laminate
$t_{eq,\sigma}$	Equivalent glass thickness for the calculation of the maximal bending stresses in the glass of the laminate

On the other hand, the equivalent thickness can be determined by using the results from our three-point bending tests.  $t_{eq,w,exp}$  is then given by the simple Eq. (IV.6)

$$t_{eq,w,exp} = \sqrt[3]{\frac{F \cdot L_{span}^3}{4E_{glass}Ww}} \tag{IV.6}$$

In this case, the load  $F$  acting in the middle of the span  $L_{span}$  on the laminated test specimen with width  $W$  causes a deflection  $w$ . When applying this equation to the results of the bending tests and using a Young’s modulus  $E_{glass}$  of 73 GPa as determined experimentally and applied in the preceding analyses of the experimental results, the equivalent thickness is drawn from Figs. IV.9 up to IV.12. The graphs are also time-shifted with the WLF-time shift equation from § IV.1.1.

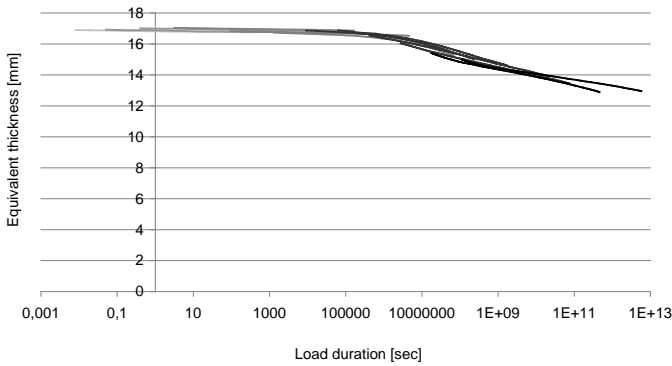


**Figure IV.9: Equivalent thickness based on the bending deformations during the bending creep experiments on test specimen of series B (1100 mm x 180 mm)**

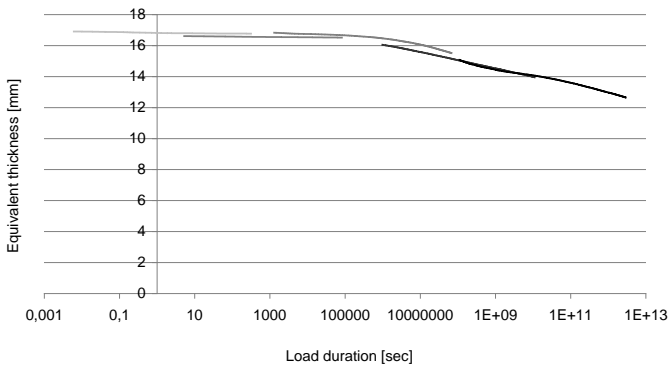


**Figure IV.10: Equivalent thickness based on the bending deformations during the bending creep experiments on test specimen of series E (1100 mm x 120 mm)**



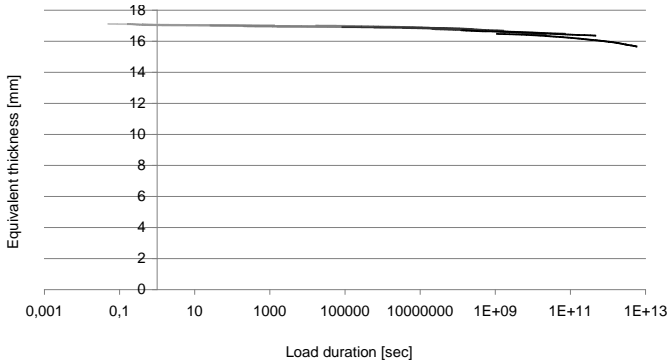


**Figure IV.11: Equivalent thickness based on the bending deformations during the bending creep experiments on test specimen of series C (3000 mm x 360 mm)**

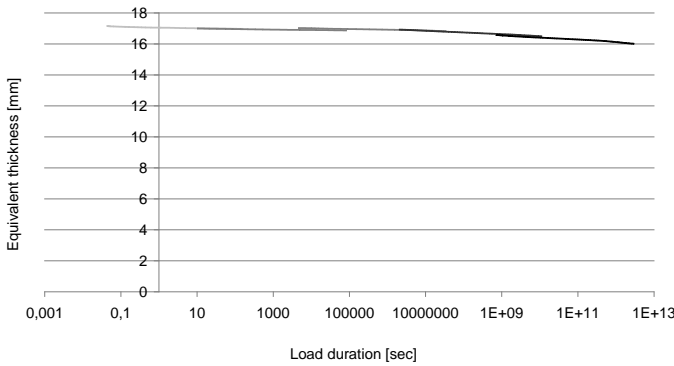


**Figure IV.12: Equivalent thickness based on the bending deformations during the bending relaxation experiments on test specimen of series C (3000 mm x 360 mm)**

From the graphs, it is seen that for longer load durations, there is a non negligible difference between the equivalent thickness for small span and large span bending experiments (compare Fig. IV.9 and IV.10 with Figs. IV.11 and IV.12). The calculations show that there does not exist one single equivalent thickness for the calculation of the bending deflections with an equal laminate composition (2x 8mm glass with 1.52 mm SG). The foregoing discussion thus reveals that the equivalent thickness does not only alter when the theory is used to calculate deformations or stresses, but is also highly sensitive to the loading situation. Therefore, it is important that the equivalent thickness derived from an experiment may not be used directly for the calculation of the bending deformations of an element having a different geometry than the elements tested.

Based on the principle that the equivalent thickness corresponds to the thickness of a monolithic glass element with equivalent mechanical behaviour of the laminate, an equation for torsional deformations can be formulated similar to Eq. (IV.6) for bending deflections. With Eq. (IV.7), the equivalent thickness for the calculation of the torsional stiffness  $t_{eq,\theta}$  can be determined.

$$t_{eq,\theta,exp} = \sqrt[3]{\frac{3ML_{span}}{WG_{glass}\theta}} \quad (IV.7)$$

In this expression, the torque  $M$  on the laminated element with width  $W$  causes a rotational twist  $\theta$  about the longitudinal axis over the length  $L$ . Figs. IV.13 up to IV.15 represent the resulting curves when applying Eq. (IV.7) on the measured results of the torsion experiments on the test specimens of series A and D with a thickness of 2x 6 mm glass and a 1.52 mm interlayer.

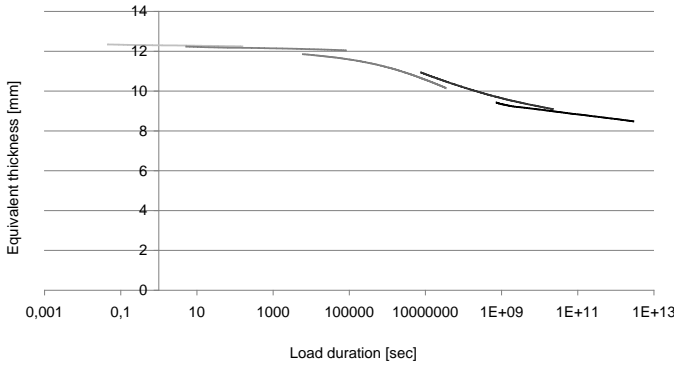


**Figure IV.13: Equivalent thickness based on the torsional deformations during the torsion creep experiments on test specimen of series A (1100 mm x 360 mm)**

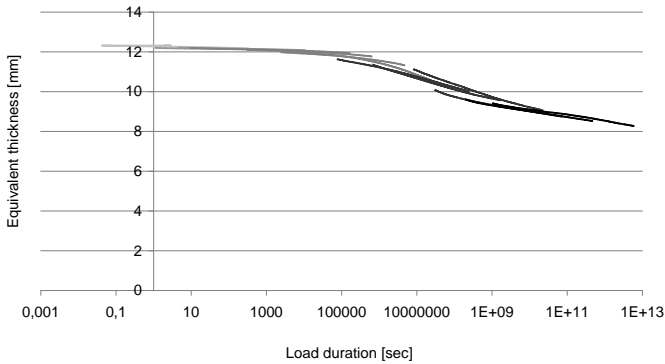


**Figure IV.14: Equivalent thickness based on the torsional deformations during the torsion relaxation experiments on test specimen of series A (1100 mm x 360 mm)**

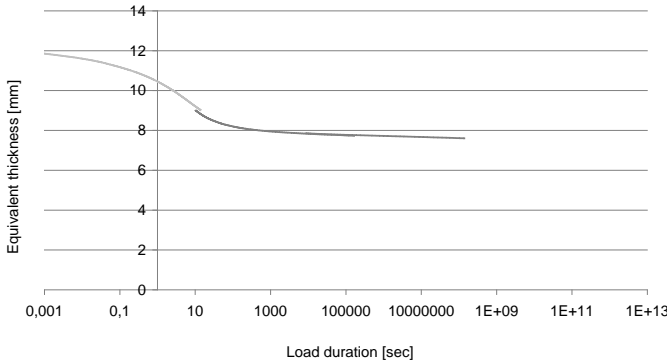


**Figure IV.15: Equivalent thickness based on the torsional deformations during the torsion relaxation experiments on test specimen of series D (1100 mm x 360 mm; PVB interlayer)**

It is obvious that the equivalent thickness from the torsion experiments is lower than the equivalent thickness from the bending tests, because the thickness of the glass plies is smaller in the former. Therefore a comparison between the calculated equivalent thickness for bending and torsion is meaningless.

However, the comparison of all these results with the minimal and maximal expected value for the equivalent thickness is relevant. When implementing  $\omega = 0$  in Eq. (IV.3), the minimum possible value of the equivalent thickness for bending deflections  $t_{eq,w,min}$  can be represented with Eq. (IV.8), while implementing  $\omega = 1$  in Eq. (IV.3) leads to Eq. (IV.9) which represents the maximal value for the equivalent thickness  $t_{eq,w,max}$ . Although Eq. (IV.3) is only given for the bending deflections, Eqs. (IV.8) and (IV.9) are also applicable for the calculation of the minimal and maximal value of the equivalent thickness for torsional deformations.

$$t_{eq,w,min} = \sqrt[3]{\sum(t_{glass,i}^3)} \quad (IV.8)$$

$$t_{eq,w,max} = \sqrt[3]{(\sum t_{glass,i})^3} = \sum t_{glass,i} \quad (IV.9)$$

$$t'_{eq,w,max} = \sum t_{glass,i} + \sum t_{int,j} \quad (IV.10)$$

Normally, the interlayer thickness  $t_{int}$  is not taken into account for the determination of the equivalent thickness. However, the calculated values presented in Figs. IV.8 up to IV.13 clearly exceed the total glass thickness from Eq. (IV.9). Therefore, an additional maximal equivalent thickness  $t'_{eq,w,max}$  was calculated with Eq. (IV.10) which does include the interlayer thicknesses  $t_{int,j}$ . Table IV.3 and Table IV.4 summarise the minimal and maximal values for all the test

samples with respectively the average values of the measured thickness and the nominal thicknesses.

**Table IV.3: Minimal and maximal equivalent thicknesses based on the average measured thickness for each sample series**

Samples	$t_{glass,mean}$ [mm]	$t_{int,mean}$ [mm]	$t_{eq,w,min}$ [mm]	$t_{eq,w,max}$ [mm]	$t'_{eq,w,max}$ [mm]
A	5.91	1.59	7.44	11.81	13.40
B	7.77	1.62	9.80	15.55	17.17
C	7.77	1.60	9.79	15.54	17.14
D	5.90	1.54	7.43	11.80	13.34
E	7.79	1.53	9.81	15.58	17.11

**Table IV.4: Minimal and maximal equivalent thicknesses based on the nominal thickness for each sample series**

Samples	$t_{glass,nom}$ [mm]	$t_{int,nom}$ [mm]	$t_{eq,w,min}$ [mm]	$t_{eq,w,max}$ [mm]	$t'_{eq,w,max}$ [mm]
A / D	6.00	1.52	7.56	12.00	13.52
B / C / E	8.00	1.52	10.08	16.00	17.52

When taking into account the interlayer thickness, all curves lie between the two limiting cases. Almost all curves start close to the maximum, which indicates that all tested laminates behave almost monolithically for short loading durations at low temperatures. For the bending experiments of series C with a span of 2950 mm, the results remain close to the upper limit, while for the torsion experiments on series D with a PVB interlayer, the lower limit is approached. Unfortunately, the graphs in Figs. IV.8 up to IV.14 clearly demonstrate that the equivalent thickness for the calculation of deformations is not only influenced by the laminate composition and the material properties of the components, but also by its dimensions and the loading configuration.

For bending therefore, the results can also be interpreted in terms of the dimensionless shear factor  $\omega$ , which can then be used to determine the equivalent thickness for the calculation of the glass stresses  $t_{eq,\sigma}$ . Because prEN 13474-3 proposes to neglect the thickness and the bending stiffness of the interlayer, the results are converted this way. Contrary to all other preceding data processing, for which a Young's modulus of 73 GPa is used based on an experimental determination of the glass stiffness, a Young's modulus of 70 GPa is used as defined in the European standard. Eq. (IV.10) is therefore only valid for this specific case.

$$\omega = \frac{\left(t_{eq,w,exp} \cdot \sqrt[3]{\frac{73}{70}}\right)^3 - N \cdot t_{glass,nom}}{t_{glass,nom}^3 \cdot (N^3 - N)} \tag{IV.10}$$

Equation (IV.10) indicates that the shear transfer coefficient  $\omega$  is only function of the equivalent thickness for the calculation of the bending stiffness  $t_{eq,w}$ , the number of glass plates  $N$  and the nominal thickness of the glass layers  $t_{glass, nom}$ . This already indicates that this dimensionless factor is also influenced by the loading condition and the dimensions of the element, as was noticed in the previous graphs of Figs. IV.8 to IV.14. The clear difference between Figs. IV.16 and IV.17 with results from the small bending on the one hand side and Figs. IV.18 and IV.19 for the larger bending experiments on the other hand side clearly demonstrate this presumption.

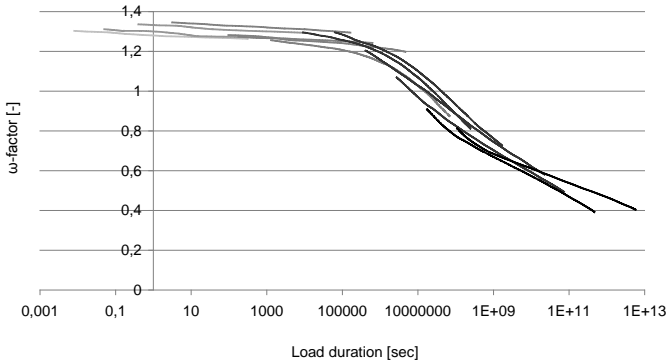


**Figure IV.16: Shear transfer coefficient  $\omega$  based on the bending deformations during the bending creep experiments on test specimen of series B (1100 mm x 180 mm)**

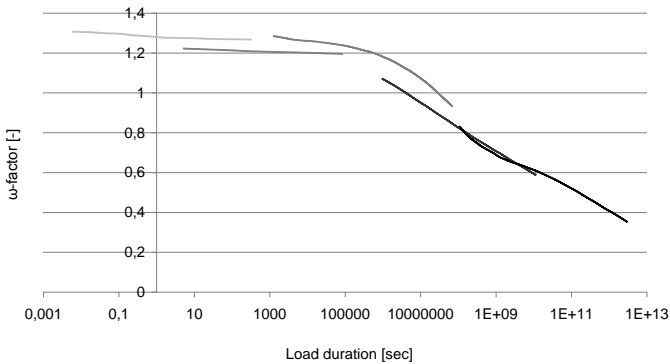


**Figure IV.17: Shear transfer coefficient  $\omega$  based on the bending deformations during the bending creep experiments on test specimen of series E (1100 mm x 120 mm)**

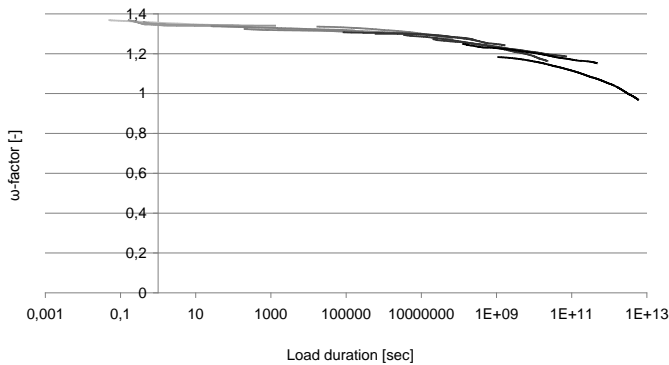


**Figure IV.18: Shear transfer coefficient  $\omega$  based on the bending deformations during the bending creep experiments on test specimen of series C (3000 mm x 360 mm)**

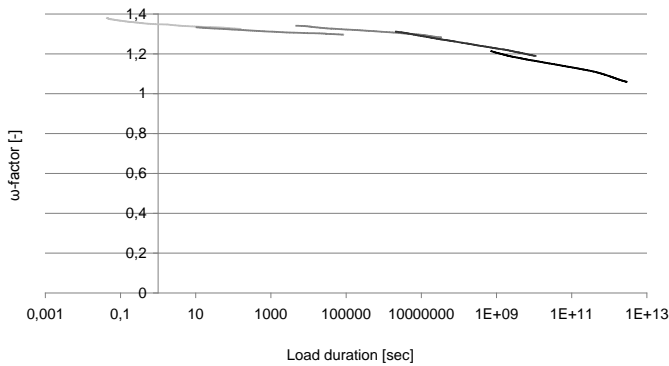


**Figure IV.19: Shear transfer coefficient  $\omega$  based on the bending deformations during the bending relaxation experiments on test specimen of series C (3000 mm x 360 mm)**

Although the basic concept of the effective thickness method seems very appealing as a relatively easy way of simplifying the problem of the mechanical behaviour of laminated glass elements, the results demonstrate that the calculated equivalent thickness or shear transfer coefficient can only be used to predict the performance of elements with a similar loading condition and an identical geometry as the tested samples. For this reason, the experimental results should be converted into a practical material model which describes the time- and temperature dependent behaviour of the interlayer material. This could eliminate the geometrical influences. Therefore, the results are recalculated analytically and numerically into a time- and temperature-dependent shear modulus model.

### 1.3 Analytical models

Several analytical models exist in literature to calculate the stiffness of laminated elements, based on their geometry and the material properties of the components. These theories can be used inversely to find the shear modulus of the interlayer from the experimentally determined stiffness. The analysis of the torsion

experiments is based on the theory developed by Scarpino [Scarpino 2002], while for the bending, the model of Wölfel is applied [Wölfel 1987].

### 1.3.1 Torsional stiffness by Scarpino

Generally, the torsional behaviour of an element is of minor interest for structural applications. Nevertheless, this can be calculated with the sandwich theory described in [Stamm & Witte 1974], which is proposed in [Haldimann et al. 2008] to predict the lateral torsional buckling load of slender laminated glass beams.

In 2002, Scarpino developed an analytical model to calculate an equivalent torsional stiffness  $G I_{t,eq}$  of a glass/interlayer laminate based on the geometry and the shear modulus of the soft interlayer material [Scarpino 2002] [Scarpino et al. 2004]. This later model is suggested in [Belis 2005] for the calculation of the torsional stiffness. Although both models are found accurate for these applications, the theory of Scarpino was chosen here because it has already been used for the numerical analysis of torsion tests on glass/PVB laminates as well [Kasper 2005].

The basis for the theory is that the actual torsion stiffness of laminated glass can be expressed as the multiplication of the torsional stiffness of the individual glass sheets with a factor  $f$ :

$$G_{glass} \cdot I_{t,eq} = G_{glass} \cdot I_{t,lower} \cdot f \quad (IV.11)$$

For a symmetric laminate with two glass plies and one soft interlayer subjected to pure torsion, meeting the additional requirements formulated in Eqs. (IV.12) up to (IV.15), its dimensionless factor of increase  $f$  can be represented by Eq. (IV.16). Since the test specimens of these experiments fulfil all the necessary requirements, this formula is applicable. In these equations, the length  $L$ , the width  $W$  and the layer thicknesses  $t_i$  determine the geometry of the laminate.

$$L \gg W \gg \sum_i t_i \quad (IV.12)$$

$$t_{int} < t_{glass} \quad (IV.13)$$

$$G_{int} \ll G_{glass} \quad (IV.14)$$

$$I_{t,lower} = 2 \cdot \frac{W \cdot t_{glass}^2}{3} \quad (IV.15)$$

$$f = \frac{6t_{glass}^3 t_{int} + \frac{G_{int}}{G_{glass}} \cdot W^2 (4t_{int}^2 + 6t_{glass} t_{int} + 3t_{glass}^2)}{t_{glass}^2 (6t_{glass} t_{int} + \frac{G_{int}}{G_{glass}} \cdot W^2)} \quad (IV.16)$$

$t_{glass}$  denotes the thickness of one individual glass sheet and  $t_{int}$  is the interlayer thickness. Because Eqs. (IV.15) and (IV.16) are only applicable for symmetric laminates, the glass thickness  $t_{glass}$  is taken as the mean measured thickness of the two glass plies of each test specimen. Because  $G_{glass} \cdot I_{t,eq}$  - with  $G_{glass} = 30\,000\text{ N/mm}^2$  - is known from the torsion experiments, Eqs. (IV.11) and (IV.16) can be combined to retrieve the interlayer instantaneous shear modulus  $G_{int}$  for each recording. This results in a correlation between the shear modulus of the interlayer, and the load duration at a certain temperature level as presented in Figs. IV.20 up to IV.24. To visualise the influence of the measured deviations on the calculated values, the results of four identical experiments on different samples and the mean results are displayed for each temperature level and test configuration.

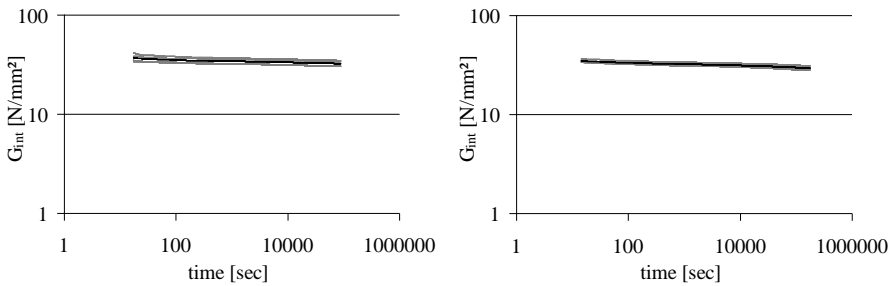


**Figure IV.20:** Correlation between the shear modulus of the interlayer and the load duration at 5 °C: torsion creep (left); torsion relaxation (right)

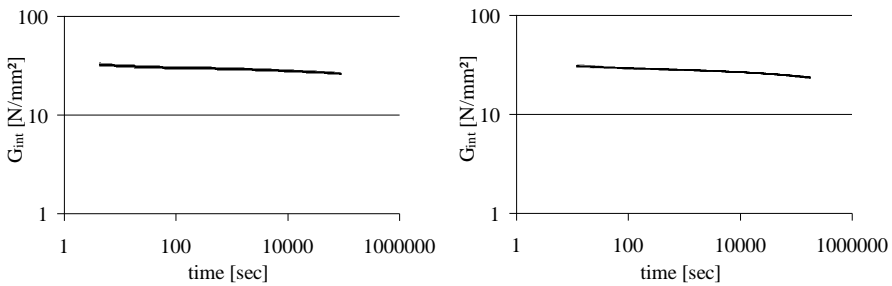


**Figure IV.21:** Correlation between the shear modulus of the interlayer and the load duration at 20 °C: torsion creep (left); torsion relaxation (right)



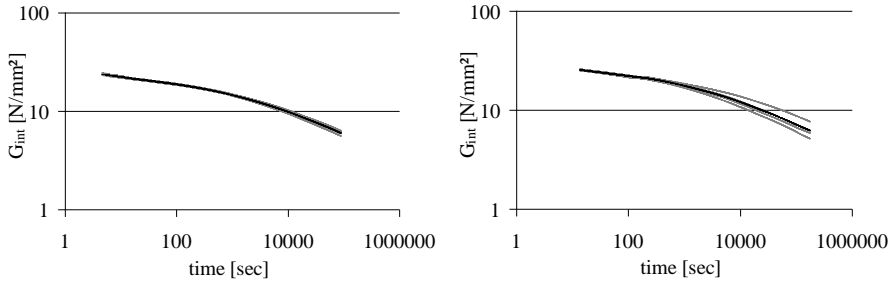


**Figure IV.22:** Correlation between the shear modulus of the interlayer and the load duration at 35 °C: torsion creep (left); torsion relaxation (right)

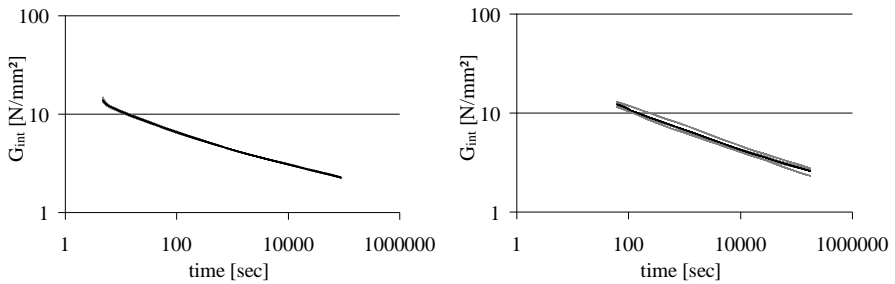


**Figure IV.23:** Correlation between the shear modulus of the interlayer and the load duration at 50 °C: torsion creep (left); torsion relaxation (right)

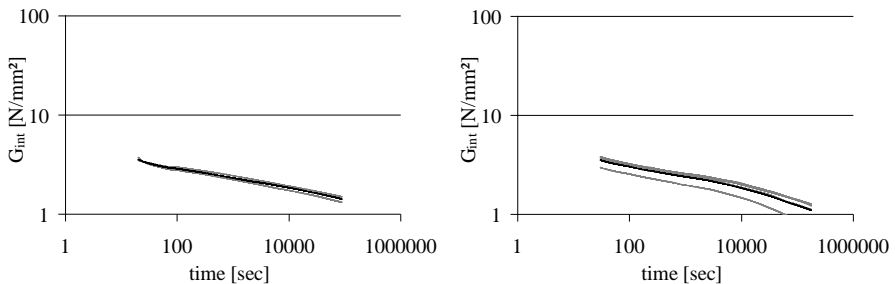


**Figure IV.24:** Correlation between the shear modulus of the interlayer and the load duration at 65 °C: torsion creep (left); torsion relaxation (right)

As was found for the proportional torsional stiffness, the difference between similar creep and relaxation experiments is negligible.

### 1.3.2 Bending stiffness by Wölfel

In literature, multiple analytical models exist to predict the mechanical behaviour of two sided supported laminated plates subjected to bending about the weak axis, e.g. [Roik & Sedlacek 1970], [Hooper 1973], [Stamm & Witte 1974], [Wölfel 1987], [Norville et al. 1998]. Already in multiple works about the stiffness of laminated

glass, different models are described and compared [Siebert 2001], [Schuler 2003], [Bucak & Meißner 2005], [Ensslen 2005] and often, Wölfel's theory is preferred to analyse experimental results [Schuler 2003], [Ensslen 2005], [Bucak et al. 2006]. Additionally, the equivalent thickness method, used in § IV.1.2, is based on this model [Bennison et al. 2009], and for these reasons, it is also applied here to transform the experimental bending results towards the interlayer material properties.

Generally, the analytical model of Wölfel can be used for the calculation of the weak axis bending stiffness of a laminate with two stiff outer planes and a softer interlayer [Wölfel 1987]. This theory was not specifically designed for laminated glass, but its validity has already been proven for applications in this field [Siebert 2001], [Stelzer et al. 2008].

As for each analytical model, there are some requirements regarding the applicability. The model is e.g. only valid for static cases with relatively small deflections of laminated elements with elastic and isotropic materials. Therefore, visco-elastic materials should be simplified to an elastic material, resembling one load duration at a certain temperature level. Furthermore, the stiffness of the interlayer must be relatively small compared to the stiffness of the outer panes, as the model only takes into account the shear transfer and neglects the bending stiffness of the interlayer. Finally, also a perfect adhesion between the different layers is assumed.

The equivalent bending stiffness of the laminate  $E_{glass} \cdot I_{b,eq}$  is the sum of the bending stiffness of all individual glass sheets  $E_{glass} \cdot I_{b,lower}$  and a substitute bending stiffness  $\overline{B}_S$  (Eq. (IV.17)). For a laminate with two stiff outer panes with equal thickness, the latter term can be calculated with Eq. (IV.18). The dimensionless factor  $k$  depends on the loading condition and Eq. (IV.19) represents the formula which is only applicable for three-point bending.

$$E_{glass} \cdot I_{b,eq} = E_{glass} \cdot I_{b,lower} + \overline{B}_S \quad (IV.17)$$

$$\overline{B}_S = \frac{1}{(1+k)} \cdot E_{glass} \cdot \frac{W t_{glass} (t_{glass} + t_{int})^2}{2} \quad (IV.18)$$

$$k = 12 \cdot \frac{E_{glass}}{G_{int}} \cdot \frac{t_{glass} t_{int}}{2L^2} \quad (IV.19)$$

Again, because the bending stiffness  $E_{glass} \cdot I_{b,eq}$  is calculated from the experimental bending results, Eqs. (IV.17) up to (IV.19) can be combined to find the shear modulus of the soft interlayer. The results are presented in Figs. IV.25 up to IV.34.

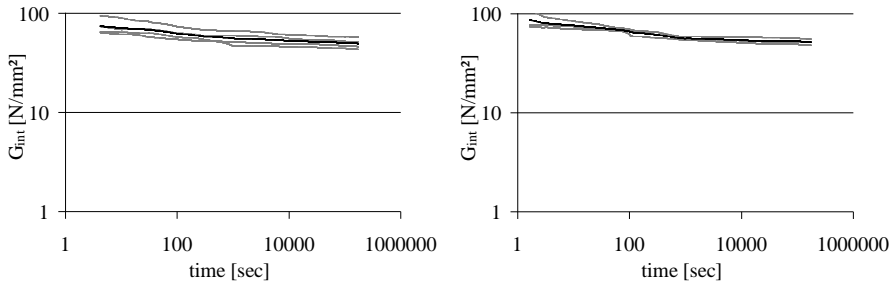


**Figure IV.25:** Correlation between the shear modulus of the interlayer and the load duration at 5 °C: bending creep on series B (width = 180 mm) (left); bending creep on series E (width = 120 mm) (right)

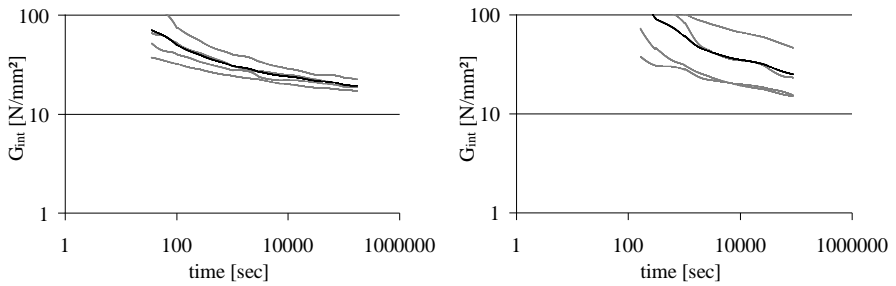


**Figure IV.26:** Correlation between the shear modulus of the interlayer and the load duration at 5 °C: bending creep on series C (left); bending relaxation on series C (right)

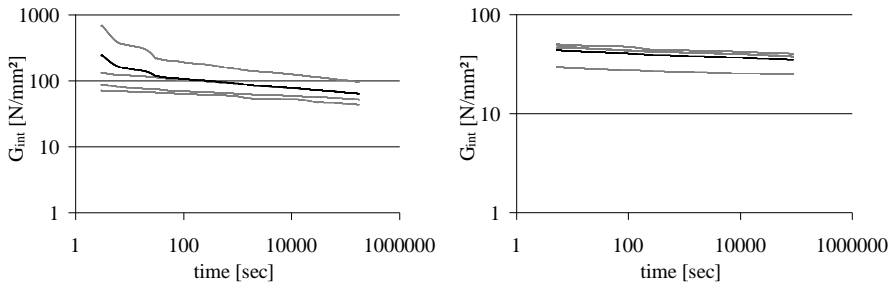


**Figure IV.27:** Correlation between the shear modulus of the interlayer and the load duration at 20 °C: bending creep on series B (width = 180 mm) (left); bending creep on series E (width = 120 mm) (right)

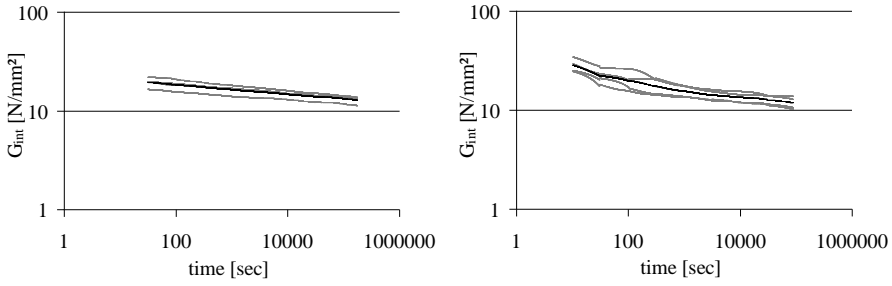


**Figure IV.28:** Correlation between the shear modulus of the interlayer and the load duration at 20 °C: bending creep on series C (left); bending relaxation on series C (right)

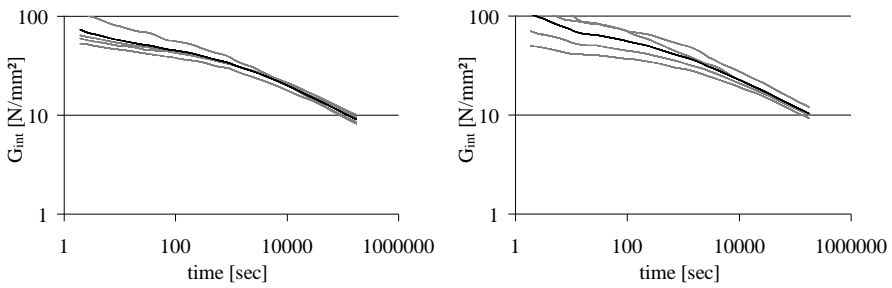


**Figure IV.29:** Correlation between the shear modulus of the interlayer and the load duration at 35 °C: bending creep on series B (width = 180 mm) (left); bending creep on series E (width = 120 mm) (right)

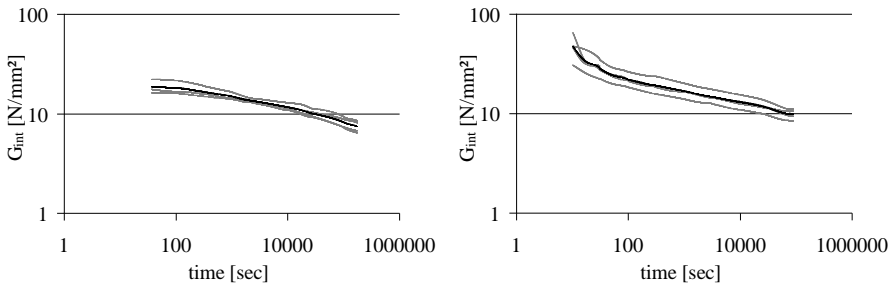


**Figure IV.30:** Correlation between the shear modulus of the interlayer and the load duration at 35 °C: bending creep on series C (left); bending relaxation on series C (right)

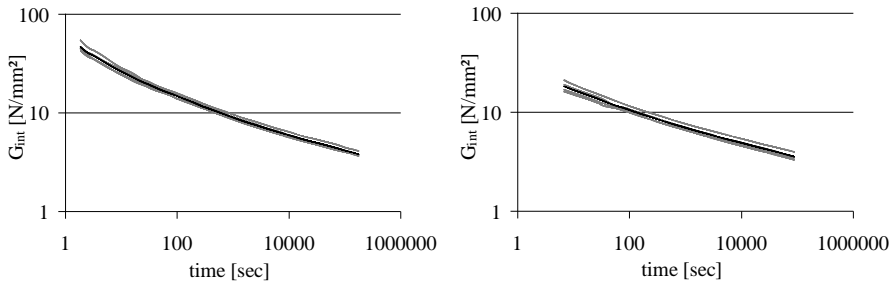


**Figure IV.31:** Correlation between the shear modulus of the interlayer and the load duration at 50 °C: bending creep on series B (width = 180 mm) (left); bending creep on series E (width = 120 mm) (right)

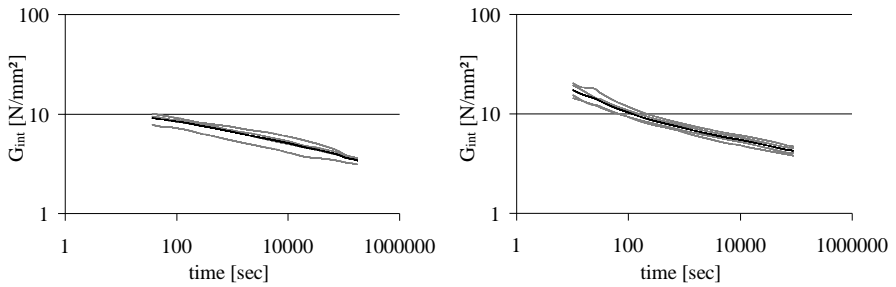


**Figure IV.32:** Correlation between the shear modulus of the interlayer and the load duration at 50 °C: bending creep on series C (left); bending relaxation on series C (right)

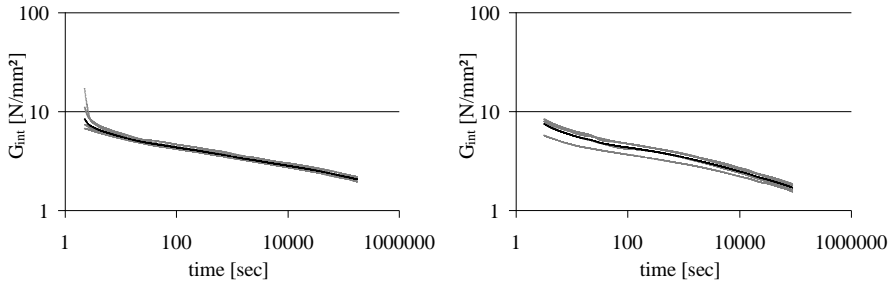


**Figure IV.33:** Correlation between the shear modulus of the interlayer and the load duration at 65 °C: bending creep on series B (width = 180 mm) (left); bending creep on series E (width = 120 mm) (right)

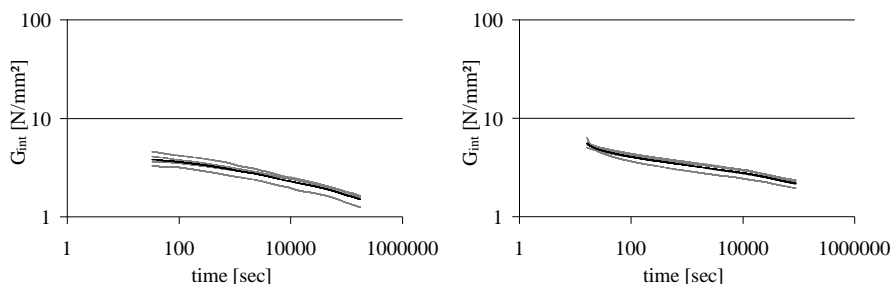


**Figure IV.34: Correlation between the shear modulus of the interlayer and the load duration at 65 °C: bending creep on series C (left); bending relaxation on series C (right)**

Again, there is little difference between the small bending experiments on series B (180 mm x 1100 mm) and E (120 mm x 1100 mm) (compare the left to the right graphs of Figs. IV.25, IV.27, IV.29, IV.31 and IV.33) and between the creep and relaxation bending experiments on series C (360 mm x 3000 mm) (difference between the left and the right graphs of Figs. IV.26, IV.28, IV.30, IV.32 and IV.34). The difference between the small bending experiments with a span of 1050 mm and the large tests with a span of 2950 mm is significantly reduced compared to the difference between the proportional bending stiffness.

### 1.3.3 Combined results

In Fig. IV.35, all the results presented in Figs. IV.20 up to IV.34 are combined in averaged and time-shifted curves for both the bending and the torsion experiments.

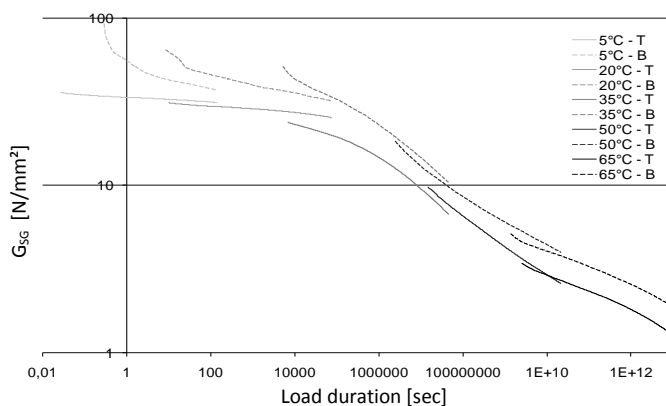


**Figure IV.35: WLF time-shifted correlation between the shear modulus of the interlayer averaged over all bending B (dotted lines) and over all torsion results T (continuous lines), and the load duration**

Although the material properties of the polymer interlayer material SG should only be determined by the load duration and the temperature, a clear influence of the loading conditions is visible. Because it is possible that this deviation is due to the

applied analytical models, the results are further compared with FE simulations of the test setups presented in § III.4.2 and § III.5.2.

Although recently, also new improved analytical models are developed [Feldmann & Langosch 2011], [Galuppi & Royer-Carfagni 2011a], [Galuppi & Royer-Carfagni 2011b] which might increase the accuracy, it seems more appropriate to analyse the results with FE models. With the latter, also seemingly negligible side effects are taken into consideration, such as the small parts of the test sample which extend beyond the supports (25 mm for the bending experiments and 50 mm for the torsion tests), the non-bending deformations due to shear loads (see Appendix L) or the small bending or torsional stiffness of the interlayer itself, which are generally neglected in the analytical models.

## 2 Numerical analysis

FE models have been built for the simulation of the tested loading conditions. Subsequently, they have been used to determine the stiffness of an element with different interlayer shear modules numerically. Finally, these results are compared with the tests and an experimental shear modulus of the interlayer is deduced.

### 2.1 Finite element models

#### 2.1.1 Torsion model

To simulate the torsion experiments, a FE model was developed in Abaqus Standard, version 6.8-1 [Abaqus 2008]. Although the laminated elements seem very compatible with shell elements, the use of volumetric elements was preferred. Based on Abaqus models for laminated glass in literature [Bennison et al. 2008] [D'Haene & Savineau 2007] and a mesh-study [Nachtergaele 2009] (see also appendix M), solid 8-node linear brick elements with incompatible mode (C3D8I) are preferable for the glass panes, while the interlayer materials is best simulated with 8-node linear brick with incompatible modes and hybrid with linear pressure (C3D8IH) elements. In Fig. IV.36, the applied mesh is presented. In the longitudinal direction of the plates  $26 + 56 + 26$  elements were used, while there were  $6 + 20 + 6$  in transversal direction. This higher density of the mesh at the edges, especially in the clamped region, enables a more realistic stress analysis. The glass panes consisted of three layers of elements, and the interlayer contained two element layers. The amount of elements is summarised in Table IV.5.

The laminated plate is caught between half cylindrical bars, of which the displacements can be imposed by rotating tie constrained rigid body elements.

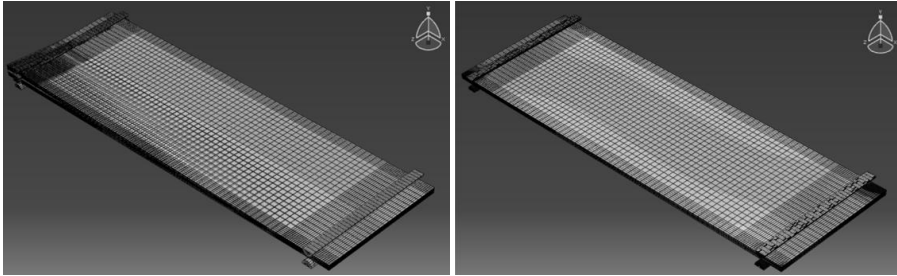


**Figure IV.36: FE model for torsion setup: Deformed and undeformed mesh (left); deformed shape with indication of the maximal principal stresses (right)**

**Table IV.5: Number of elements in the FE models for torsion (A and D) and bending (B, C and E)**

Sample series	# elements in length	# elements in width	# elements in thickness
A and D	26 + 56 + 26	6 + 20 + 6	3 + 2 + 3
B	34 + 10	18	3 + 2 + 3
C	54 + 10	18	3 + 2 + 3
E	34 + 10	12	3 + 2 + 3

Initially, this numerical model was also utilised for the optimization of the torsion setup, by performing simulations with different boundary conditions and applying an eccentricity of the rotational axis [Callewaert et al. 2007].

### 2.1.2 Bending model

Also for bending, a numerical model was built, with similar element types as the torsion model. However, because the loading situation for three-point bending has two axes of symmetry, the model could be limited to one quarter of the setup. This significantly reduces the calculation time and digital file sizes. Figs. IV.37 and IV.38 depict these models.

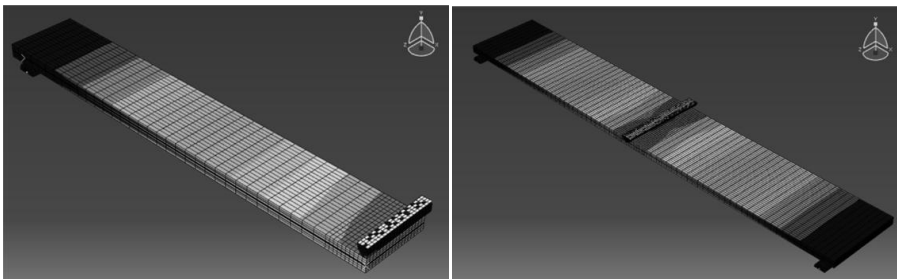


**Figure IV.37: FE model for bending setup of series B (1100 mm x 180 mm): simulated quarter of the test setup (left); deformed shape with indication of the stresses (right)**

In the right picture of Fig. IV.37, the full laminated plate is generated by mirroring the calculated results which are represented in the left picture of Fig. IV.37. Fig. IV.38 represents the mesh for the samples of series C and E. The applied number of



elements in the simulated quadrant are summarized in Table IV.5. In the centre of the plate, where the line-load is implemented, a fine mesh is used to enhance the imaging of the local stresses.

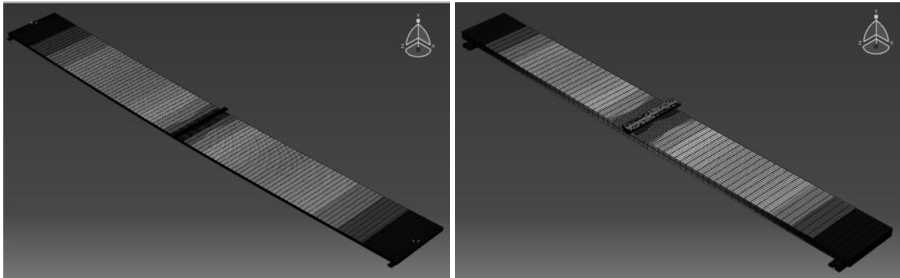


**Figure IV.38:** FE model for bending setup: for test series E (1100 mm x 120 mm) (left); for test series C (3000 mm x 360 mm) (right)

## 2.2 Analytical versus numerical stiffness

To check the validity of the models, a comparison was made between the results of a FE simulation and a calculation based on the theoretical models used in the previous chapter. The mean thickness of a test series and the applied test load were implemented, as well as different values for the shear modulus of the interlayer. Fig. IV.39 shows that both methods give almost the same results for the torsion experiments. In this graph, the black and the gray markers represent the analytical and the numerical values, respectively.

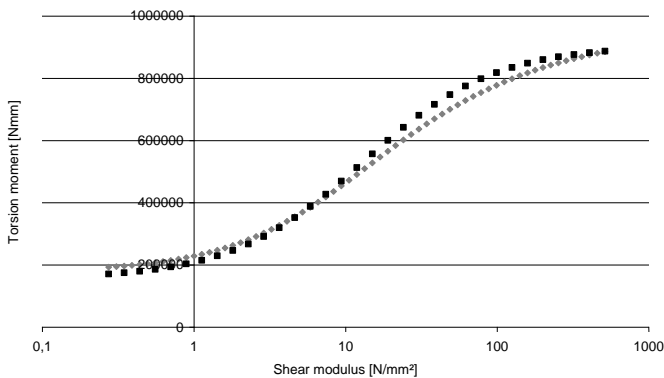


**Figure IV.39:** Analytical (black markers) and numerical (grey markers) torsion moment of sample series A (1100 mm x 360 mm) with a specific angle of torsion of  $6^\circ / 1000$  mm in function of the shear modulus of the interlayer

The largest relative difference appears at the lowest interlayer shear stiffness values. Although the absolute values do not deviate that much there, the relative difference between the analytical and numerical torsional moment values raises up to 11.5 %. For an interlayer shear modulus of about  $40 \text{ N/mm}^2$ , the analytical torsional moment exceeds the numerical value with 7 %.

A likewise comparison was made for the bending models. Figs. IV.40 up to IV.42 depict the numerical and analytical bending deformations for specimen series B, E and C with a load of 147 N, 98 N and 392 N, respectively. Here again, the grey dots corresponds with the numerical results, while the black makers represent the analytical values.

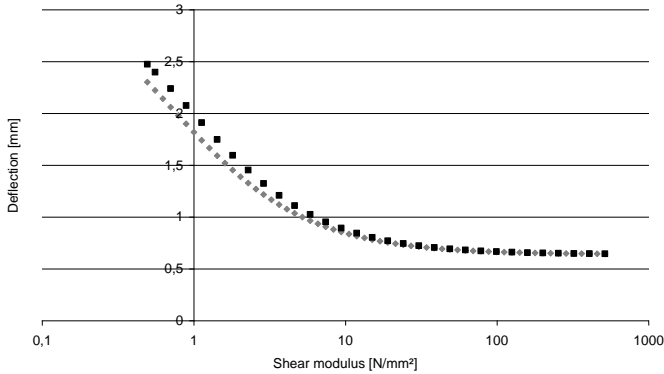


**Figure IV.40: Analytical (black markers) and numerical (grey markers) bending deflection of sample series B (1100 mm x 180 mm) with a load of 147 N in function of the shear modulus of the interlayer**

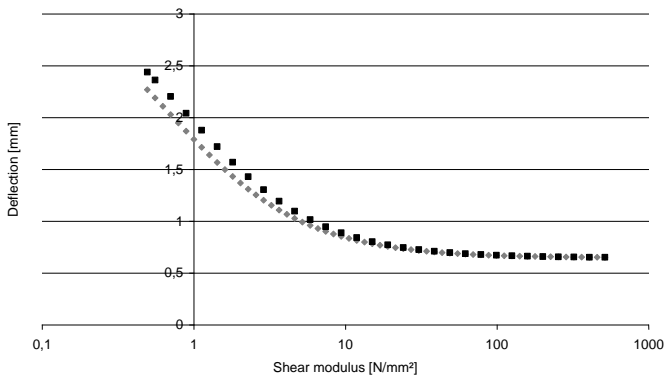


**Figure IV.41: Analytical (black markers) and numerical (grey markers) bending deflection of sample series E (1100 mm x 120 mm) with a load of 98 N in function of the shear modulus of the interlayer**

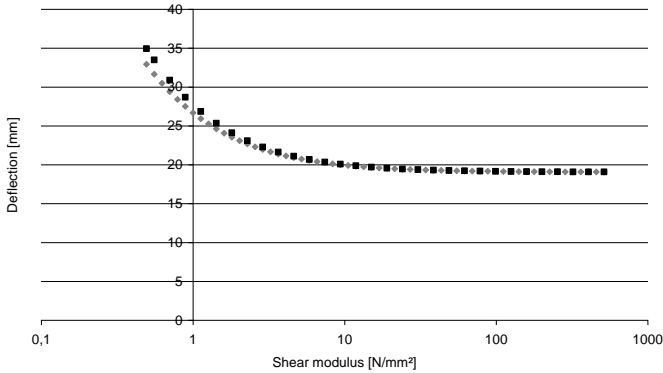


**Figure IV.42: Analytical (black markers) and numerical (grey markers) bending deflection of sample series C (3000 mm x 360 mm) with a load of 392 N in function of the shear modulus of the interlayer**

For both bending series B and E, the maximal relative deviations of almost 10 % occurs at a shear modulus of 1.5 N/mm<sup>2</sup>. The small difference between these two figures clearly proves that also numerically, little edge influence exists when scaling the load proportionally to the width of the specimen, without changing other factors.

The deformations in Fig. IV.42 are obviously much larger, because of the bigger load and span of the test sample series C. However, the deviation between numerical and analytical results is smaller than for the previous models and remains restricted to 6 % in the evaluated range of the interlayer shear modulus.

In general, this demonstrates that the numerical models give accurate results. Nevertheless, the differences between the numerical and analytical values are not completely negligible, but can be explained by some small imperfections of the test setup compared to the conditions of the analytical models, as explained in § IV.1.3.1 and § IV.1.3.2. Therefore, the experimental results are also analysed based on the numerically simulated stiffness of the laminated elements.

### 2.3 Numerically deduced interlayer stiffness

To evaluate the test results with the numerical model, elastic simulations were executed with different shear moduli for the interlayer material, of which the results are already compared to analytical results in § IV.2.2.

Because it was not possible to perform simulations with different shear moduli for each measured deformation and stiffness, a series of simulations was executed with a load comparable to the experiments. The numerical results were therefore converted into a ratio of load versus deformation, which was compared to the same ratio derived from the experimental results. This way, the experimental results were again recalculated in a reversed way into a shear modulus of the interlayer in function of load duration and temperature.

To reduce the difference between the numerical simulations and the similar experiments, the results were approached analogically. For torsion, this means that the vertical displacements of four nodes on top of the glass surface were monitored, situated at the same location as the LVDT measuring instruments during the actual experiments. The torsional deformation was then not determined by the rotation of the supports, but, as for the experiments, by recalculating the angle of twist based on these four vertical displacements. By simultaneously recording the torsional moment in the numerical model, the numerical proportional stiffness could be calculated. In Figs. IV.43 and IV.44, the calculated SG shear modulus  $G_{SG}$  is represented in function of the load duration.

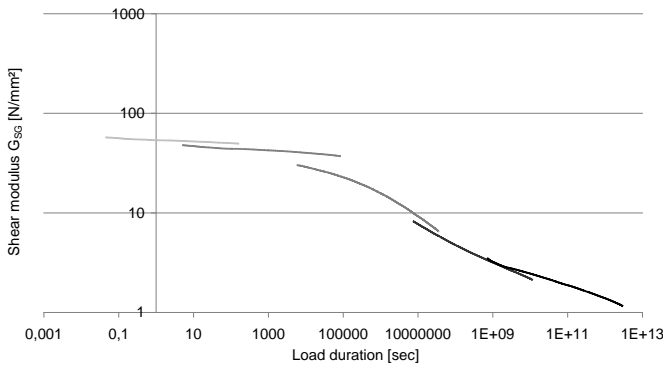


**Figure IV.43: Numerically analysed shear modulus of the SentryGlas interlayer  $G_{SG}$  from torsion relaxation experiments on sample series A (1100 mm x 360 mm)**

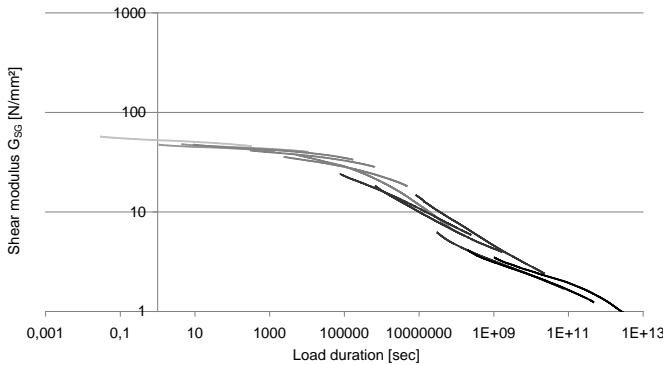


**Figure IV.44: Numerically analysed shear modulus of the SentryGlas interlayer  $G_{SG}$  from torsion creep experiments on sample series A (1100 mm x 360 mm)**

As could be expected, these results are very similar to the preceding analytical analyses, presented in Figs. IV.20 up to IV.24. The relatively small differences between analytical and numerical analysing presented in Fig. IV.39 do not dramatically alter the resulting material properties.

Also for bending, the experimental results were processed by comparison to FE simulations. The displacements of the laminated glass surface were registered at the same location as the LVDT's during the experiments. By comparing the discrete number of simulated load - deflection ratio to the experimentally determined values, a quasi continuous relation between the shear modulus of the interlayer and the load duration was put together. Figs. IV.45 and IV.46 depict these results for the small bending experiments with a span of 1050 mm, while Figs. IV.47 and IV.48 represent the values for the larger bending experiments on sample series C with a span of 2950 mm.

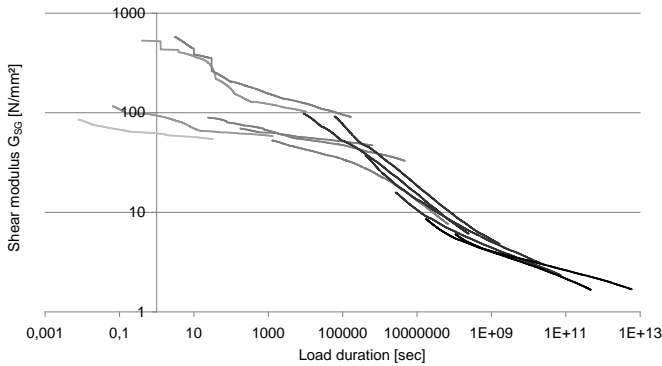


**Figure IV.45: Numerically analysed shear modulus of the SentryGlas interlayer  $G_{SG}$  from bending creep experiments on sample series B (1100 mm x 180 mm)**

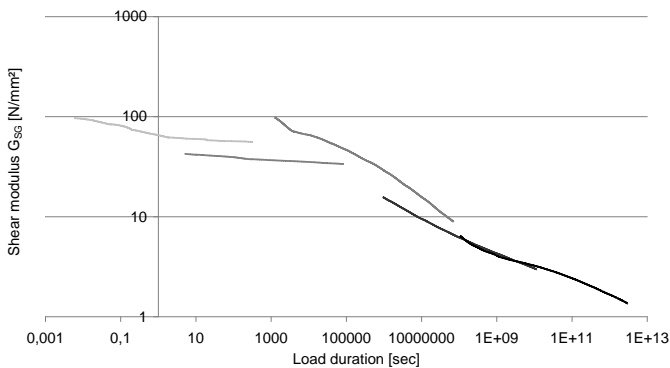


**Figure IV.46: Numerically analysed shear modulus of the SentryGlas interlayer  $G_{SG}$  from bending creep experiments on sample series E (1100 mm x 120 mm)**

As already noticed before, the time shifted results from the bending experiments on test specimen series E at 35 °C are slightly higher than would be expected in comparison with the shifted results from the experiments at 20 °C and 50 °C, but the dispersion of the comparable bending results of series B indicates that this is normal.

However, it should be noted that the dispersion at shorter load durations is larger for the numerically analysed results than for the analytically processed experiments. This can be annotated to the tiny difference in deformations that arise at higher interlayer shear moduli. The difference in displacement deflection between  $G_{SG}$  of 50 N/mm<sup>2</sup> and 500 N/mm<sup>2</sup> is restricted to less than 7 % for the small bending setup (see Figs. IV.40 and IV.41). A limited change in measured deformation, therefore results in a considerably different analysed shear modulus. Although this is also valid for the analytical analysis, the numerical analysis was based on a FE model with the average glass thickness of the entire series instead of the actual thickness of each specimen. This was necessary to limit the amount of simulations, although this slightly reduces the accuracy of the analysis.

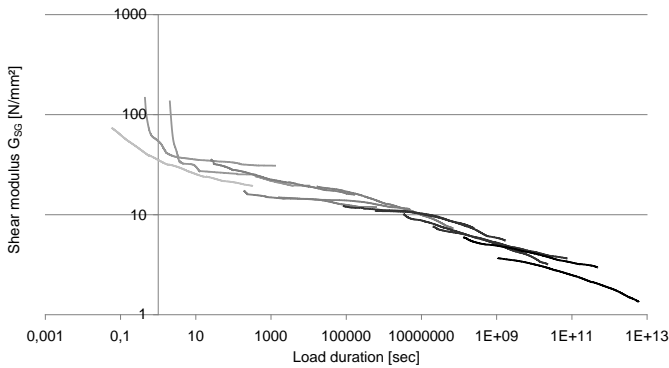


**Figure IV.47: Numerically analysed shear modulus of the SentryGlas interlayer  $G_{SG}$  from bending creep experiments on sample series C (3000 mm x 360 mm)**

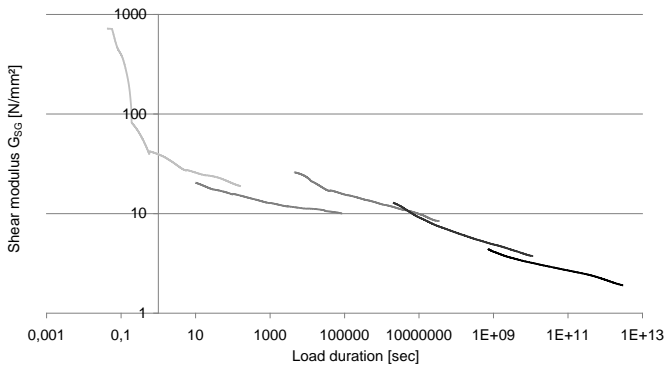


**Figure IV.48: Numerically analysed shear modulus of the SentryGlas interlayer  $G_{SG}$  from bending relaxation experiments on sample series C (3000 mm x 360 mm)**

Although the slightly lower results of the shear modulus from the larger bending experiments at shorter load durations visible in Figs. IV.47 and IV.48 compared to the results from the smaller bending experiments on series B and E, the curves display a comparable result. It should also be noticed, once again, that each line in

the above graphs already represents the mean value of four identical experiments, each analysed separately.

### 3 Discussion

In this chapter, the experimental results presented in Chapter III were further analysed. First, the time-shift constants for a linear visco-elastic WLF-time shift of the results were determined by comparing the load duration at the end of an experiment, with a certain experimental stiffness, to the load duration with the same experimental stiffness at a higher temperature. For SG, the experimentally deduced values ( $C_1 = 135$ ;  $C_2 = 760$  °C ;  $T_{ref} = 20$ °C) differ from the values which could be found in literature ( $C_1 = 135$ ;  $C_2 = 600$  °C;  $T_{ref} = 25$  °C) [Belis 2005] [Bennison et al. 2008], but they yield better results. With the model of Bennison et al., the results at higher temperature are shifted too far to the right, causing a clear gap between the different curves. The latter time shift is represented in Fig. IV.49, which shows the same averaged results as presented in Fig. IV.35 in which the shear modulus is time-shifted with the found shift constants.

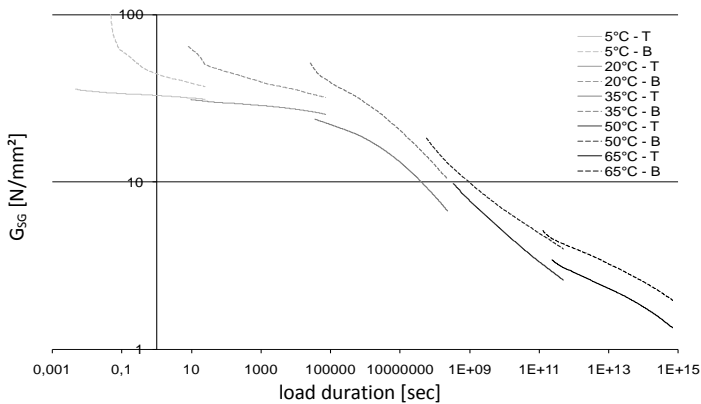


**Figure IV.49: Correlation between the shear modulus of the interlayer averaged over all bending (B; dotted lines) and over all torsion results (T; continuous lines), and the load duration, with WLF-time shift with time-shift constants from literature ( $C_1 = 135$ ;  $C_2 = 600$  °C;  $T_{ref} = 25$  °C)**

In a second step, the results were converted to an equivalent thickness. This should have lead towards an easy usable property for the use in mechanical calculations, but as was already clear from the representation of the results as a proportional stiffness, these values are highly regulated by the applied loading condition. E.g. even with equal thickness composition, the influence of the span of an element subjected to bending is very significant. Deriving the torsional stiffness from an equivalent bending thickness seems impossible.

Therefore, the results were further converted into a correlation between the shear modulus of the interlayer and the load duration, because it ought to be insensitive to the applied loading conditions. At first, this was done with existing analytical models, which especially use the shear modulus to determine the mechanical behaviour of laminated elements.

For bending, the theory of Wölfel was used, which forms the basis behind the method to calculate the equivalent thickness, but which retains the possibility of inserting the actual loading conditions and mechanical properties of the composing materials (see § IV.1.3.2). By doing so, the analysed results are interchangeable, even with the torsion results when using the theory developed by Scarpino (see § IV.1.3.1). With the latter, the torsional stiffness of a laminated glass element can be determined. Both methods were used in a reversed way, reproducing the shear modulus of SentryGlas in function of the temperature and the load duration.

Because it was uncertain which was the influence of the small deviations between the experimental setup and the analytical models, FE models were built to simulate the real setup accurately. As a result, e.g. also the influence of the small parts protruding the supports was taken into account. With the FE analysis, the test results could finally be used to develop the relation between the shear modulus and the load duration at the reference temperature of 20 °C. Fig. IV.50 represents all these results in one single graph (see also Appendix O).

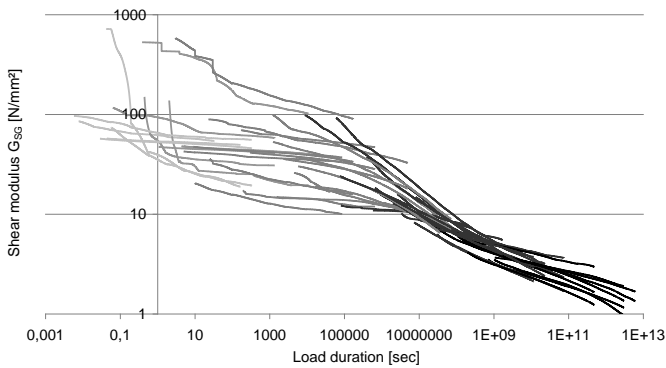


**Figure IV.50: Numerically deduced values for the shear modulus from all experimental results**

In Chapter V, these resulting interlayer shear modulus with rather large variation are simplified into a usable material model for the interlayer material.



# Chapter V: SentryGlas<sup>®</sup> material model

In this section, the results of the previous chapter are summarised in a single material model. In the first paragraph, the proposed material model is built, while in the second paragraph, it is compared to material properties for SG from literature. In the next paragraph, a number of experiments are simulated and recalculated based on the composed material model and compared with the experimental results.

## 1 Material model

### 1.1 Rheology

The time dependent behaviour of a visco-elastic material can be described using simplified rheological models [Schuler 2003]. These idealised, mechanical models are composed by a specific combination of linear springs and viscous dampers. The elastic component is characterised by the springs, which behave according to the Hooke's law summarised in Eq. (V.1), while Eq. (V.2) presents the theoretical behaviour of a viscous damper.

$$\sigma_s = E \cdot \varepsilon_s \quad (V.1)$$

$$\sigma_d = \eta \cdot \dot{\varepsilon}_d = \eta \cdot \frac{d\varepsilon_d}{d \text{ time}} \quad (V.2)$$

In Eq. (V.1), the stress in the spring  $\sigma_s$  is proportional to the elastic constant  $E$  and the strain in the spring  $\varepsilon_s$ . Eq. (V.2) indicates that the stress in the damper  $\sigma_d$  is proportional to the viscosity of the material  $\eta$  and the time derivative of strain  $\dot{\varepsilon}_d$ , as depicted visually in Fig. V.1.

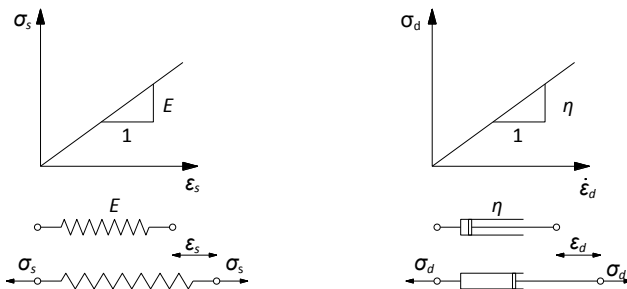


**Figure V.1: Basic rheological components: Linear elastic spring (left); Linear viscous damper (right)**

When combining these two basic elements, a mathematical description appears for creep and relaxation, respectively. A parallel combination leads to a so-called Kelvin-Voigt model for which the creep deformation under constant stress can be calculated based on Eq. (V.4). This is deduced from the sum of Eqs. (V.1) and (V.2) with equal strain because of the parallel positioning of the elements.

$$\sigma = E \cdot \varepsilon + \eta \cdot \dot{\varepsilon} = \sigma_0 \tag{V.3}$$

$$\varepsilon(\text{time}) = \frac{\sigma_0}{E} \left[ 1 - \exp\left(-\frac{E}{\eta} \cdot \text{time}\right) \right] \tag{V.4}$$

A linear spring and damper in series corresponds to a Maxwell model and can be used to determine the relaxation stress in a material under constant strain with Eq. (V.6). The stress in both the spring and the damper remains equal due to their position. Both a single Kelvin-Voigt element and a Maxwell element are represented in Fig. V.2.

$$\dot{\varepsilon} = \frac{\dot{\sigma}}{E} + \frac{\sigma}{\eta} = 0 \tag{V.5}$$

$$\sigma = \sigma_0 \cdot \exp\left(-\frac{E}{\eta} \cdot \text{time}\right) \tag{V.6}$$

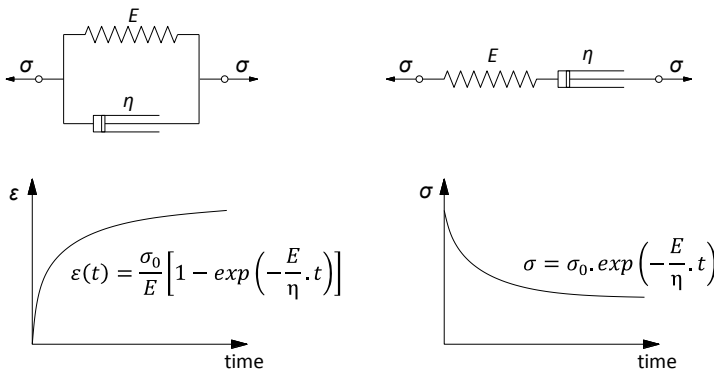


**Figure V.2: Kelvin-Voigt model for creep (left); Maxwell model for relaxation (right)**

More complex time-dependent material behaviour can be approximated by combining multiple Kelvin-Voigt elements in series with a spring, or a number of Maxwell elements in parallel with a spring. Fig. V.3 represents these more complex models for which the creep and relaxation function can be defined and described according to Eqs. (V.7) and (V.8), respectively.

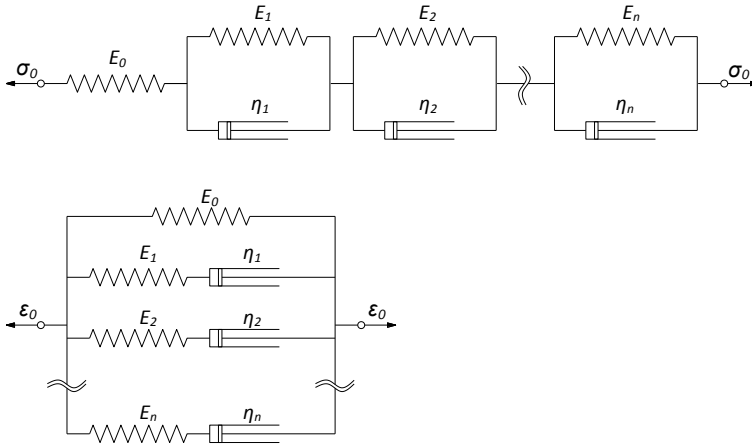


**Figure V.3: Combination of multiple elements for the approximation of more complex time-dependent material behaviour: Creep model with multiple Kelvin-Voigt elements (upper); Relaxation model with multiple Maxwell elements (lower)**

$$J(\text{time}) = \frac{\epsilon(t)}{\sigma_0} = \frac{1}{E_0} + \sum_{i=1}^n \frac{1}{E_i} \left( 1 - \exp\left(-\frac{E_i}{\eta_i} \cdot \text{time}\right) \right) \quad (\text{V.7})$$

$$E(\text{time}) = \frac{\sigma(\text{time})}{\epsilon_0} = E_0 + \sum_{i=1}^n E_i \cdot \exp\left(-\frac{E_i}{\eta_i} \cdot \text{time}\right) \quad (\text{V.8})$$

The last model is also referred to as the generalised Maxwell model, or the Maxwell-Weichert model. It is already used in literature to describe the visco-elastic mechanical behaviour of PVB and SG [Bennison et al. 1999], [Belis 2005] and [D'Haene & Savineau 2007] and therefore, it is also employed in the next section § V.1.2 to approach the numerically analysed experimental results.

The above mentioned models assume a linear visco-elastic behaviour of the material. Their instantaneous and delayed elastic strains are thus linearly proportional to stress. Generally, this is a good assumption for modest stresses, and accompanying small strains. Based on the rather large variation of the experimentally determined  $G_{SG}$  (see Fig. IV.50 and Appendix O), it is very unlikely that the use of more complex material models will yield a significant better approximation of the results.

Additionally, the difference in stress level in the three test setups (see Appendix N) does not seem to lead to remarkable differences in the material properties, which indicate the absence of non-linear stress-strain behaviour. Furthermore, the goal of this research is also to provide a practical model of the interlayer material to

predict the mechanical behaviour of a laminated glass element. Based on Figs. III.20 and III.22, it seems that relatively small inaccuracies of the interlayer stiffness will not directly lead to large differences in overall mechanical behaviour of the element. In [Moore & Turner 2001] it is even stated *'it is questionable whether the response to a stress change will ever be quantifiable via non-linear viscoelastic theory, mainly because crucial facts are non derivable from the relaxation or creep experiments.'*<sup>1</sup>

## 1.2 SG material model

In paragraph § IV.3, all results were summarised in Fig. IV.50. Unfortunately, the thousands of instantaneous values for the interlayer shear modulus deriving from the measured data point of the experiments are impracticable. Consequently, they are transformed and simplified into a single series of terms which can be inserted in a generalised Maxwell model and time-shifted with a WLF-function to describe the entire visco-elastic behaviour of SG.

Firstly, the results of the six different experimental configurations are averaged at the six main experimental temperature levels. Because the shear modulus of the interlayer is always represented with a double logarithmic scale, the mean value is calculated with Eq. (V.9) for each load duration. Accordingly, the highest values do not lead towards an overestimation of the actual properties. Fig. V.4 depicts the resulting averaged curves in red.

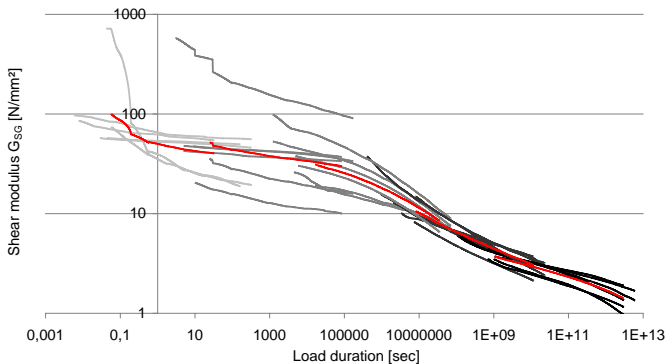


**Figure V.4: Numerically analysed shear modulus of SG for a reference temperature of 20 °C with averaged results  $G_{SG,mean}$  in red**

The mean value was preferred over the characteristic value or the lower limit because it is unclear whether the scattering of the results initiate from material inhomogeneities or from inevitable experimental inaccuracies. Additionally, this mean value can be more easily compared to test results described in literature, which often seem to be based on experiments on only one sample.

<sup>1</sup> [Moore & Turner 2001] p. 70

$$G_{SG,mean} = 10^{\left(\frac{\sum \log(G_{SG,i})}{n}\right)} \quad (V.9)$$

In spite of the relatively large scatter in results, especially from the experiments performed at 20°C, the averaged curves almost perfectly fuse together in a smooth mastercurve. It was therefore relatively easy to approach the results with a limited number of points, which could further be used to fit the Maxwell series.

Fig. V.5 depicts the chosen points in black, which were divided evenly over the logarithmic load duration. At the beginning of the first curve, one point was chosen in the close vicinity of the averaged resulting curve, because it displayed a twist in the graph mainly caused by one test series. Also at the transition between the first and second curve, three points needed to be aligned, because the head of the curve retrieved from the experiments at 20 °C was slightly higher than the tail of the curve retrieved from the experiments at 5 °C. As the stiffness cannot rise when the load duration is increased, therefore, some chosen points were slightly adapted. Finally, also at the transition regions between the other curves, where two different values were available for the same load duration, the mean value of both results was calculated.

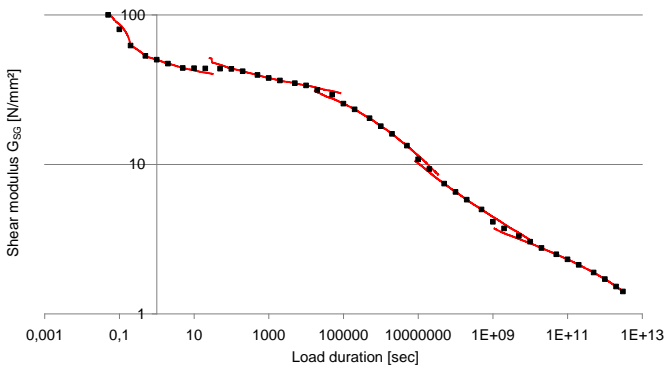


**Figure V.5: Approximation of the averaged numerically analysed shear modulus of SG by carefully chosen points**

This limited amount of data points can be fitted by a Maxwell series which describes the experimental results. By inputting these data points in Abaqus as relaxation test results, the best fitting Maxwell series was calculated [Abaqus 2008]. The only unknowns that have to be determined first are the instantaneous shear modulus of SG  $G_{SG,0}$  and the long term shear modulus  $G_{SG,\infty}$ .

No exact method exists to extract these values directly from the experimental results, because it is impossible to perform a static test with a load duration of 0 sec or an infinite time. Furthermore, because of the complexity of the material behaviour, it is impossible to precisely predict what could be the behaviour beyond the tested limits. It is therefore necessary that these values are chosen conservatively.

Initially, the lower value  $G_{SG,\infty}$  was chosen to be close to 0 N/mm<sup>2</sup> as a safe assumption. For the upper value  $G_{SG,0}$ , 375 N/mm<sup>2</sup> can be found in literature [Belis 2005] [Bennison et al. 2008]. Nevertheless, this value seems too high compared to the averaged experimental results, where the maximum deduced shear modulus does not exceed 100 N/mm<sup>2</sup>. It seems therefore not appropriate to use 375 N/mm<sup>2</sup> and  $G_{SG,0}$  was chosen to be 150 N/mm<sup>2</sup>, a value reasonably little above the highest averaged result.

When recalculating the SG shear modulus with the Maxwell series from Abaqus with the above mentioned input, it is clear that the input values are well approximated. The green and blue curves in Fig. V.6 depict these results for a Maxwell series with 10 and 13 terms respectively. Up to a load duration of about 10<sup>7</sup> seconds, both curves are quasi identical, but above this load duration, the green curve starts to fluctuate around the input values. Fig. V.7 represents the undulations more in detail.

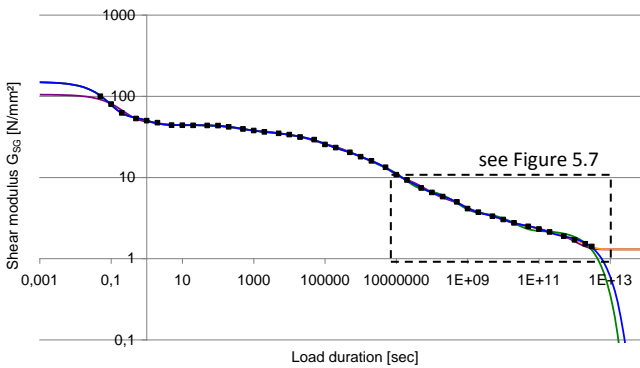


**Figure V.6:** SG shear modulus  $G_{SG}$  at  $T_{ref} = 20$  °C: input from experimental results (black markers); Maxwell series with 10 terms (green); Maxwell series with 13 terms (blue); Maxwell series with 13 terms but with  $G_{SG,\infty} = 1.3$  N/mm<sup>2</sup> (orange); Maxwell series with 13 terms but with  $G_{SG,0} = 105$  N/mm<sup>2</sup> and  $G_{SG,\infty} = 1.3$  N/mm<sup>2</sup> (purple)

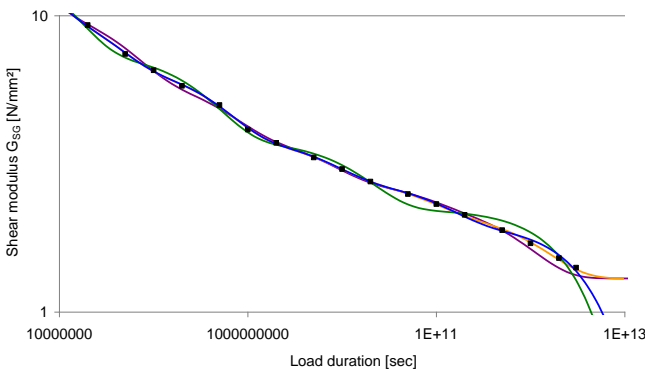


**Figure V.7:** Detail of the shear modulus of SG versus time curve from Figure V.6

The detail in Fig. V.7 also demonstrates that the blue curve from the Maxwell series with 13 terms approximates well the black markers, which embody the input points. The orange curve represents the results from a Maxwell series with 13 terms and a  $G_{SG,\infty}$  of 1.3 N/mm<sup>2</sup>, a value only slightly underneath the minimal test result. This curve follows the input values slightly closer, but provides an implausibly high value outside the tested load duration. Although the admissible application range of the model will be clearly defined, it seems safer not to use this last model which probably overestimates the actual stiffness at too long load durations. By doing so, there is no need to verify if the calculated or simulated loading case complies with the application scope of the model.

Finally, the purple curve in Figs. V.6 and V.7 represent the values of a Maxwell series with  $G_{SG,0} = 105$  N/mm<sup>2</sup> and  $G_{SG,\infty} = 1.3$  N/mm<sup>2</sup>. Although this provides a safe value for too short load durations, this curve is not selected. Not only does it yield a more undulating shape than the blue curve, it also leads to a poor approximation of the input both at the beginning and the end of the tested load duration range.

For these reasons, the blue curve is preferred, as being the resulting Maxwell series with 13 terms nicely fitting the input points in a safe way with the chosen  $G_{SG,0} = 150$  N/mm<sup>2</sup> and  $G_{SG,\infty} = 0$  N/mm<sup>2</sup>. The values of the Maxwell series are summarised in Table V.1. With these, the shear modulus of the interlayer can be calculated for any load duration and temperature within the tested range with Eqs. (V.10) up to (V.12). The valid temperature range of the model corresponds to the tested interval of 5 °C up to 65 °C. Also when the model yields a shear modulus above 100 N/mm<sup>2</sup> or below 1.4 N/mm<sup>2</sup>, the load situation falls outside the application range of our model.

**Table V.1: Proposed Maxwell series for SG:  $G_{SG,0} = 150$  N/mm<sup>2</sup>;  $G_{SG,\infty} = 0$  N/mm<sup>2</sup>;  $T_{ref} = 20$  °C;  $C_1 = 135$  and  $C_2 = 760$  °C; Valid in the temperature range 5 °C – 65 °C**

$i$	$G_{SG,i} / G_{SG,0}$	$\tau_i$ [sec]
1	5.9320E-01	6.5173E-02
2	1.1220E-01	9.6690E-01
3	-5.1988E-03	8.2310E+01
4	4.9333E-02	4.4630E+02
5	2.0831E-02	5.6480E+03
6	6.1392E-02	6.5132E+04
7	4.3697E-02	5.0406E+05
8	5.0251E-02	4.9084E+06
9	2.9005E-02	3.3452E+07
10	1.9283E-02	5.2363E+08
11	7.3690E-03	7.7396E+09
12	5.4495E-03	1.2613E+11
13	1.3155E-02	8.3316E+12

$$G_{SG}(time) = G_{SG,\infty} + \sum_{i=1}^n G_{SG,i} \cdot e^{-\frac{time}{\tau_i}} \quad (V.10)$$

$$\log a_T = -\frac{C_1 \cdot (T - T_{ref})}{C_2 + (T - T_{ref})} \quad (V.11)$$

$$a_T = \frac{\tau(T)}{\tau_{ref}(T_{ref})} \quad (V.12)$$

In Table V.2, the shear modulus is calculated for different load durations at several temperature levels within the tested range. For the load situations which fall out the application scope of our model, the values were replaced by n/a. These material properties can be used directly to perform an elastic calculation of the mechanical behaviour of laminated glass based on existing analytical models. It can also be used to avoid the long calculation time of a numerical visco-elastic simulation.

**Table V.2: Values for the shear modulus of SG  $G_{SG}$  for seven load durations at different temperature levels**

$G_{SG}$ [N/mm <sup>2</sup> ]	1 sec	3 sec	1 min	1 hour	1 day	1 month	10 years
5 °C	n/a	n/a	74	44	42	35	20
10 °C	n/a	n/a	50	44	37	30	13
15 °C	71	56	44	40	33	22	7.9
20 °C	50	45	44	36	27	15	5.4
25 °C	44	44	40	31	19	9.2	3.6
30 °C	44	42	36	23	13	6.1	2.8
35 °C	40	37	31	17	8.1	4.1	2.2
40 °C	36	34	24	11	5.7	3.2	1.8
45 °C	32	28	18	6.9	3.8	2.5	n/a
50 °C	25	21	12	5.0	3.0	2.0	n/a
55 °C	18	15	7.4	3.5	2.4	1.5	n/a
60 °C	13	9.6	5.4	2.8	1.9	n/a	n/a
65 °C	8.1	6.4	3.7	2.2	1.4	n/a	n/a

From these values, also the Young's modulus and Poisson's ratio can be deduced by using Eqs. (V.13) and (V.14). The bulk modulus of SG  $K_{SG}$  is a constant and can be taken equal to 2000 N/mm<sup>2</sup> [Belis, 2005]. The values for the same load durations and temperature levels presented in Table V.2 are provided in Appendix P.

$$E_{SG}(time, T) = \frac{9 \cdot K_{SG} \cdot G_{SG}(time, T)}{3 \cdot K_{SG} + G_{SG}(time, T)} \quad (V.13)$$

$$\nu_{SG}(time, T) = \frac{3 \cdot K_{SG} - 2 \cdot G_{SG}(time, T)}{2 \cdot (3 \cdot K_{SG} + G_{SG}(time, T))} \quad (V.14)$$



## 2 Comparison with existing material models

In this paragraph, the proposed material model for SG is compared with the models introduced in § II.2.2. In total, three different models were available. For the first two, a Maxwell series with twelve terms in combination with the WLF time-shift constants was provided for a linear visco-elastic material model [Belis 2005] and [Bennison & Gizzi 2007]. The third and last model provides some material properties for different loading durations at a number of temperature levels in the form of some tables [Bennison et al. 2008] (see Fig. II.7).

The first available material model from the interlayer producer dates from 2005 and was communicated to Belis, who published it in [Belis 2005]. It concerned a Maxwell series with 12 terms describing the master curve for SG at the reference temperature of 25 °C. Additionally to the Maxwell series, it was assumed that the long term value would never drop below the so-called *plateau value* for  $G_{SG}$  of 2 N/mm<sup>2</sup>. The comparison between this model and our model is presented in the next figure.

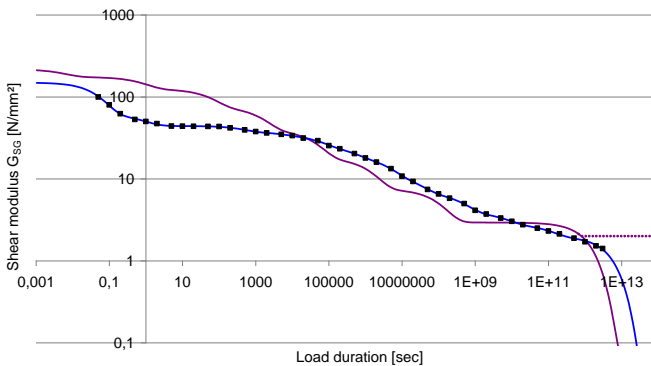


**Figure V.8: Shear modulus of SG at 20 °C: proposed material model (blue); first material model from literature (purple) with indication of the plateau-value of 2 N/mm<sup>2</sup> [Belis 2005]**

Initially, our model seems to underestimate the material behaviour as predicted by the producer. Then, for a certain period there is a slight overestimation, followed by a final underestimation at the end of the mastercurve with the plateau value of 2 N/mm<sup>2</sup>. The latter currently seems unsafe, because it was experimentally demonstrated that the shear modulus can descend underneath this value and nothing indicates that the shear modulus would stop lowering pointing this particular stiffness region.

Later on, in 2007, a new Maxwell series was presented during a workshop at GPD [Bennison & Gizzi 2007], which was not published in literature. Fig. V.9 depicts the comparison between this model and ours.

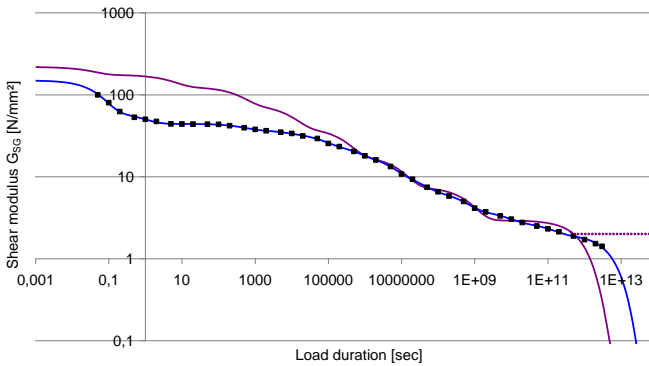


**Figure V.9: Shear modulus of SG at 20 °C: proposed material model (blue); second material model from literature (purple) with indication of the plateau-value of 2 N/mm<sup>2</sup> [Bennison & Gizzi 2007]**

Basically, this is the same as the first model, with exactly the same values for  $G_i / G_0$  but with other reduced times  $\tau_i$ , meaning that almost the entire curve is shifted to the right. Only at load durations above 1E+10 seconds, the new model renders slightly lower values than the first model. Due to this modification, our model yields almost constantly lower material properties, and at the points where our model is higher, this is mainly caused by undulations of the material model from [Bennison & Gizzi 2007]. In spite of these deviations, the close fitting of both models in the second half of the mastercurves in Fig. V.9 is remarkable.

Only in 2008, the producer published some values for the material properties of SG in literature [Bennison et al. 2008]. In this, some values were summarised in a table for different temperatures between 10 °C and 80 °C and for load durations between 1 second and 10 years (see Fig. II.7). The shear modulus was also calculated with our model for these values and compared to the properties from literature in Fig. V.10.

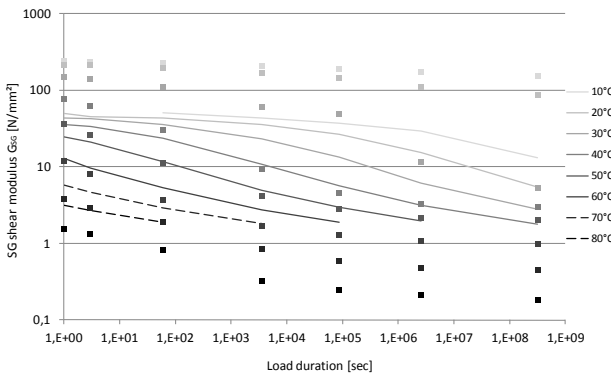


**Figure V.10: Shear modulus of SG at different temperatures: proposed material model (continuous curves); material properties from literature (square markers) [Bennison et al. 2008]**

A first observation is that a plateau value does no longer appear, which seems logic, especially when stated that the third material model from literature is also applicable for a load duration of 10 years at 80 °C. This is well above the maximal temperature of 60 °C to which the previous two models were accepted to be accurate.

A second important observation seems to be the non thermorheologically simple material model used to compose the published material properties. This is clearly visible, when time shifting the given values. The properties time shifted with the determined time-shift constants  $C_1 = 135$  and  $C_2 = 760$  °C, are represented in Figure V.11. Also shifting with other time-shift constants cannot lead towards a smooth mastercurve representing a thermorheologically simple behaviour as presented in Fig. IV.1, because it is clearly visible that the curves at different temperatures can impossibly be simply moved horizontally to overlap a curve at an other temperature.

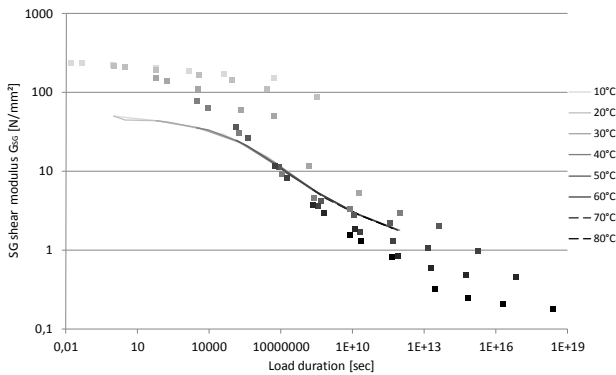


**Figure V.11: Time shifted shear modulus of SG at different temperatures: proposed material model (continuous curves); material properties from literature (square markers) [Bennison et al. 2008]**

Although it is evident that a linear visco-elastic material model can only be an approximation of reality, the experimental research indicated that it could be an easy and reliable tool. Experimental results can always be described in a better way by more complex models, but it can be discussed whether this enhances the applicability of the model. Furthermore, it should be noticed that a load duration of 10 years at 80 °C corresponds to a load duration of 1 day at a temperature above 110 °C according to the determined time shift function. This seems irreconcilable with the melting temperature of SG, which is accepted to be only 94 °C [DuPont 2008].

When comparing our material model with this last model from literature, again lower properties are rendered by our model at short load durations and/or lower temperature levels. Consequently, it might be erratically concluded that our analysis is based on too safe assumptions. However, our model renders higher

values at temperatures above 50 °C. Additionally, the lowest possible proportional stiffness was never reached, not even during the torsion experiments on glass/PVB laminates. This indicates that the assumptions were most likely not too conservative.

The significance of the difference between the models, importantly depends on the geometry of the element and the loading situation as well. When looking at certain load durations, the differences can be interpreted by comparing the shear modulus with the expected proportional stiffness represented in Fig. V.12.

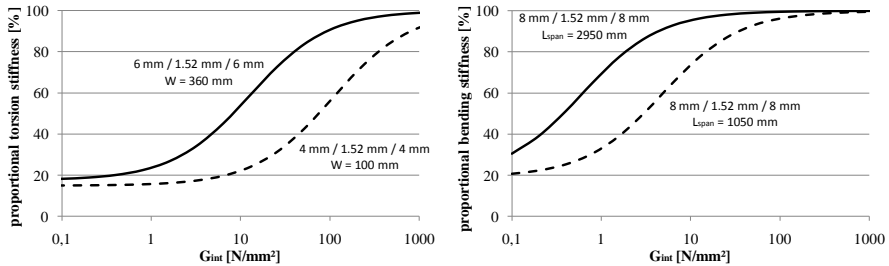


**Figure V.12: Proportional stiffness in function of the shear modulus of the interlayer: torsional stiffness (left); bending stiffness (right)**

For a load duration of e.g. 3 sec at 20 °C, our model predicts a shear modulus for SG  $G_{SG}$  of 45 N/mm<sup>2</sup>, which is well below the outcome of the three models from DuPont, varying between 125 and 211 N/mm<sup>2</sup>. It is clear that this difference has a tremendous impact on the torsional stiffness of an element with a limited width, while the influence is much less pronounced for a width of 360 mm and above. For the proportional bending stiffness of an element with a span of over 1 m, the effect is restricted to less than 10 %.

Furthermore,  $G_{SG} = 1.9$  N/mm<sup>2</sup> for our model for a load duration of 1 day at 60 °C, while the first two models from the producer reach their so-called plateau-value of 2 N/mm<sup>2</sup> at this point and the last model yields a value of 1.29 N/mm<sup>2</sup>. Contrary to the previous example, these different values result to the highest influence on the proportional stiffness for the bended elements with a large span, although the influence on the bending stiffness with a span of 1 m could certainly not be neglected either. By further reducing the span, e.g. for a glass tread spanning only about 300 mm, the effect is further reduced. The impact of the difference between 1.29 and 2 N/mm<sup>2</sup> on the proportional torsional stiffness of an element with a span of only 100 mm is almost negligible, but it raises when increasing the width.

### 3 Recalculation with proposed material model

Finally, the proposed material model is checked by recalculating the experiments. This way, the acceptability of the chosen assumptions and averaging is verified by comparing different calculation methods.

### 3.1 Numerical simulations with visco-elastic material model

First, visco-elastic simulations were performed, based on the numerical models described in § IV.2.1. The Maxwell series is implemented and visco-elastic simulations were performed for a load duration of 1 day at temperatures of 5, 20, 35, 50 and 65 °C. For torsion, the torsional deformation was applied in 10 sec and then, the relaxation was measured by monitoring the torque and the vertical displacements of four points onto the glass surface as discussed in § IV.2.3. The results are presented as a proportional stiffness in function of the load duration at the reference temperature  $T_{ref}$  of 20 °C. The continuous grey curves are the actual results from the torsional creep and relaxation experiments on sample series A, while the coloured markers depict the numerical stiffness at the end of each simulated time increment.

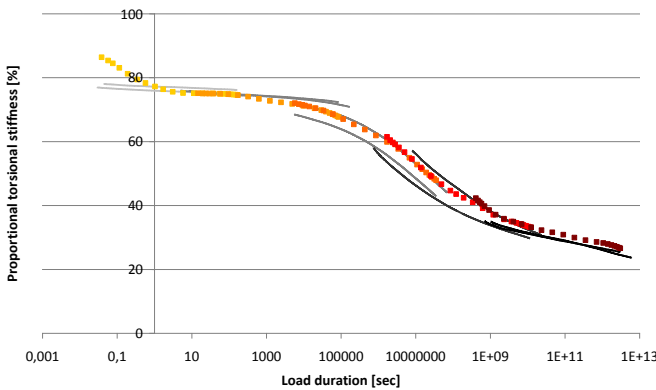


**Figure V.13: Proportional torsional stiffness for torsion experiments on series A: experimental results (continuous grey curves); numerical results from visco-elastic simulations (coloured markers)**

In general, the torsional experiments are well approximated by the simulations. Only at short and long load durations, the test values are overestimated by the simulations, which results in a slightly unsafe prediction of the actual torsional stiffness. However, this could be expected, because the model is based on averaged results of all six loading configurations and not on the lowest outcome. It is therefore important to state that the model is set up as an average approximation as close as possible to reality.

The small bending experiments were only simulated for test series B, because the differences in proportional bending stiffness compared with the experiments on series E are negligible. A laminated plate with a width of 180 mm is therefore subjected to 3-point bending. The load of 147 N was applied in 10 sec to the centre of the laminate, spanning 1050 mm, after which the deformations were registered for a creep duration of 1 day. The proportional bending stiffness is represented in Fig. V.14 for both the test results of bending experiments on series B and E (grey continuous lines), and the numerical outcome (coloured markers).

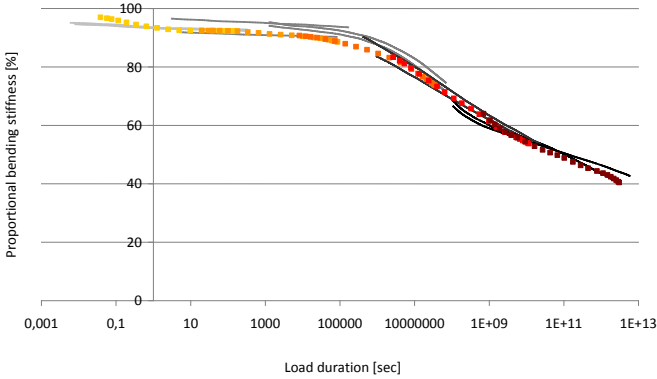


**Figure V.14: Proportional bending stiffness for small bending experiments on series B and E: experimental results (continuous grey curves); numerical results from visco-elastic simulations (coloured markers)**

Again, the simulated results closely fit the experimentally measured stiffnesses. In general a slight underestimation of the actual stiffness of the small bending experiments is observed. However, the proportional deviation remains restricted to a maximum of 6 %.

Finally, also the large bending experiments are simulated with the visco-elastic material model. Again, the load was gradually increased in 10 sec until the experimental load was reached, and after this, the creep deformations were simulated for a load duration of 1 day. Fig. V.15 depicts the experimental and numerical results.

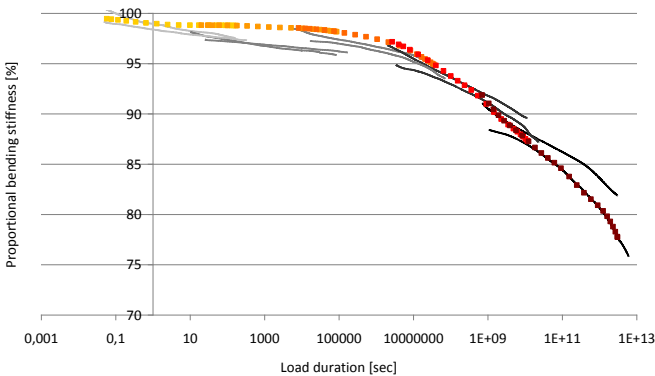


**Figure V.15: Proportional bending stiffness for large bending experiments on series C: experimental results (continuous grey curves); numerical results from visco-elastic simulations (coloured markers)**

Contrary to the previous two graphs, the origin of the Y axis does not correspond to a proportional stiffness of 0 % due to the high stiffness values obtained even at long load durations. Therefore, the deviations between the experimental and

numerical outcome might seem bigger although the largest relative overestimation is limited to only 3 %.

### 3.2 Numerical simulations with elastic material behaviour

Because visco-elastic calculations consume considerably more computational time than elastic calculations, the latter were also executed based on the instantaneous elastic properties which can be extracted from the Maxwell series by applying Eqs. (V.10) up to (V.14). This way, the validity of an extracted instantaneous shear modulus  $G_{SG}(t, T)$  at temperature  $T$  and for load duration  $time$ , can be checked.

**Table V.3: Instantaneous material properties for SG after several load durations time at  $T_{ref} = 20\text{ }^{\circ}\text{C}$**

$time$ [sec]	$G_{SG}(time, T_{ref})$ [N/mm <sup>2</sup> ]	$E_{SG}(time, T_{ref})$ [N/mm <sup>2</sup> ]	$\nu_{SG}(time, T_{ref})$ [-]
0.1	79	233	0.481
1	50	149	0.488
10	44	131	0.489
100	43	129	0.489
1000	38	112	0.491
10000	34	100	0.492
100000	35	77	0.494
1000000	18	54	0.496
10000000	11	33	0.497
100000000	6.5	19	0.498
1E+09	4.2	13	0.499
1E+10	3.0	9.1	0.499
1E+11	2.3	7.0	0.499
1E+12	1.8	5.3	0.499

The material properties were calculated for a number of logarithmically distributed load durations  $t$  at the reference temperature  $T_{ref}$  and are summarised in Table V.3. These values were entered into the numerical model and elastic simulations were performed. Because these simulations no longer display a time dependent behaviour, the load was applied in a single step and the stiffness was derived at the end of the calculated increment. These numerical results are also compared to the experimental results, which are shown in Figs. V.15 to V.17.

The simulations yield quasi identical results compared to the visco-elastic simulations presented in the previous paragraph (§ V.3.1). The numerical simulations follows the trends from the experimental proportional stiffness for both torsion and bending, and the deviation between experiment and simulation remain limited.

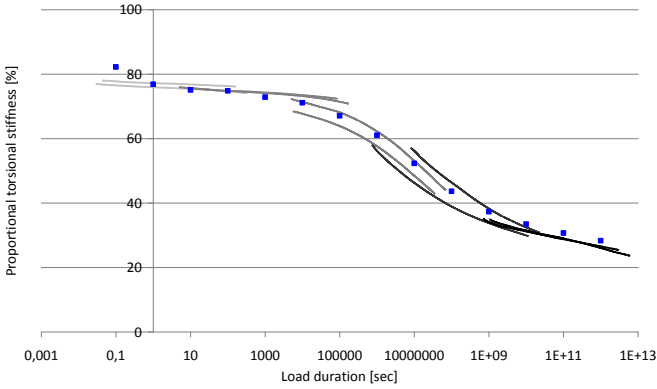


**Figure V.16: Proportional torsional stiffness for torsion experiments on series A: experimental results (continuous grey curves); numerical results from elastic simulations (blue markers)**

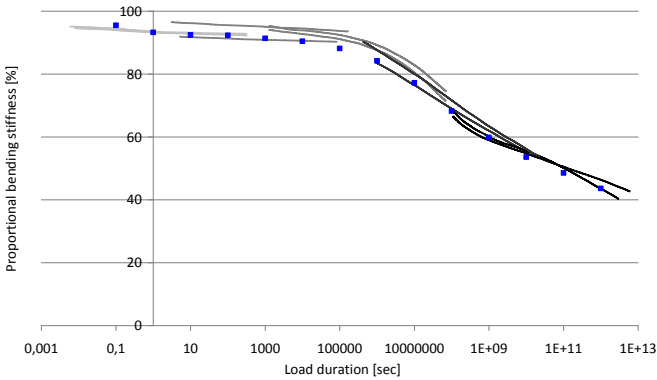


**Figure V.17: Proportional bending stiffness for small bending experiments on series B and E: experimental results (continuous grey curves); numerical results from elastic simulations (blue markers)**

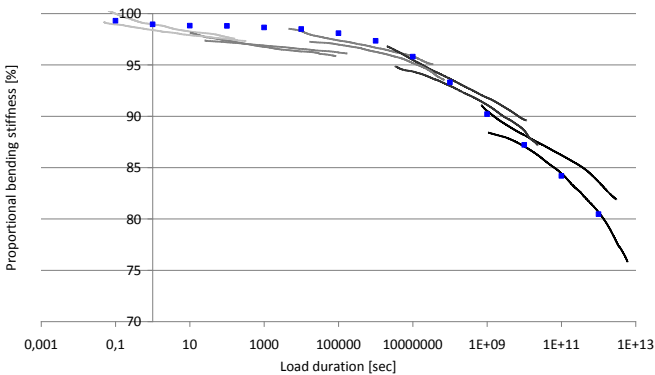


**Figure V.18: Proportional bending stiffness for large bending experiments on series C: experimental results (continuous grey curves); numerical results from elastic simulations (blue markers)**



### 3.3 Analytical calculations with elastic material behaviour

The same instantaneous material properties used in the previous paragraph § V.3.2, were also applied as input for the calculation of the laminated stiffness based on the analytical models from [Scarpino 2002] and [Wölfel 1987]. The derived proportional torsional stiffness is compared with the experimental stiffness in Fig. V.19.

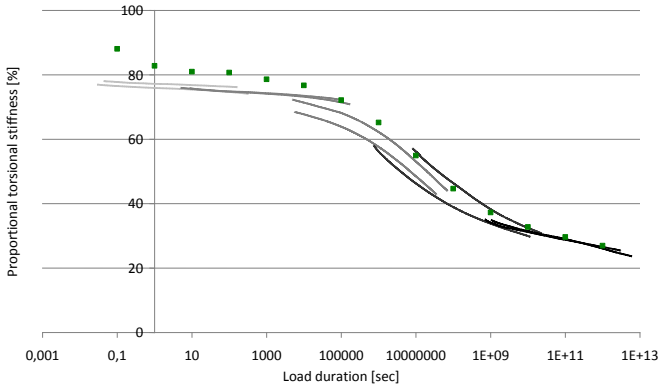


**Figure V.19: Proportional torsional stiffness for torsion experiments on series A: experimental results (continuous grey curves); theoretic results from elastic calculations (green markers)**

In general, the analytically calculated proportional stiffness is slightly overestimating the actually measured stiffness. When looking back at Fig. IV.38, this performs according to expectations because the analytical stiffness noticeably overrates the required torsional moment compared to the numerical simulations at values for the shear modulus of the interlayer between 10 N/mm<sup>2</sup> and 200 N/mm<sup>2</sup>. More than half of the calculated conditions, situated at shorter load durations, fit in this range. For longer load durations, and therefore also lower shear moduli, the curves approach each other more closely.

The theory of Wölfel, presented in paragraph § IV.3.1.2, was used to approach the bending experiments. As already pointed out by the comparison between the analytical model and the numerical simulations, presented in Figs. IV.39 to IV.41, the analytical proportional stiffness will be slightly lower than the numerical proportional stiffness. The analytical calculations, represented in Figs. V.19 and V.20, are slightly lower than the numerical results from Figs. V.16 and V.17 resulting in a somewhat safer approach. Nevertheless, the experimental results are also closely approached by the much easier analytical models with simple elastic input.

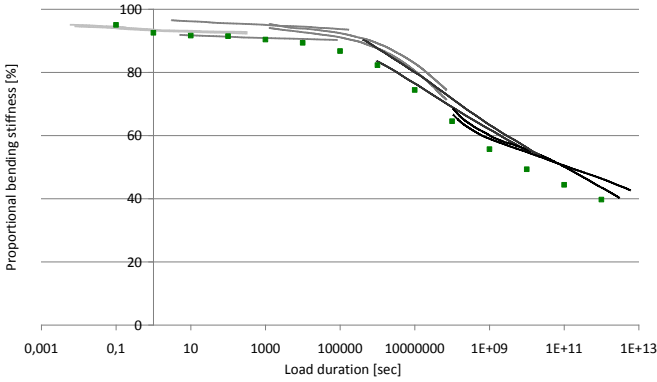


**Figure V.20: Proportional bending stiffness for small bending experiments on series B and E: experimental results (continuous grey curves); theoretic results from elastic calculations (green markers)**

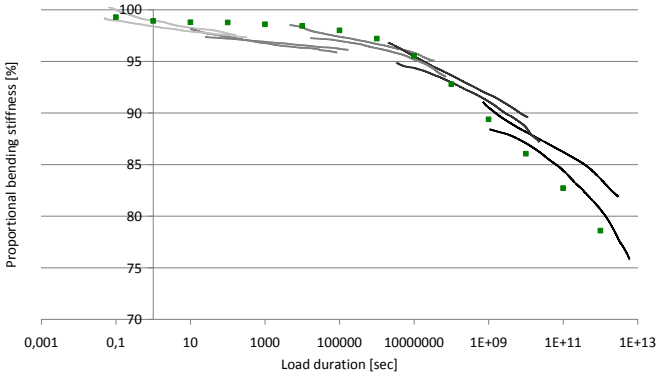


**Figure V.21: Proportional bending stiffness for large bending experiments on series C: experimental results (continuous grey curves); theoretic results from elastic calculations (green markers)**

## 4 Discussion

In this chapter, the experimental results are reduced into a workable material model for the visco-elastic behaviour of SentryGlas®. By firstly reducing the experimental output, a linear visco-elastic Maxwell model was developed. Doing so, much attention was given to rechecking the intermediate results. E.g. at the point where the instantaneous shear modulus  $G_{SG,0}$  and long term shear modulus  $G_{SG,\infty}$  had to be chosen, different Maxwell series were recalculated to assist in establishing a well-founded assumption. By extending the recalculated mastercurves beyond the tested time-range, not only the fitting to the input seemed important, but also a built-in safety in case the application scope of the Maxwell series is involuntary exceeded.

Compared to the previously published material properties of SentryGlas®, the proposed material yields similar behaviour. Although our proposed model clearly provides lower values at shorter load durations and lower temperatures, there does not seem a structural overconservative approach because the models approximate each other at longer load durations and higher temperatures. This is especially clear in Fig. V.9 for the theoretical load durations above 1 million seconds, at which the second Maxwell series from the producer really fluctuates around our proposed model.

Finally, the model is validated by performing both numerical simulations and analytical calculations. All these outcomes are compared to the experimental proportional stiffnesses and summarised in Figs. V.22 up to V.24.

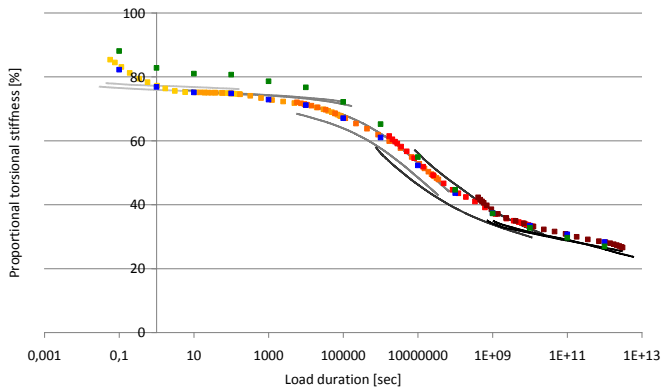


**Figure V.22: Proportional torsional stiffness for torsion experiments on series A: experimental results (continuous grey curves); numerical results from visco-elastic simulations (yellow, orange, red and brown markers); numerical results from elastic simulations (blue markers); theoretic results from elastic calculations (green markers)**

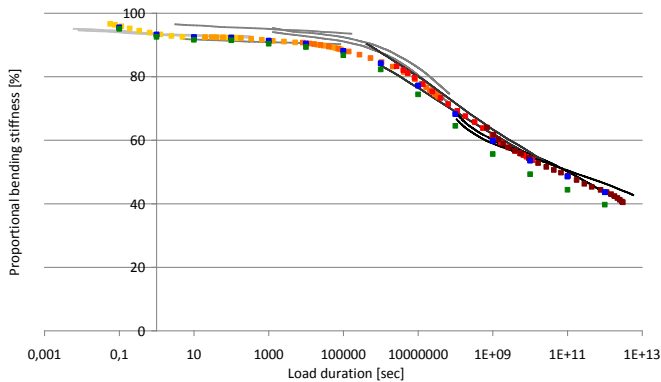


**Figure V.23: Proportional bending stiffness for small bending experiments on series B and E: experimental results (continuous grey curves); numerical results from visco-elastic simulations (yellow, orange, red and brown markers); numerical results from elastic simulations (blue markers); theoretic results from elastic calculations (green markers)**

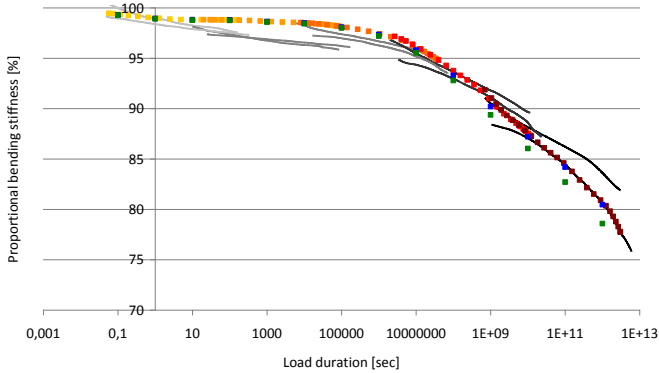


**Figure V.24: Proportional bending stiffness for large bending experiments on series C: experimental results (continuous grey curves); numerical results from visco-elastic simulations (yellow, orange, red and brown markers); numerical results from elastic simulations (blue markers); theoretic results from elastic calculations (green markers)**

In general, there are slightly larger deviations between the analytically calculated stiffness (green markers) and the experiments. Obviously, this is a direct consequence of the applied method for determining our material model, which is based on the numerically derived shear modulus. Nevertheless, both methods yield very acceptable results.

Although the analytically determined deformations should be approached with a slightly larger safety coefficient, the calculation can be performed faster by much less means compared to finite element simulations. The instantaneous material properties can easily be determined and the elastic simulations proved these are evenly reliable as more complex visco-elastic simulations. With the superposition principle of Boltzmann, even a combination of loading conditions can be composed by a simple superposition of the different loads. The deformation under e.g. a long term uniform self weight and a short term point load can be superimposed by adding the deformations from two separate calculations with two different instantaneous material properties.

An additional advantage of the elastic calculations, is the straightforward possibility to verify whether the loading condition goes together with the application range of the Maxwell series. Firstly, the temperature must be within the tested temperature range of 5 °C up to 65 °C. Secondly, the shear modulus  $G_{SG}(t, T)$  must lay between the two ultimately measured values, namely 1.4 N/mm<sup>2</sup> and 100 N/mm<sup>2</sup>. If the instantaneous shear modulus is lower than 1.4 N/mm<sup>2</sup>, no interaction at all should be taken into account. If it exceeds 100 N/mm<sup>2</sup>, it is safer to use this maximum value.

For more complex loading situations, for which e.g. no analytical models exist to approximate the mechanical behaviour of the laminated material, the more complex visco-elastic finite element simulations can be helpful.

# Chapter VI: Conclusions

---

Throughout the previous chapters, the mechanical behaviour of glass/SG laminates is investigated. The main conclusions are presented in this chapter. Finally, in the last paragraph, also a proposition for future research is made.

## 1 Conclusions

At the beginning of this research, three objectives were stated:

- Improvement of the understanding of the mechanical behaviour of laminated glass with a stiff interlayer under different loading conditions
- Determination of the visco-elastic material properties of SG
- Verification of the applied analysing techniques

Firstly, an experimental programme was composed. Relatively large laminated samples were preferred as they directly demonstrate the mechanical behaviour of an element under loading conditions which can be expected in reality. Consequently, the interlayer has also a realistic humidity level. For the investigation of the time and temperature dependent behaviour of the interlayer material, long duration experiments at different temperature levels seemed essentially. Firstly, to increase the temperature of the test sample, a technique with longitudinal IR-heaters was examined, but it was rather impossible to uniformly heat up a test specimen to an exact temperature level for a long period. Therefore, all test were performed inside a room with controlled environment.

The results of some preliminary test series with several loading configurations on old laminated samples, proved that no direct correlation exists between the proportional stiffness of the laminate on the one hand side, and a certain load duration at a temperature level on the other. These results had two important findings. Firstly, the stiffness of the laminated element based on experiments with a single test setup must be handled with care. An experimental proportional stiffness can not be used directly to predict the mechanical behaviour of a building component with identical load duration and temperature but with a divergent loading configuration. Secondly, the choice of test setup configurations can determine its capability to reveal changes in the mechanical behaviour of the interlayer material and thus its accuracy. To this insight, a complementary test programme was set up, which again confirmed the importance of the loading conditions and the geometry of the element.

A first step in the analyse of the results, was to find a correlation between the time and temperature dependency. Therefore, the results were time shifted with a

Williams-Landel-Ferry equation. By fitting the end of a double logarithmic stiffness-time curve with the beginning of a similar curve of the results at a higher temperature level, the shift constants were determined empirically. With  $C_1 = 135$  and  $C_2 = 760$  °C at  $T_{ref} = 20$  °C, values which slightly differ from values which could be found in literature, a smooth transition between the curves at different temperature levels became visible.

Furthermore, the results were transformed into an equivalent thickness and an  $\omega$  shear factor as proposed in [prEN 13474-3]. As could be expected based on the findings of the proportional stiffness analysis, the loading conditions and the geometry of the element had an important influence on these values as well. An experimental equivalent thickness can not be easily extrapolated to other situations.

Accordingly, the mechanical properties of the interlayer were deduced from the experimental results. The outcome was analysed based on both analytical models and numerical simulations. This showed that the shear modulus of the interlayer  $G_{SG}$  is only determined by the load duration and the temperature level. This makes the results interchangeable with other building components, e.g. four sided supported floor plates or laminated glass stiffeners.

By performing tests directly on laminated elements, the condition of the interlayer material is identical to real laminated glass elements in structural applications. As a consequence, the variation on the material properties is also influenced by uncertainties about the glass sheets. Consequently, there was a relatively large variation on the results, especially on the results at the lower temperatures. Nevertheless, the results could be used as the basis for a simplifying linear visco-elastic material model for SG. All tests performed at a certain temperature were averaged and the resulting five curves could be well approximated with a Maxwell series.

Finally, the proposed material model was also implemented in the different analysing techniques to recalculate the laminate stiffness. This validated the presented model, as well as the applied analysing techniques. The limited difference between existing analytical models and the numerical simulations indicated that the analytical models have a good reliability. Elastic material properties, extrapolated from the Maxwell series, can be used to perform simplified calculations or simulations, while the visco-elastic material model can be implemented in FE-software to simulate more complex situations.

## 2 Further research

Unfortunately this kind of extensive experimental research can impossibly be required for each new interlayer material or minor change to an existing one. It is therefore advisable to compare these outcomes to standardised dynamic analyses

more in detail. The latter can compare different materials relatively fast, and the influence on the stiffness of the interlayer from minor modifications to the material e.g. to enhance the adhesion to the glass surface can be verified quickly. [prEN 13474-3] gives a good start to a classification of interlayer materials to certain stiffness families, although the elaboration does not yet seem validated. Nevertheless, it would be very interesting if the test programme could be partially repeated with other stiff interlayers. Then twenty torsion tests are proposed for interlayer materials with a comparable stiffness to SG. This could provide a valuable comparison between different materials from the same stiffness family.

Additionally, also the influence of artificial aging of the test specimen on the long term mechanical behaviour of laminated elements should be further investigated. Bucak et al. already performed experiments on a limited amount of aged glass/SG samples [Bucak & Meißner 2005], but the load duration was restricted to maximum 120 sec. Additionally, the dispersion of identical tests was almost as large as the influence of the aging for these short load durations. In [Parmentier et al. 2007], again an impression of the influence of UV-light and humidity aging was provided for 1.1 m long glass/SG laminated samples. Unfortunately, the load duration on the aged specimen was limited to 300 sec at room temperature. The combined effect of long load durations, elevated temperatures and UV or humidity influences on laminated elements, is thus still unknown.

As a final suggestion concerning the pre-failure investigations, it might be worthwhile to expand the experimental temperature range to the range -20 °C up to +80 °C, which is described in several standards concerning building components. Tests at those low temperatures might increase the short time SG stiffness, while the higher test temperature can increase the application field of the material model.

Additionally, a lot of research is still needed to predict the post-failure behaviour of laminated glass, particularly with a stiff interlayer material. This should be focussing both on large element, like e.g. [Bucak & Meißner 2005] and on intermediate scale samples, like e.g. [Delincé et al. 2010].

Finally, the possibility of bonding glass to metal with an ionomer interlayer looks very promising to increase the transparency of the connections between different building components. However, the technique is not yet fully developed and durability issues are for this kind of applications extremely important [Belis et al. 2011].





# References

---

- [Abaqus 2008] Abaqus, Inc. Abaqus version 6.8. Manuals, 2008
- [Amston 1997] Amston, J. S. Handbook of Glass in Construction. New York: McGraw-Hill, 1997, ISBN 0-07-001619-4
- [ASTM C1048-04] Standard Specification for Heat-Treated Flat Glass—Kind HS, Kind FT Coated and Uncoated Glass. 2004. doi:10.1520/C1048-04
- [ASTM D638-10] Standard test method for tensile properties of plastics. 2010. doi:10.1520/D0638-10
- [ASTM D2990-09] Standard Test Methods for Tensile, Compressive, and Flexural Creep and Creep-Rupture of Plastics. 2009. doi:10.1520/D2990-09
- [ASTM D4065-06] Standard Practice for Plastics: Dynamic Mechanical Properties: Determination and Report of Procedures. 2006. doi:10.1520/D4065-06
- [Austin 1984] Austin, G. T. Shreve's Chemical Process Industries. Fifth edition - Singapore : McGraw-Hill, 1984, ISBN 0-07-066167-7
- [Belis 2005] Belis, J. Kipsterkte van monolitische en gelamineerde glazen liggers. Ghent: Ghent University, 2005, ISBN 90-8578-034-9
- [Belis et al. 2007] Belis, J., Vander Beken, J., Van Impe, R. & Callewaert, D. Performance of glass-ionoplast laminates above room temperature. Proceedings of Glass performance Days (GPD) 2007, Tampere, pp. 639-642
- [Belis et al. 2008] Belis, J., Vander Beken, J., Callewaert, D. & Van Impe, R. Temperature Dependent Bending and Buckling of Glass/Ionomer Laminates. Proceedings of 6th International Conference on Mechanics of Time Dependent Materials (MTDM) 2008, Monterey, California
- [Belis et al. 2009] Belis, J., Depauw, J., Callewaert, D., Delincé, D. & Van Impe, R. Failure mechanisms and residual capacity of annealed glass/SGP laminated beams at room temperature. Engineering Failure Analysis, Vol. 16, No.

- 6, 2009, pp. 1866–1875.  
doi:10.1016/j.engfailanal.2008.09.023
- [Belis et al. 2011] Belis, J., Van Hulle, A., Out, B., Bos, F., Callewaert, D. & Poulus, H. Broad screening of adhesives for glass-metal bonds. Proceedings of Glass Performance Days (GPD) 2011, Tampere, pp. 286-289
- [Bennison et al. 1999] Bennison, S. J., Jagota, A. & Smith, C. A. Fracture of Glass/Poly(ninyl Butyral) (Butacite®) Laminates in Biaxial Flexure. Journal of the American Ceramic Society , Vol. 82, No. 7, July 1999, pp. 1761-1770. doi:10.1111/j.1151-2916.1999.tb01997.x
- [Bennison et al. 2008] Bennison, S. J., Qin, M. HQ & Davies, P. S. High-Performance Laminated Glass for Structurally Efficient Glazing. HKIE/IStructE Joint Structural Division Annual Seminar: Innovative Leight-weight Structures and Sustainable Facades, 2008, Hong Kong
- [Bennison et al. 2009] Bennison, S. J., Stelzer, I., Davies P. S., Sloan, J. G., Xiaokun H. & Gang L. Calculation Methods for the Structural Behavior of Laminated Glass. Proceedings of Glass Performance Days (GPD), Tampere, 2009, pp. 433-434
- [Bennison & Gizzi 2007] Bennison, S. & Gizzi, V. Structural Properties of Laminated Glass. Glass Performance Days (GPD) 2007, Tampere workshop, not published
- [Bricolli Bati et al. 2010] Bricolli Bati, S., Ranocchiai, G., Reale, C. & Rovero, L. (2010). Time-Dependent Behaviour of Laminated Glass. Journal of Materials in Civil Engineering, Vol. 22, No. 4, April 2010, pp. 389-396. doi:10.1061/(ASCE)MT.1943-5533.0000032
- [Bucak et al. 2006] Bucak, Ö., Schuler, C. & Meißner, M. Verbund im Glasbau – Neues und Bewährtes. Stahlbau, Vol. 75, No. 6, 2006, pp. 529-543. doi:10/1002/stab.200610056
- [Bucak & Meißner 2005] Bucak, Ö & Meißner, M. Trag- und Resttragfähigkeitsuntersuchungen an Verbundglas mit der Zwischenlage "SentryGlas® Plus". AIF FH3-Abschlussbericht, Munich: Fachhochschule München, 2005

- [Callewaert et al. 2007] Callewaert, D., Belis, J., Van Impe, R., Lagae, G. & Vanlaere, W. Refined test set-up for pure torsion of laminated glass. Proceedings of Glass Performance Days (GPD) 2007, Tampere, pp. 118-121
- [Callewaert et al. 2008] Callewaert, D., Delincé, D., Belis, J. & Van Impe, R. Temperature-dependent behaviour of glass/ionomer laminates: preliminary test results. Proceedings of Challenging Glass, Delft, 2008, pp. 431-437
- [clfg 2011] Ultra-thick float glass. Online: [www.clfg.com/english](http://www.clfg.com/english), 2011
- [Delincé et al. 2010] Delincé, D., Callewaert, D., Belis, J., Van Impe, R., Galmart, F. & Matthijs, N. Influence of temperature on post-breakage behaviour of laminated glass beams : experimental approach. Proceedings of Challenging Glass 2, Delft, 2010, pp. 407-410
- [Depaepe 2008] Depaepe, J. Buigstijfheid van glas/ionomeer laminaten in functie van temperatuur en belastingsduur. Ghent: Ghent University, 2008, Master thesis
- [De Vogel 2008] De Vogel, K. Torsiestijfheid van glas/ionomeer laminaten in functie van temperatuur en belastingsduur. Ghent: Ghent University, 2008, Master thesis
- [D'Haene & Savineau 2007] D'Haene, P. & Savineau, G. Mechanical properties of laminated safety glass - FEM Study. Proceedings of Glass Performance Days (GPD) 2007, Tampere, pp. 594-598
- [DIN 1249-10] Flachglas im Bauwesen: Chemische und physikalische Eigenschaften. 1990
- [DuPont 2008] DuPont™ SentryGlas®: Architectural safety glass interlayer. Technical documentation: K-02065-1 (09/08), 2008
- [Ensslen 2005] Ensslen, F. Zum Tragverhalten von Verbund-Sicherheitsglas unter Berücksichtigung der Alterung der Polyvinylbutyral-Folie. Buchum: Ruhr-Universität Bochum, 2005. ISBN 978-3-8322-4456-9
- [Feldmann & Langosch 2011] Feldmann M. & Langosch K. Zum Biegeverhalten vor VSG-Laminaten unter Quer- oder Längsbelastung.

Stahlbau Special 2011: Glasbau/Glass in Building, Ernst & Sohn. pp. 52-60

- [Ferry 1980] Ferry, J. D. Viscoelastic Properties of Polymers – 3<sup>rd</sup> Edition. John Wiley & Sons Inc., 1980. ISBN 0-471-04894-1
- [Froli & Lani 2010] Froli, M. & Lani, L. Adhesion and Viscoelasticity Properties of PVB in Laminated Safety Glass. Proceedings of International Symposium on the Application of Architectural Glass (ISAAG) 2010, Munich, pp. 1-7
- [Galuppi & Royer-Carfagni 2011a] Galuppi L. & Royer-Carfagni G. Simple Models for Laminated Glass. April 28<sup>th</sup> 2011
- [Galuppi & Royer-Carfagni 2011b] Galuppi L. & Royer-Carfagni G. Effective Thickness of Laminated Glass beams. New expression via a variational approach. Submitted October 15<sup>th</sup> 2011
- [Greenyer 2009] Greenyer, B. Laminating thin film PV modules with pre-nip technology and autoclave process. Proceedings of Glass Performance Days (GPD) 2009, Tampere, pp. 535-538
- [Haldimann 2006] Haldimann, M. Fracture Strength of Structural Glass Elements—analytical and numerical modelling, testing and design. Lausanne: Ecole polytechnique fédérale de Lausanne, 2006, ISBN 978-3-8381-0534-5
- [Haldimann et al. 2008] Haldimann, M., Luible, A., Overend, M. Structural Engineering Documents 10: Structural Use of Glass. Zurich: IABSE-AIPC-IVBH, 2008, ISBN 978-3-85748-119-2
- [Henze-Glas 2010] Henze-Glas auf der Glasstec 2010. Online: [www.henzeglas.de](http://www.henzeglas.de), 2010
- [Hinckley 2005] Hinckley, J. & Robinson, J. G. The Big Book of Car Culture: The Armchair Guide to Automotive Americana. Saint Paul, Minnesota: Motorbooks, 2005, ISBN-10 0-7603-1965-0.
- [Hooper 1973] Hooper, J. A. On the Bending of Architectural Laminated Glass. International journal of mechanical science, Vol. 15, No. 4, 1973. pp. 309-322

- [Jagota et al. 2000] Jagota, A., Bennison, S. J. & Smith, C. A. Analysis of a compressive shear test for adhesion between elastomeric polymers and rigid substrates. International Journal of Fracture, Vol. 104, No. 2, 2000, pp. 105-130. doi:10.1023/A:1007617102311
- [Kashyap 2008] Kashyap, S. S. Noviflex®–The Original Structural Interlayer. Online: www.GlasNovations.com, 2008
- [Kasper 2005] Kasper, R. Tragverhalten von Glasträgern. Aachen: Shaker Verlag, 2005, RWTH Aachen, ISBN 978-3-8322-4407-1
- [Kott & Vogel 2006] Kott, A. & Vogel, T. Versuche zum Trag- und Resttragverhalten von Verbundsicherheitsglas. Zurich: ETH Zürich, 2006. doi:10.3929/ethz-a-005287655
- [Lindqvist et al. 2011] Lindqvist, M., Vandebroek, M., Louter, C. & Belis, J. Influence of edge flaws on failure strength of glass. Proceedings of Glass Performance Days (GPD) 2011, Tampere, pp. 126-129
- [Meißner & Sackmann 2006] Meißner, M. & Sackmann, V. On the Effect of Artificial Weathering on the Shear Bond and the Tear Strength of two different Interlayers of Laminated Glass. Proceedings of International Symposium on the Application of Architectural Glass (ISAAG) 2006, Munich, pp. 1-11
- [Moore & Turner 2001] Moore, D. R. & Turner S. Mechanical evaluation strategies for plastics. Woodhead publishing limited, 2001. ISBN 1-85573-379-X
- [Nachtergaele 2009] Nachtergaele, S. Materiaaleigenschappen van een ionomeer tussenlaag in gelamineerd glas. Ghent: Ghent University, 2009, Master thesis
- [NBN EN 572-1] Glass in building - Basic soda lime silicate glass products – Part 1: Definitions and general physical and mechanical properties. 2004
- [NBN EN 572-2] Glass in Building - Basic soda lime silicate glass products - Part 2: Float glass. 2004
- [NBN EN 1288-2] Glass in building - Determination of the bending strength of glass - Part 2: Coaxial double ring test on flat specimens with large test surface areas. 2000

- [NBN EN 1288-3] Glass in building - Determination of the bending strength of glass - Part 3: Test with specimen supported at two points (four point bending). 2000
- [NBN EN 12150-1] Glass in building - Thermally toughened soda lime silicate safety glass - Definition and description. 2000
- [NBN EN ISO 527] Plastics - determination of tensile properties. 1996
- [NBN EN ISO 899] Plastics - Determination of creep behaviour. 2003
- [NBN EN ISO 6721] Plastics - Determination of dynamic mechanical properties. 2011
- [Norville & Minor 1985] Norville, H.S. & Minor, J.E. The strength of weathered window glass. American Ceramic Society bulletin, Vol. 64, No. 11, 1985, pp. 1467-1470
- [Norville et al. 1998] Norville, H. S., King, K. W. & Swofford, J. L. Behavior and Strength of Laminated Glass. Journal of engineering mechanics, Vol. 124, No. 1, 1998. pp. 46-63
- [Pardos 2004] Pardos, F. Plastic Films: Situation and Outlook. Shrewsbury: Rapra Technology Limited, 2004, ISBN 1-85957-480-7
- [Parmentier et al. 2007] Parmentier, B., Delincé, D., Zarmati, G. & Belis, J. Utilisation du verre feuilleté dans les applications structurales. Belgium: CSTC - WTCB - BBRI, 2007.
- [prEN 13474-3] Glass in building - Determination of the strength of glass panes - Part 3: General method of calculation and determination of strength of glass by testing. October 2009
- [Roik & Sedlacek 1970] Roik, K., Sedlacek, G. Erweiterung der technischen Biege- und Verdrehtheorie unter Berücksichtigung von Schubverformungen. Die Bautechnik, Vol. 47, No. 1, 1970. pp. 20-32
- [Sackmann et al. 2004] Sackmann, V., Schuler, C. & Gräf, H. Testing of Laminated Safety Glass. Proceedings of International Symposium on the Application of Architectural Glass (ISAAG) 2004, Munich, pp. 1-8
- [Scarpino 2002] Scarpino, P. Berechnungsverfahren zur Bestimmung einer äquivalenten Torsionssteifigkeit von Trägern in

- Sandwichbauweise. Aachen: RWTH Aachen, 2002, Master thesis
- [Scarpino et al. 2004] Scarpino, P., Kasper, R. & Sedlacek, G. Saint Venantsche Torsionswiderstände von Querschnitten in Sandwichbauweise. Bauingenieur, Vol. 79, 2004, 167-175
- [Scherer 1992] Scherer G. W. Relaxation in Glass and Composites. Krieger Publishing Company, 1992. ISBN 0-89464-643-5
- [Schneider & Wörner 2006] Schneider, F. & Wörner, J.-D. Delayed elastic behaviour of glass at room temperature. Proceedings of IABSE symposium: Responding to Tomorrow's Challenges in Structural Engineering, Budapest, 2006
- [Schuler 2003] Schuler, C. Einfluss des Materialverhaltens von Polyvinylbutyral auf das Tragverhalten von Verbund-sicherheitsglas in Abhängigkeit von Temperatur und Belastung. Munich: Technische Universität München, 2003, ISSN 0941-925X
- [Siebert 2001] Siebert, G. Entwurf und Bemessung von tragenden Bauteilen aus Glas. Berlin: Ernst & Sohn, 2001, ISBN 3-433-01614-3
- [Sobek et al. 1999] Sobek, W., Kutterer, M. & Messmer, R. Shear Stiffness of the Interlayer in Laminated Glass. Proceedings of Glass Processing Days (GPD) 1999, Tampere, pp. 360-365
- [Stamm & Witte 1974] Stamm K. & Witte H. Sandwichkonstruktionen – Berechnung, Fertigung, Ausführung. Springer-Verlag, 1974. ISBN 3-211-81121-4
- [Stelzer 2010] Stelzer, I. High Performance Laminated Glass. Proceedings of Challenging Glass 2 - Conference on Architectural and structural Applications of Glass, 2010, Delft, pp. 467-474
- [Stelzer et al. 2008] Stelzer, I, Bennison, S. J. & Qin, M. HX. High-Performance Laminated Glass for Structurally Efficient Glazing. Proceedings of International Symposium on the Application of Architectural Glass (ISAAG) 2008, Munich, pp. 65-77

- [Schwarzl 1990] Schwarzl F. R. Polymermechanik – Struktur und mechanisches Verhalten von Polymeren. Springer-Verlag, 1990. ISBN 3-540-51965-3
- [Trimm 2005] Trimm, Harold H. Forensics The Easy Way. New York : Barron's Educational Series, Inc., 2005, ISBN-10 0-7641-3050-1.
- [Trosifol 2011] Laminated safety glass: testing of windscreens. Online: www.trosifol.com, 2011
- [Vandebroek et al. 2011] Vandebroek, M., Lindqvist, M., Belis, J. & Louter, C. Edge strength of cut and polished glass beams. Proceedings of Glass Performance Days (GPD) 2011, Tampere, pp. 476-479
- [Vander Beken 2006] Vander Beken, J. Temperatuursafhankelijk gedrag van gelamineerd glas met ionoplast tussenlaag. Ghent: Ghent University, 2006, Master thesis
- [Van Duser et al. 1999] Van Duser, A., Jagota, A. & Bennison, S. J. Analysis of Glass/Polyvinyl Butyral Laminates Subjected to Uniform Pressure. Journal of engineering Mechanics, Vol. 125, No. 4, 1999, pp. 435-442. doi:10.1061/(ASCE)0733-9399(1999)125:4(435)
- [Van Russelt 1997] Van Russelt, M. How to make a good laminated safety glass for windscreens. Proceedings of Glass Processing Days (GPD) 1997, Tampere, pp. 475-479
- [Veer & Rodichev 2010] Veer, F. & Rodichev, Y. The strength of glass, hidden damage. Proceedings of Challenging Glass 2, Delft, 2010, pp. 395-404
- [Weller et al. 2005] Weller, B., Wünsch, J. & Härth, K. Experimental Study on Different Interlayer Materials for Laminated Glass. Proceedings of Glass Processing Days (GPD) 2005, Tampere, pp. 120-123
- [WG8-N260E 2009] Glass in building - Laminated glass and laminated safety glass – Determination of interlayer shear transfer coefficient. Working document CEN/TC129/WG8 - N260E, Oktober 2009
- [Williams et al. 1955] Williams M. L., Landel, R. F. & Ferry, J. D. The Temperature dependence of Relaxation Mechanisms in Amorphous Polymers and Other Glass-forming Liquids. Journal of the American Chemical Society,



Vol. 77, No. 14, 1955, pp. 3707-3707.  
doi:10.1021/ja01619a008

[Wölfel 1987]

Wölfel, E. Nachgiebiger Verbund Eine  
Näherungslösung und deren  
Anwendungsmöglichkeiten. Stahlbau, Vol. 56, No. 6,  
1987, pp. 173-180



# Appendix A: Sensitivity analysis of the experimental setups

The influence of some possible inaccuracies on the calculated material properties of the interlayer was determined for the three chosen test setups. For this, the deformation was each time calculated analytically while the value of only one parameter was changed with 1%. With the resulting deformation, the shear modulus of the interlayer was then recalculated (analogically to § IV.1.3). As a reference, a laminated element was chosen with the nominal dimensions of the applied test samples. Tables A.1 up to A.3 summarise this sensitivity analysis, performed each time with three different reference values of  $G_{int}$ .

It must be emphasised that most parameters were determined with a much better accuracy than +/- 1 %. The calculated values are thus only illustrative.

The negative recalculated values of  $G_{int}$  of table A.2 initiate from a lower deformation than the deformation with full shear transfer, which is theoretically impossible.

**Table A.1: sensitivity of torsion test setup**

	twist deformation			recalculated shear modulus [N/mm <sup>2</sup> ]		
	$G_{int} = 100$	$G_{int} = 10$	$G_{int} = 1$	$G_{int} = 100$	$G_{int} = 10$	$G_{int} = 1$
reference	0.7109	1.1965	2.7395	100.0	10.00	1.000
$t_{glass} +1\%$	0.6928	1.1689	2.6679	138.5	10.65	1.114
$t_{glass} -1\%$	0.7295	1.2251	2.8136	77.44	9.399	0.890
$t_{SG} +1\%$	0.7092	1.1978	2.7431	102.7	9.973	0.995
$t_{SG} -1\%$	0.7125	1.1953	2.7358	97.51	10.03	1.006
$W +1\%$	0.7026	1.1758	2.6995	114.8	10.48	1.063
$W -1\%$	0.7194	1.2178	2.7803	88.38	9.547	0.939
$L +1\%$	0.7180	1.2085	2.7669	90.11	9.742	0.959
$L -1\%$	0.7037	1.1846	2.7121	112.5	10.27	1.043
$G_{glass} +1\%$	0.7045	1.1891	2.7188	111.1	10.17	1.033
$G_{glass} -1\%$	0.7174	1.2040	2.7606	90.88	9.838	0.968
$M +1\%$	0.7180	1.2085	2.7669	90.15	9.743	0.959
$M -1\%$	0.7037	1.1846	2.7121	112.5	10.27	1.043
$\theta +1\%$	0.7180	1.2085	2.7669	90.17	9.744	0.959
$\theta -1\%$	0.7037	1.1846	2.7121	112.5	10.27	1.043

**Table A.2: sensitivity of large bending test setup**

	deflection [mm]			recalculated shear modulus [N/mm <sup>2</sup> ]		
	$G_{int} = 100$	$G_{int} = 10$	$G_{int} = 1$	$G_{int} = 100$	$G_{int} = 10$	$G_{int} = 1$
reference	17.920	18.705	25.743	100.0	10.00	1.000
$t_{glass} +1\%$	17.438	18.209	25.112	-22.57 ( $\infty$ )	23.28	1.097
$t_{glass} -1\%$	18.419	19.219	26.396	14.91	6.251	0.915
$t_{SG} +1\%$	17.875	18.666	25.754	205.6	10.47	0.998
$t_{SG} -1\%$	17.965	18.744	25.732	65.96	9.565	1.002
$W +1\%$	17.742	18.520	25.488	-99.16 ( $\infty$ )	12.72	1.037
$W -1\%$	18.101	18.894	26.003	32.69	8.200	0.964
$L +1\%$	18.461	19.254	26.379	13.92	6.094	0.917
$L -1\%$	17.389	18.166	25.118	-20.09 ( $\infty$ )	26.28	1.096
$E_{glass} +1\%$	17.743	18.528	25.558	-100.1 ( $\infty$ )	12.57	1.027
$E_{glass} -1\%$	18.100	18.885	25.931	32.80	8.269	0.974
$P +1\%$	18.099	18.892	26.000	32.92	8.215	0.965
$P -1\%$	17.741	18.518	25.486	-97.23 ( $\infty$ )	12.76	1.038
$w +1\%$	18.099	18.892	26.000	32.92	8.215	0.965
$w -1\%$	17.741	18.518	25.486	-97.23 ( $\infty$ )	12.76	1.038

**Table A.3: sensitivity of small bending test setup**

	deflection [mm]			recalculated shear modulus [N/mm <sup>2</sup> ]		
	$G_{int} = 100$	$G_{int} = 10$	$G_{int} = 1$	$G_{int} = 100$	$G_{int} = 10$	$G_{int} = 1$
reference	0.6264	0.8190	1.8310	100.0	10.00	1.000
$t_{glass} +1\%$	0.6098	0.7987	1.7857	350.3	11.13	1.074
$t_{glass} -1\%$	0.6437	0.8400	1.8778	57.11	9.031	0.929
$t_{SG} +1\%$	0.6250	0.8190	1.8349	106.3	10.00	0.994
$t_{SG} -1\%$	0.6278	0.8190	1.8270	94.39	10.00	1.006
$W +1\%$	0.6202	0.8109	1.8128	136.5	10.43	1.029
$W -1\%$	0.6327	0.8273	1.8495	78.50	9.597	0.972
$L +1\%$	0.6449	0.8398	1.8734	55.39	9.041	0.936
$L -1\%$	0.6083	0.7986	1.7891	451.0	11.14	1.068
$E_{glass} +1\%$	0.6204	0.8128	1.8191	134.7	10.32	1.019
$E_{glass} -1\%$	0.6325	0.8253	1.8430	79.13	9.692	0.981
$P +1\%$	0.6327	0.8272	1.8493	78.66	9.601	0.972
$P -1\%$	0.6202	0.8108	1.8127	137.0	10.43	1.029
$w +1\%$	0.6327	0.8272	1.8493	78.66	9.601	0.972
$w -1\%$	0.6202	0.8108	1.8127	137.0	10.43	1.029

# Appendix B: Measured test specimen geometry

---

The actual geometry of the test specimen was determined meticulously. The thickness of the individual glass panes  $t_{glass}$  was measured twice for each pane, prior to lamination (Fig. B.1). After the further production of the samples, also the total thickness of the laminate  $t_{total}$  (Fig. B.2) and the length  $L$  (Fig. B.3) and width  $W$  (Fig. B.4) of each pane was measured several times.

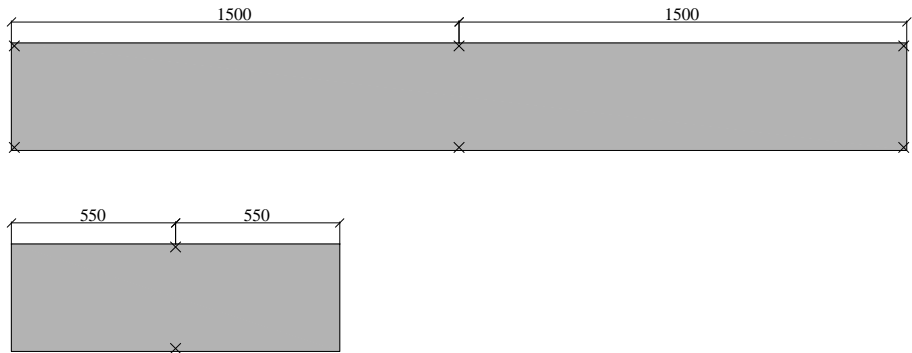


**Figure B.1: Measurement locations of the individual thickness of the single glass panes  $t_{glass}$  prior to lamination: test specimen of series C (upper); test specimen of series A, B, D and E (lower)**

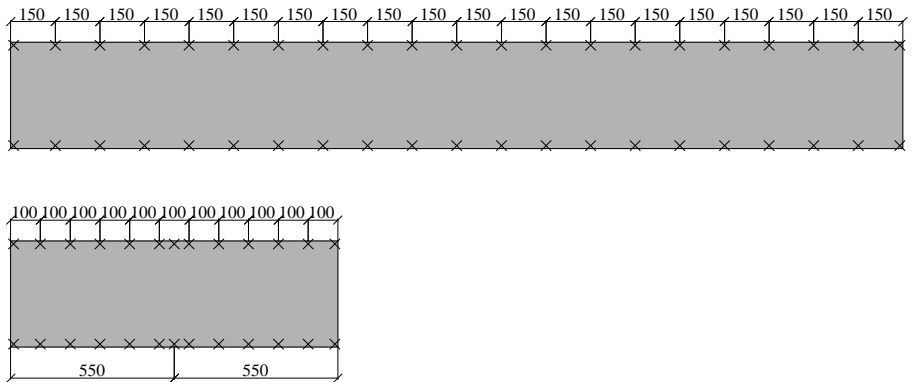


**Figure B.2: Measurement locations of the overall total thickness of the laminate  $t_{total}$  after lamination: test specimen of series C (upper); test specimen of series A, B, D and E (lower)**

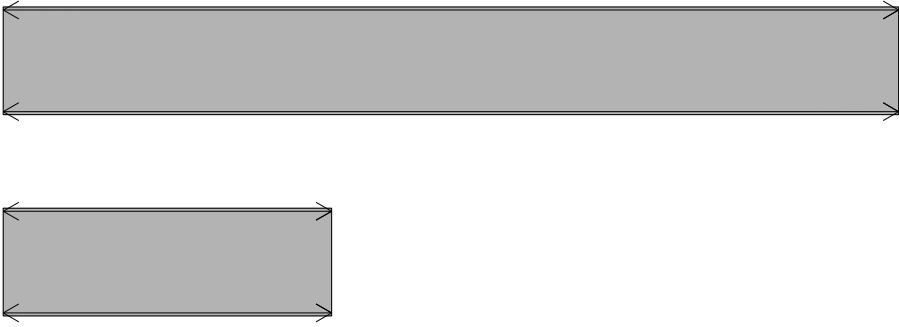


**Figure B.3: Measurement locations of the length  $L$ : test specimen of series C (upper); test specimen of series A, B, D and E (lower)**

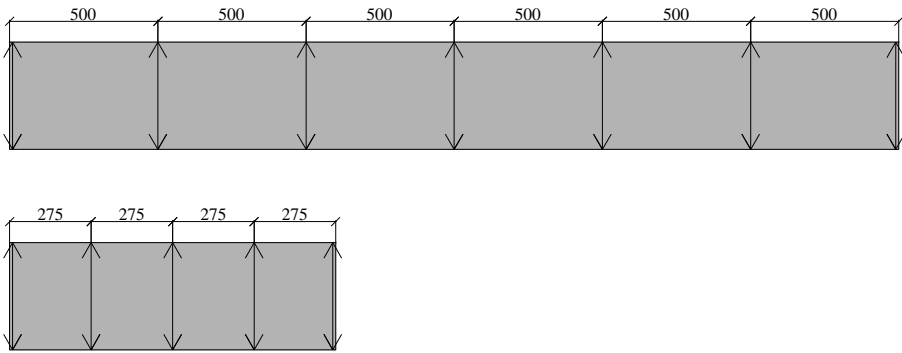


**Figure B.4: Measurement locations of the width  $W$ : test specimen of series C (upper); test specimen of series A, B, D and E (lower)**

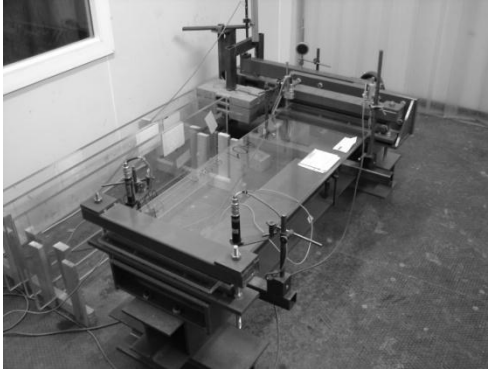


**Figure B.5: Torsion creep test on test specimen A01**

**Table B.1: Mean values of the measured specimen geometry for test series A (torsion)**

Sample	$L$ [mm]	$W$ [mm]	$t_{total}$ [mm]	$t_{glass,1}$ [mm]	$t_{int}$ [mm]	$t_{glass,2}$ [mm]
A01	1100.25	360.98	13.42	5.91	1.64	5.88
A02	1100.25	360.97	13.39	5.95	1.56	5.88
A03	1100.00	360.95	13.35	5.87	1.57	5.91
A04	1100.00	360.97	13.33	5.89	1.56	5.89
A05	1100.00	360.00	13.38	5.92	1.59	5.88
A06	1100.00	360.00	13.40	5.92	1.57	5.92
A07	1100.00	360.00	13.42	5.94	1.58	5.90
A08	1100.00	360.00	13.42	5.91	1.63	5.89
A09	1100.25	361.00	13.49	5.95	1.64	5.91
A10	1100.25	361.00	13.48	5.95	1.62	5.91
A11	1100.25	360.99	13.44	5.90	1.64	5.90
A12	1100.50	361.00	13.40	5.91	1.59	5.91
A13	1100.00	360.97	13.36	5.93	1.55	5.88
A14	1100.00	360.99	13.33	5.93	1.52	5.89
A15	1100.25	360.98	13.42	5.90	1.59	5.93
A16	1100.50	360.99	13.41	5.88	1.59	5.95
A17	1100.00	360.98	13.39	5.94	1.56	5.89
A18	1100.25	360.99	13.37	5.94	1.56	5.88
A19	1100.00	360.92	13.47	5.92	1.60	5.96
A20	1100.00	360.92	13.36	5.88	1.60	5.89



**Figure B.6: Small bending creep test on test specimen B14**

**Table B.2: Mean values of the measured specimen geometry for test series B (small bending)**

Sample	L [mm]	W [mm]	$t_{total}$ [mm]	$t_{glass,1}$ [mm]	$t_{int}$ [mm]	$t_{glass,2}$ [mm]
B01	1099.00	181.12	17.29	7.85	1.58	7.86
B02	1099.00	179.73	17.06	7.75	1.60	7.71
B03	1098.00	179.60	17.14	7.75	1.64	7.75
B04	1099.50	179.43	17.29	7.86	1.59	7.85
B05	1099.00	179.90	17.34	7.85	1.63	7.86
B06	1099.00	181.54	17.31	7.81	1.70	7.80
B07	1099.75	182.27	17.03	7.73	1.57	7.73
B08	1099.00	179.23	17.16	7.76	1.65	7.75
B09	1099.50	182.87	17.27	7.83	1.62	7.83
B10	1099.75	181.35	17.31	7.81	1.70	7.81
B11	1098.00	182.38	17.23	7.81	1.62	7.81
B12	1100.00	181.81	17.15	7.82	1.52	7.82
B13	1099.25	182.49	17.14	7.80	1.53	7.81
B14	1099.25	181.21	17.07	7.72	1.61	7.75
B15	1100.00	181.54	17.06	7.73	1.61	7.72
B16	1098.50	181.54	17.04	7.71	1.62	7.71
B17	1099.25	181.66	17.30	7.75	1.79	7.76
B18	1099.00	181.71	17.14	7.72	1.68	7.74
B19	1098.75	182.11	17.04	7.77	1.53	7.75
B20	1098.50	181.81	16.98	7.71	1.57	7.71





**Figure B.7:** Large bending relaxation test on specimen C01 (left); Torsion relaxation test setup with specimen D01 (right)

**Table B.3:** Mean values of the measured specimen geometry for test series C (large bending)

Sample	$L$ [mm]	$W$ [mm]	$t_{total}$ [mm]	$t_{glass,1}$ [mm]	$t_{int}$ [mm]	$t_{glass,2}$ [mm]
C01	3000.00	360.00	17.10	7.76	1.57	7.77
C02	3000.00	360.00	17.11	7.76	1.59	7.77
C03	3000.00	360.00	17.10	7.76	1.58	7.76
C04	3000.00	360.00	17.12	7.76	1.61	7.76
C05	2999.75	360.75	17.26	7.82	1.62	7.82
C06	3000.00	360.46	17.12	7.76	1.62	7.74
C07	2999.75	360.95	17.17	7.80	1.62	7.75
C08	3000.00	360.45	17.11	7.77	1.57	7.77

**Table B.4:** Mean values of the measured specimen geometry for test series D (torsion PVB)

Sample	$L$ [mm]	$W$ [mm]	$t_{total}$ [mm]	$t_{glass,1}$ [mm]	$t_{int}$ [mm]	$t_{glass,2}$ [mm]
D01	1100.00	360.94	13.31	5.92	1.44	5.95
D02	1100.00	361.07	13.36	5.93	1.50	5.93
D03	1100.00	360.97	13.38	5.88	1.63	5.87
D04	1100.00	360.99	13.39	5.87	1.65	5.87
D05	1100.00	360.98	13.38	5.95	1.51	5.92
D06	1100.00	360.96	13.29	5.88	1.54	5.87
D07	1100.00	360.97	13.31	5.90	1.53	5.89
D08	1100.00	360.99	13.30	5.91	1.52	5.88



**Figure A.8: Small bending creep test on test specimen E12**

**Table A.5: Mean values of the measured specimen geometry for test series E (small bending)**

<b>Sample</b>	<b>L [mm]</b>	<b>W [mm]</b>	<b><math>t_{total}</math> [mm]</b>	<b><math>t_{glass,1}</math> [mm]</b>	<b><math>t_{int}</math> [mm]</b>	<b><math>t_{glass,2}</math> [mm]</b>
E01	1100.00	119.72	17.23	7.79	1.65	7.79
E02	1100.50	119.90	17.19	7.79	1.61	7.79
E03	1101.00	120.45	17.21	7.79	1.63	7.79
E04	1100.25	120.19	17.16	7.79	1.58	7.79
E05	1100.50	121.02	17.15	7.79	1.57	7.79
E06	1101.50	119.93	17.18	7.79	1.60	7.79
E07	1101.50	120.97	17.10	7.79	1.52	7.79
E08	1101.50	120.26	16.99	7.79	1.41	7.79
E09	1100.75	122.34	16.99	7.79	1.41	7.79
E10	1101.25	119.99	17.17	7.79	1.59	7.79
E11	1101.25	120.74	16.99	7.79	1.41	7.79
E12	1100.50	120.21	17.21	7.79	1.63	7.79
E13	1100.00	120.11	17.23	7.79	1.65	7.79
E14	1101.25	119.97	16.97	7.79	1.39	7.79
E15	1101.25	120.27	16.99	7.79	1.41	7.79
E16	1101.25	121.49	16.98	7.79	1.40	7.79
E17	1100.50	120.30	17.18	7.79	1.60	7.79
E18	1100.50	120.18	17.15	7.79	1.57	7.79
E19	1100.75	120.78	17.14	7.79	1.56	7.79
E20	1100.25	120.86	17.00	7.79	1.42	7.79

# Appendix C: Example of torsion test results

---

During a torsion creep experiment, the vertical displacement of the lever arm and the vertical deformations on top of the glass surface are registered. These measurements are exemplarily represented in Figs. C.1 and C.2 for the torsion creep experiment at 35 °C on sample A09.

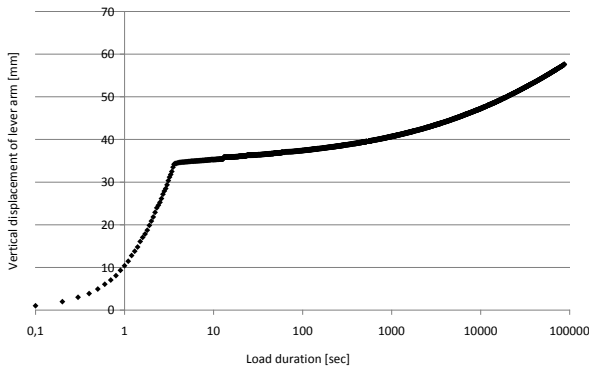


**Figure C.1: Vertical displacement of the end of the lever arm during the torsion creep experiment at 35°C on sample A09**

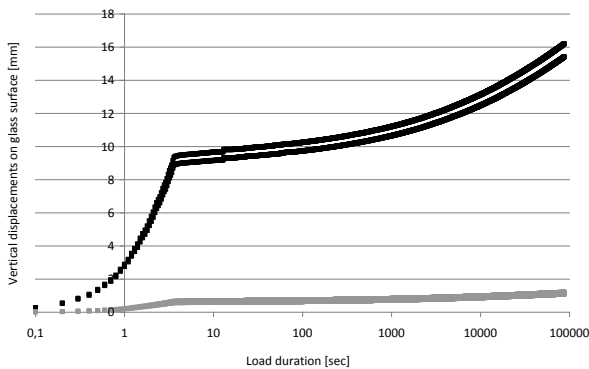


**Figure C.2: Absolute values of the vertical displacements on top of the glass surface during the torsion creep experiment at 35°C on sample A09**

During the torsion relaxation experiments, additionally also the load on the lever arm is registered. The experimental outcome of the torsion relaxation experiment on sample A17 is represented in Figs. C.3 up to C.5.

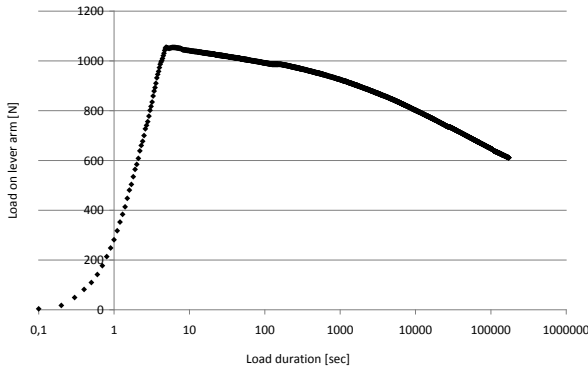


**Figure C.3:** Force on the end of the lever arm during the torsion relaxation experiment at 35 °C on sample A17

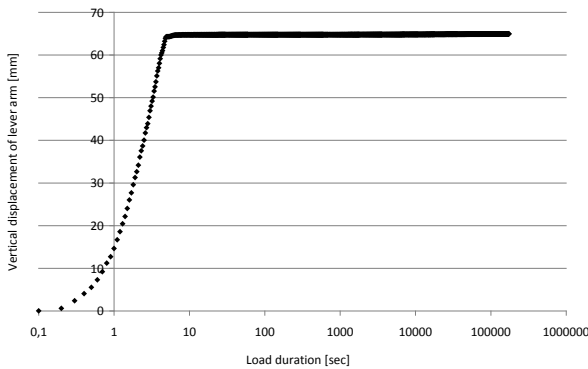


**Figure C.4:** Vertical displacement of the end of the lever arm during the torsion relaxation experiment at 35 °C on sample A17

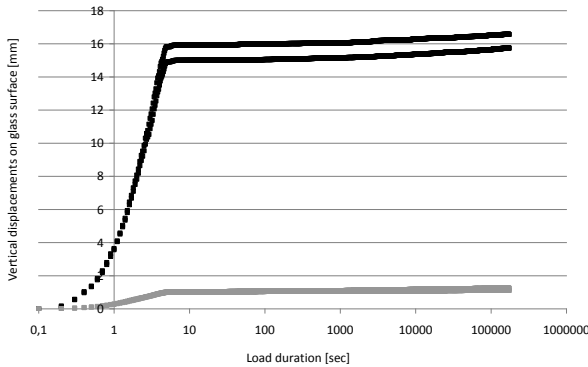


**Figure C.5:** Absolute values of the vertical displacements on top of the glass surface during the torsion relaxation experiment at 35 °C on sample A17

Figs. C.6 up to C.8 display similar outcome for the torsion relaxation experiment at 35 °C on sample D05 (with PVB interlayer).

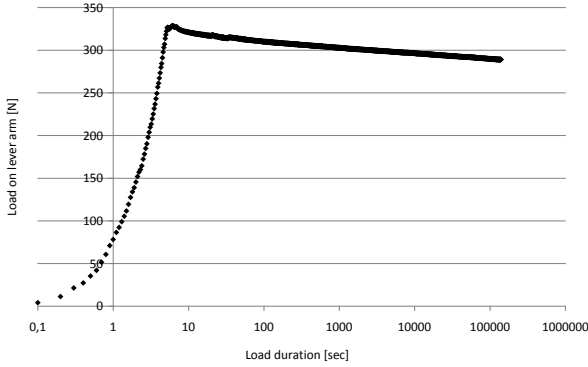


**Figure C.6:** Force on the end of the lever arm during the torsion relaxation experiment at 35 °C on sample D05 (PVB)

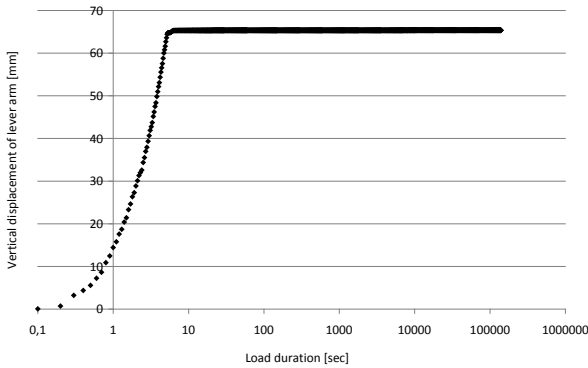


**Figure C.7:** Vertical displacement of the end of the lever arm during the torsion relaxation experiment at 35 °C on sample D05 (PVB)

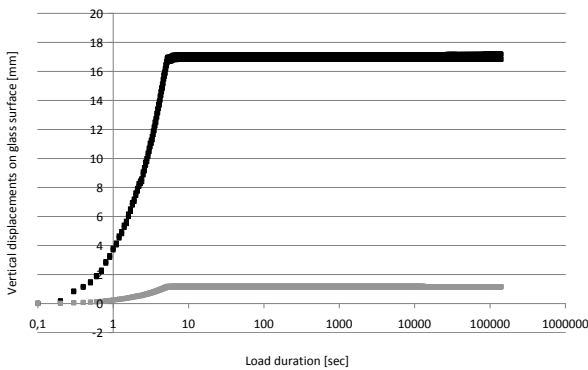


**Figure C.8:** Absolute values of the vertical displacements on top of the glass surface during the torsion relaxation experiment at 35 °C on sample D05 (PVB)



# Appendix D: Example of bending test results

---

During a bending creep experiment, the horizontal displacement at the back of the glass surface is registered simultaneously with two LVDT's at the middle between the two supports. These measurements are exemplarily represented in Figs. D.1 up to D.3 for the bending creep experiment at 35 °C on sample B13, E05 and C05 respectively.

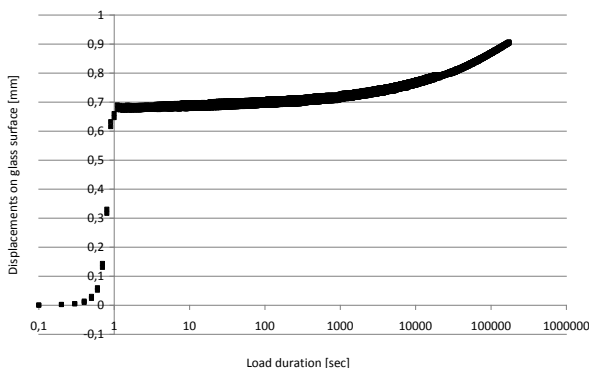


**Figure D.1: Displacements at the centre of the tested element during the bending creep experiment at 35 °C on sample B13**

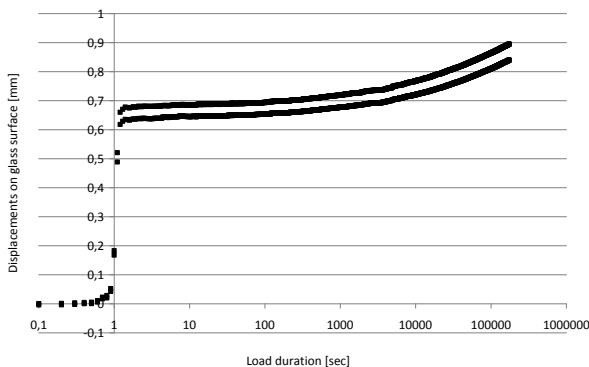


**Figure D.2: Displacements at the centre of the tested element during the bending creep experiment at 35 °C on sample E05**

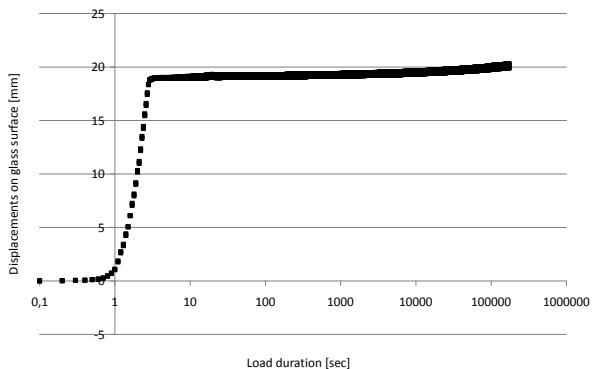


**Figure D.3: Displacements at the centre of the tested element during the bending creep experiment at 35 °C on sample C05**

During the bending relaxation tests on series C, additionally the load at the centre of the element was measured. The experimental outcome of the experiment at 35 °C on sample C01 are represented in Figs. D.4 and D.5.

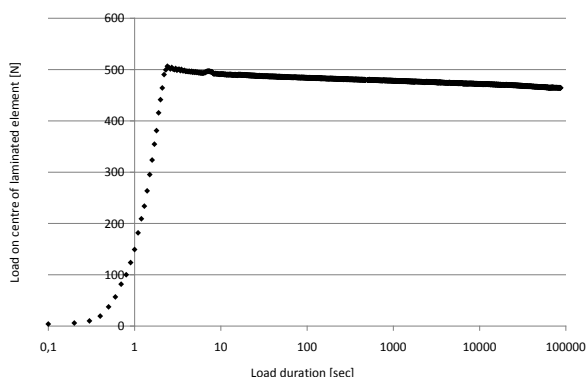


**Figure D.4: Load at the centre of the tested element during the bending relaxation experiment at 35 °C on sample C01**

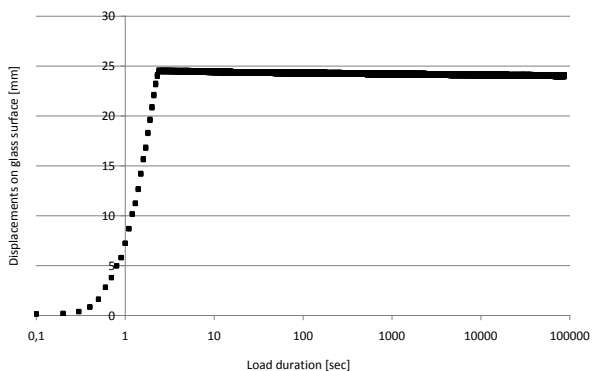
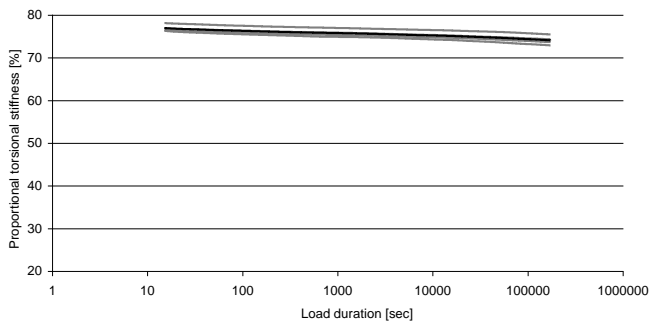


**Figure D.5: Displacements at the centre of the tested element during the bending relaxation experiment at 35 °C on sample C01**

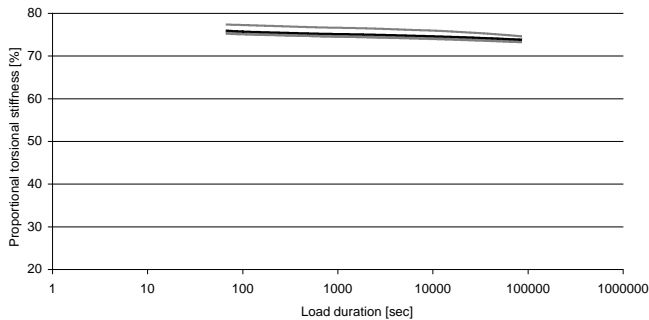


# Appendix E: Torsion relaxation results series A (SG laminates)

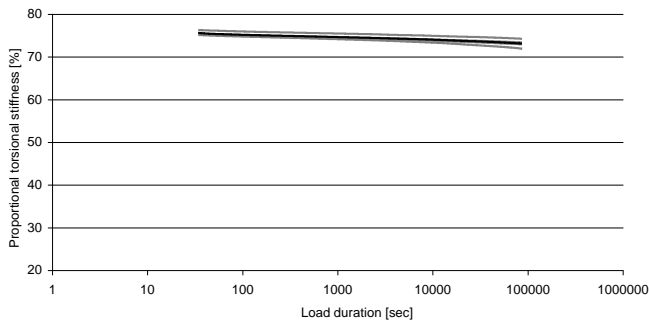
Results of torsion relaxation experiments on specimen from series A (1100 mm long, 360 mm wide and a thickness of 2x 6 mm fully tempered glass with a 1.52 mm SG interlayer)



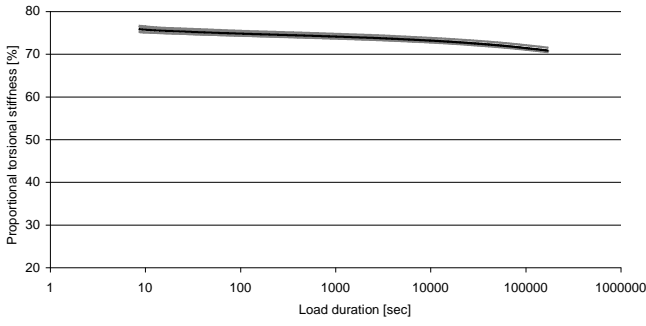
5 °C



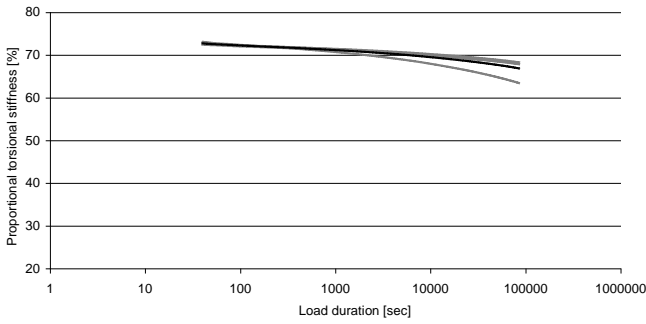
10 °C



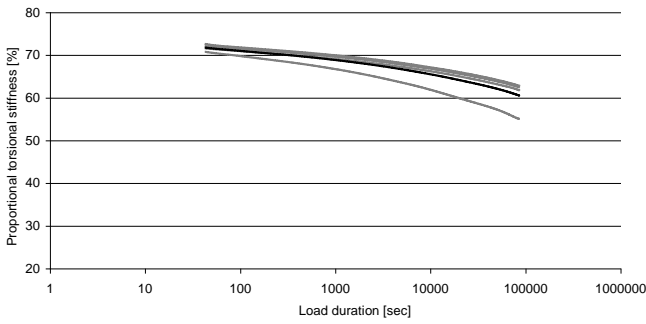
15 °C



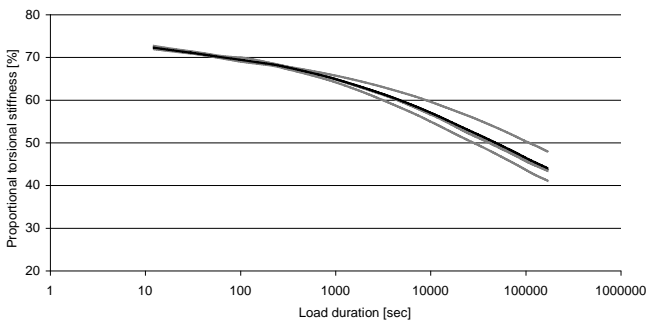
20 °C



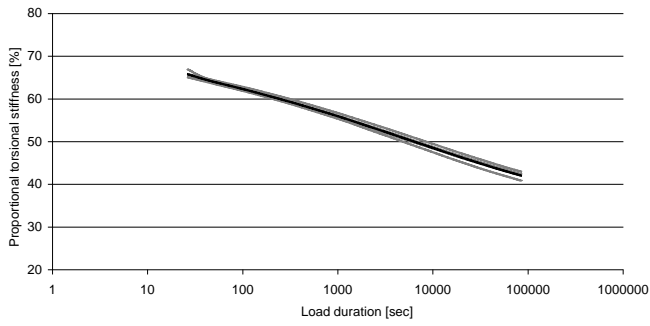
25 °C



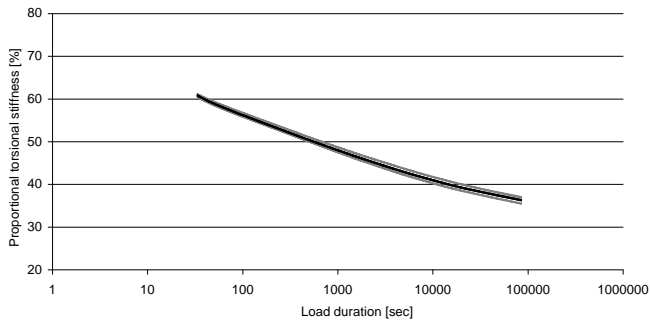
30 °C



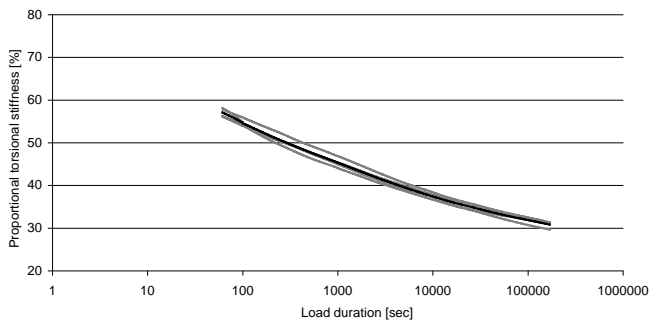
35 °C



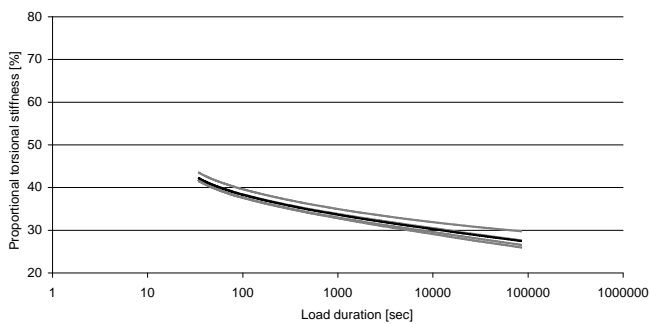
40 °C



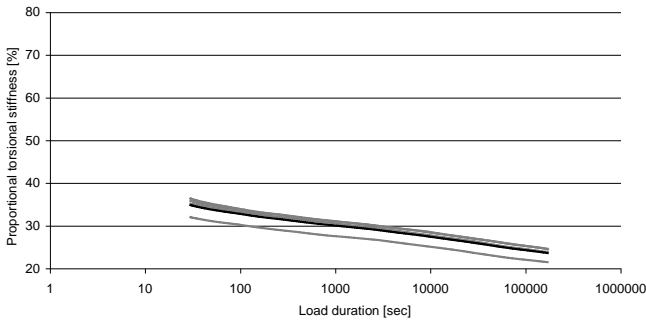
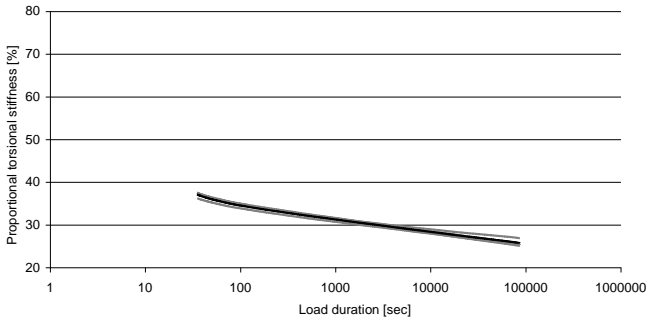
45 °C



50 °C



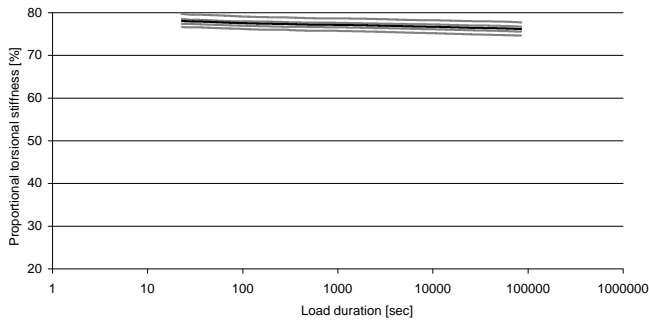
55 °C



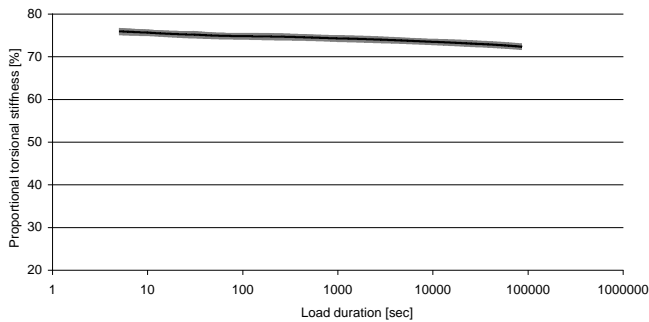
# Appendix F: Torsion creep results series A (SG laminates)

---

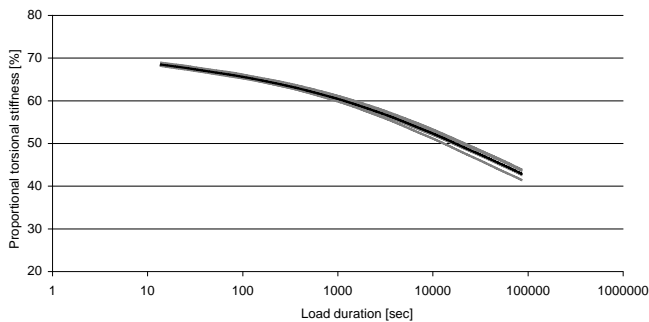
Results of torsion creep experiments on specimen from series A (1100 mm long, 360 mm wide and a thickness of 2x 6 mm fully tempered glass and a 1.52 mm SG interlayer)



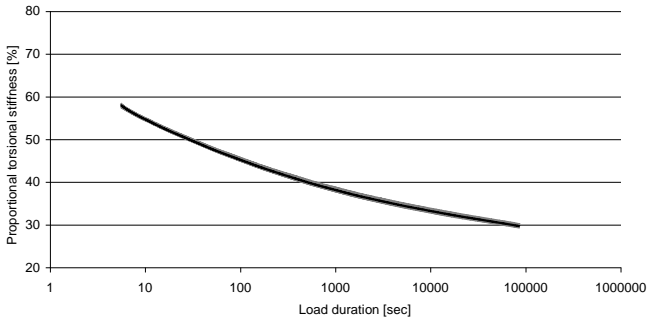
5 °C



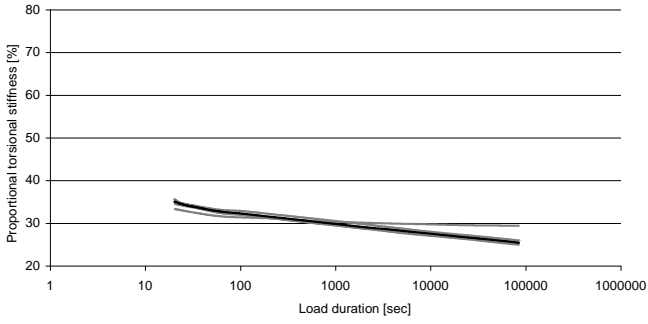
20 °C



35 °C



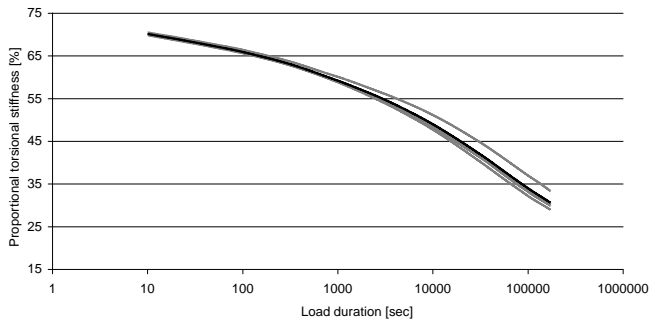
50 °C



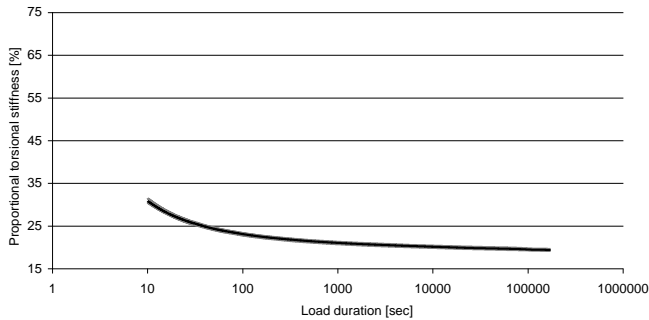
65 °C

# Appendix G: Torsion relaxation results series D (PVB laminates)

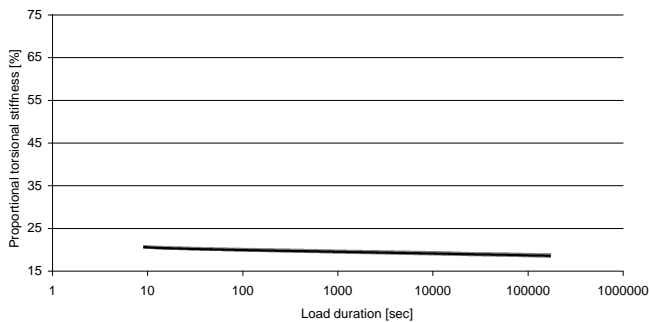
Results of torsion creep experiments on specimen from series D (1100 mm long, 360 mm wide and a thickness of 2x 6 mm fully tempered glass and a 1.52 mm PVB interlayer)



5 °C



20 °C



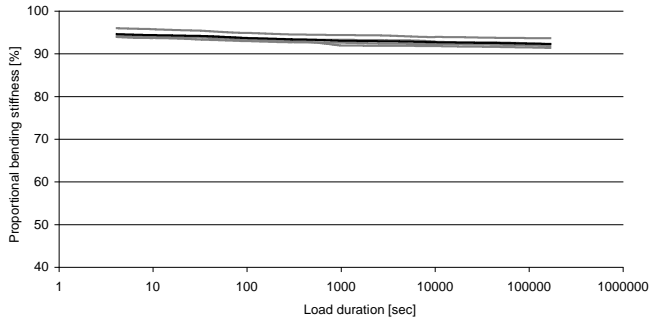
35 °C



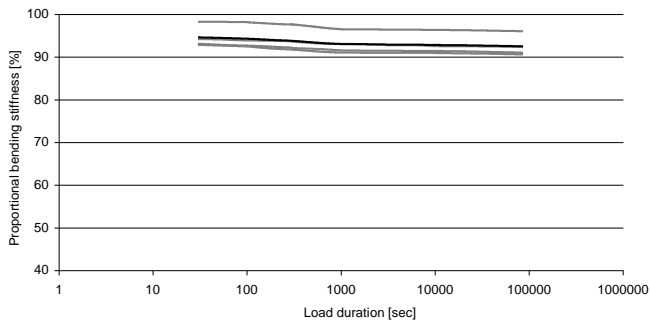


# Appendix H: Bending creep results series B

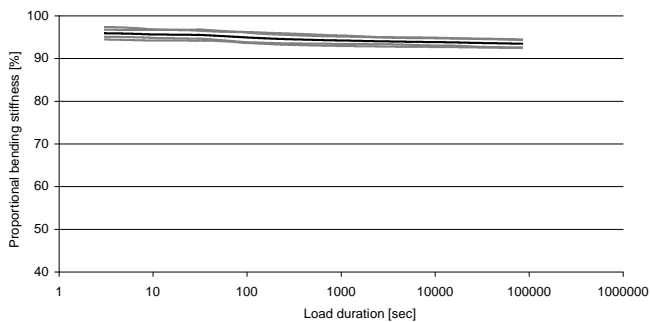
Results of bending creep experiments on specimen from series B (1100 mm long, 180 mm wide and a thickness of 2x 8 mm annealed glass and a 1.52 mm SG layer)



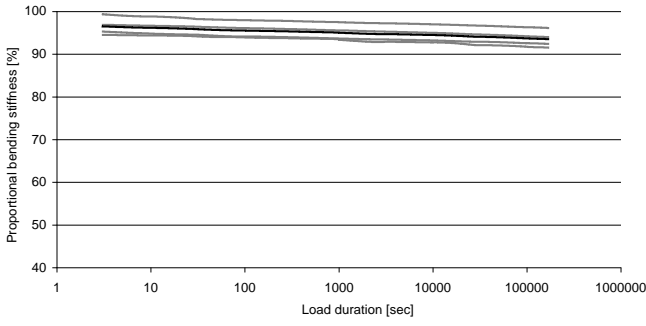
5°C



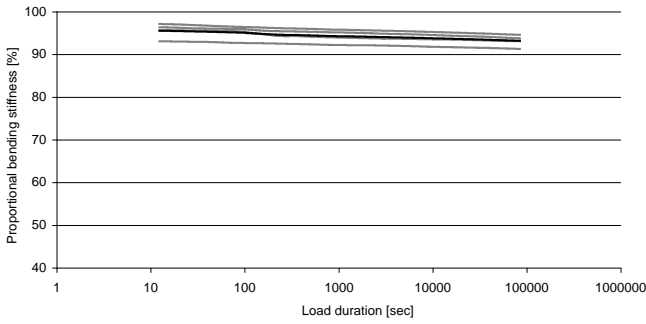
10 °C



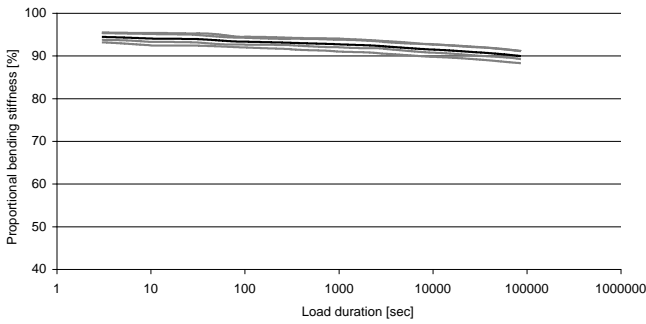
15 °C



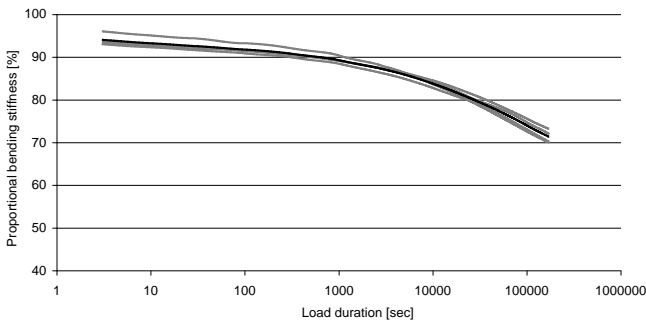
20 °C



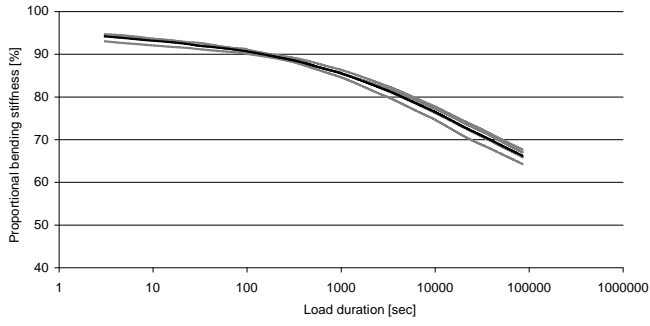
25 °C



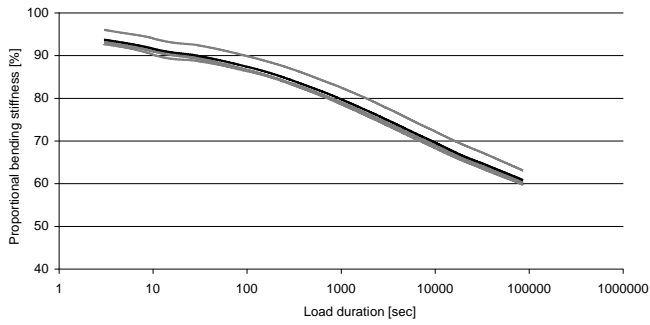
30 °C



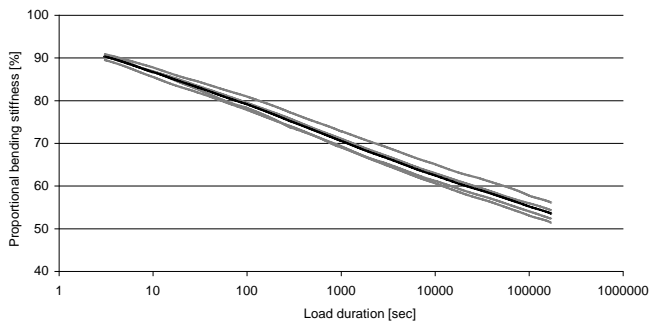
35 °C



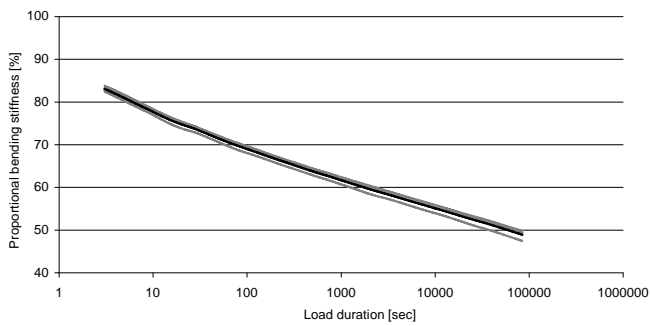
40 °C



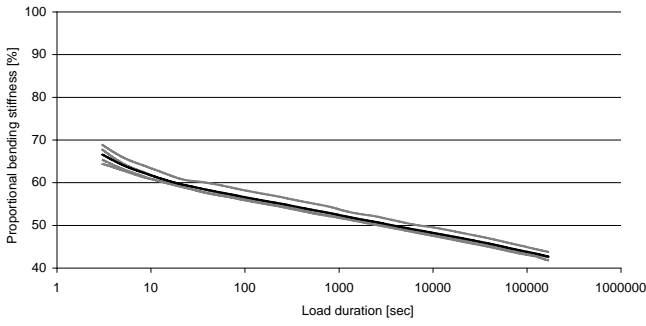
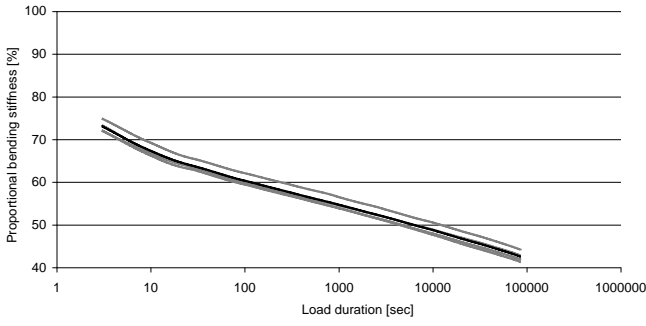
45 °C



50 °C

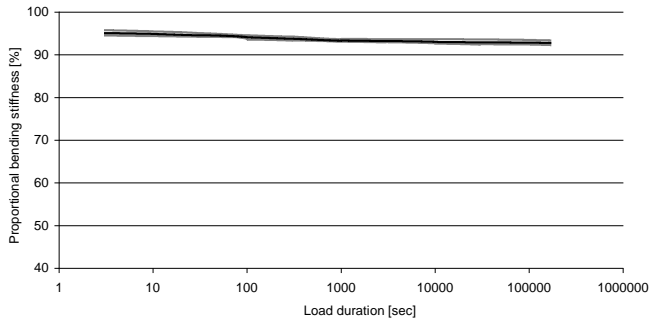


55 °C

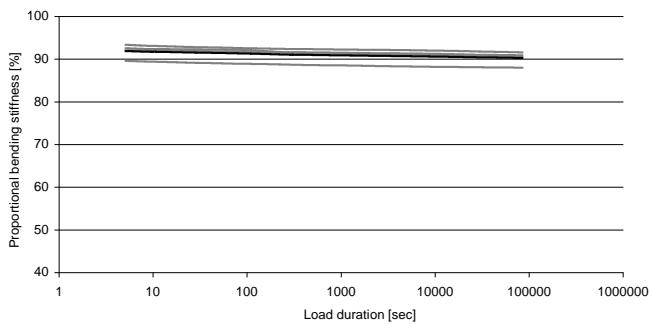


# Appendix I: Bending creep results series E

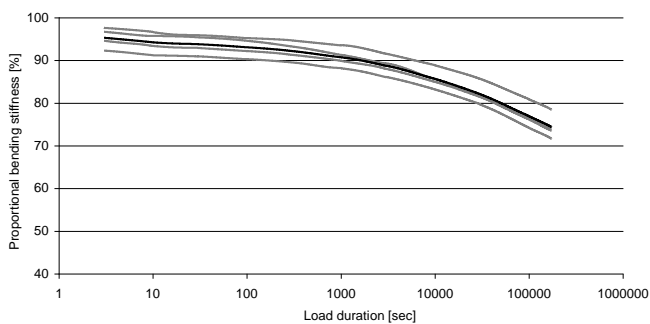
Results of bending creep experiments on specimen from series E (1100 mm long, 120 mm wide and a thickness of 2x 8 mm annealed glass and 1.52 mm SG)



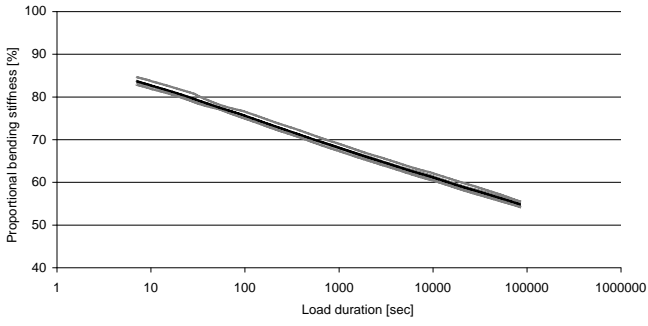
5 °C



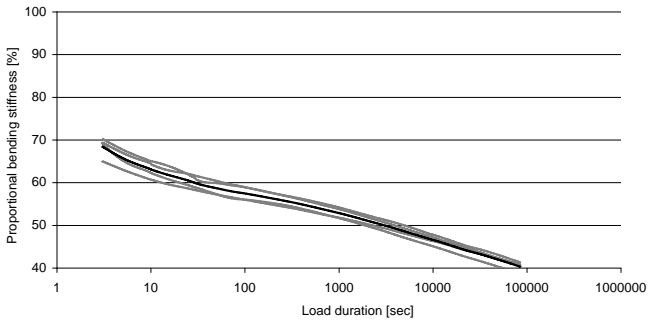
20 °C



35 °C



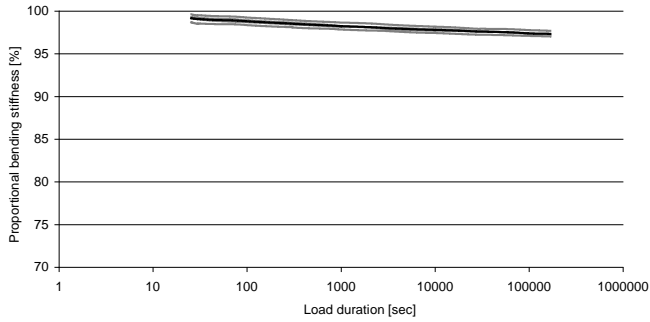
50 °C



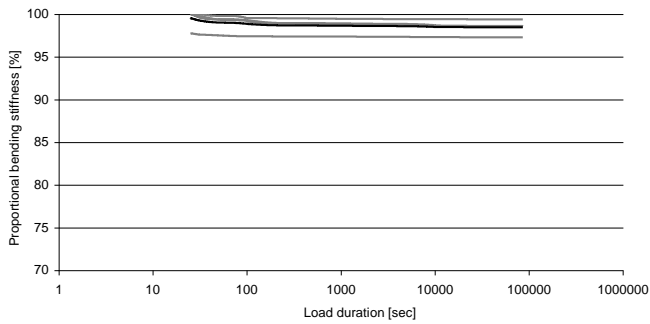
65 °C

# Appendix J: Bending creep results series C

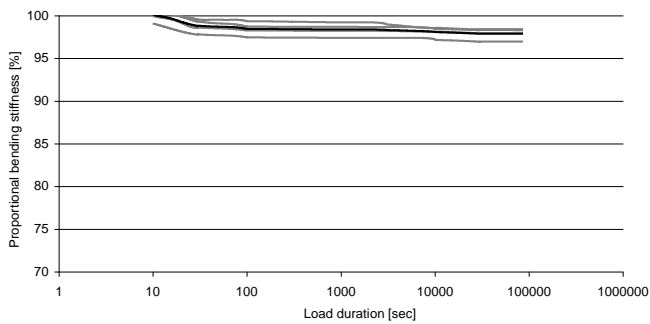
Results of bending creep experiments on specimen from series C (3000 mm long, 360 mm wide and a thickness of 2x 8 mm annealed glass and 1.52 mm SG)



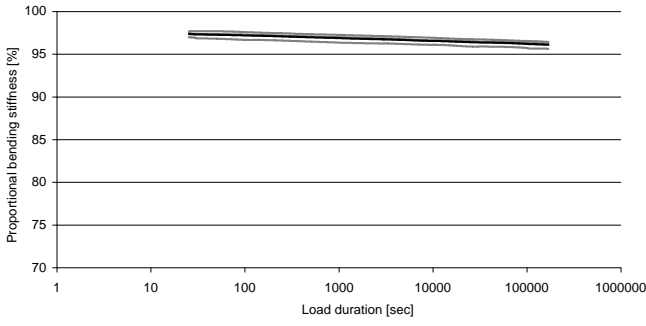
5 °C



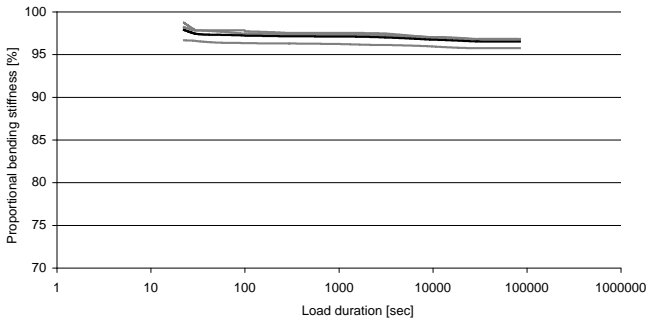
10 °C



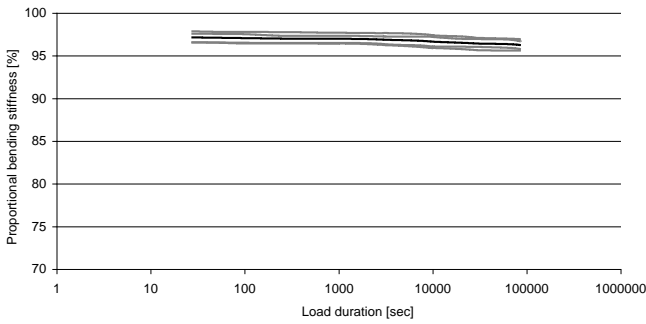
15 °C



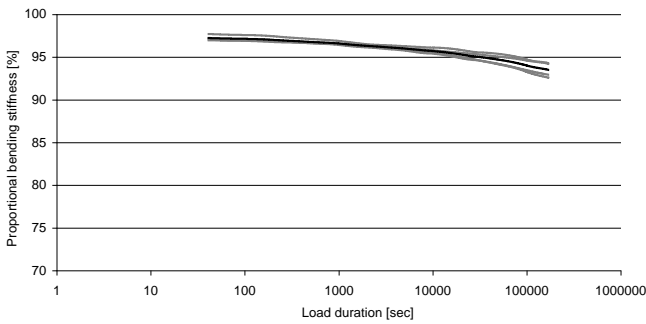
20 °C



25 °C

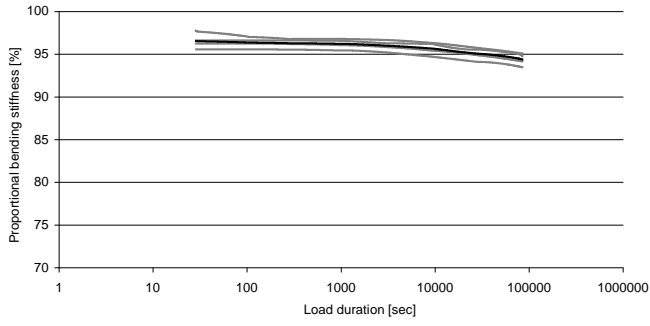


30 °C

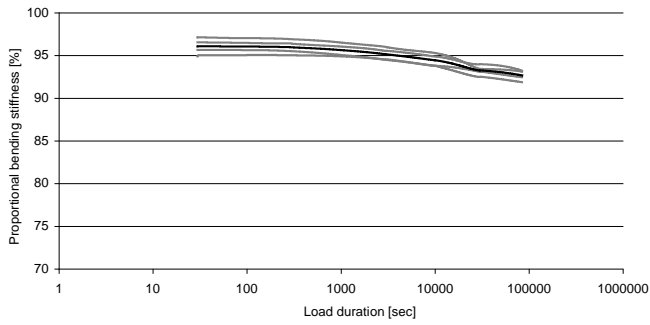


35 °C

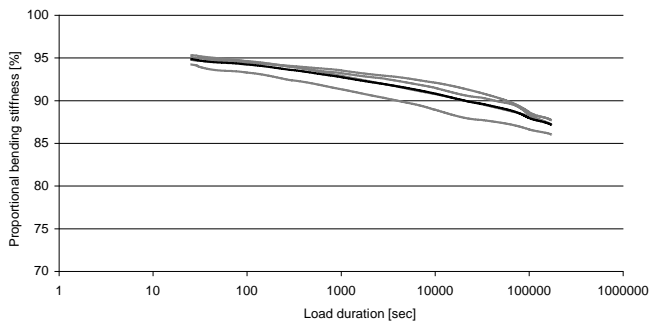




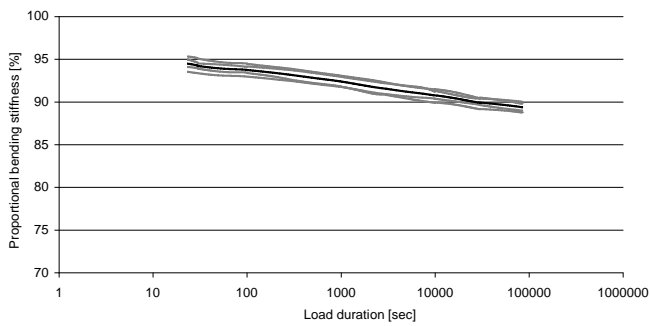
40 °C



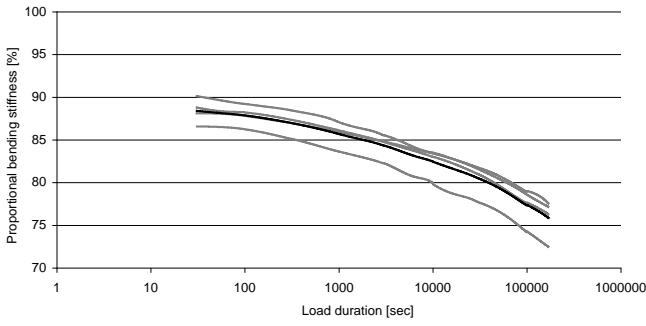
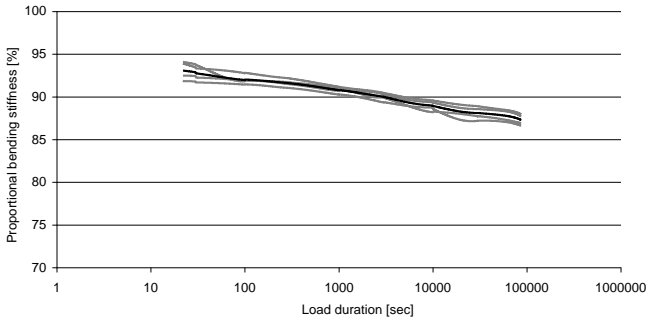
45 °C



50 °C



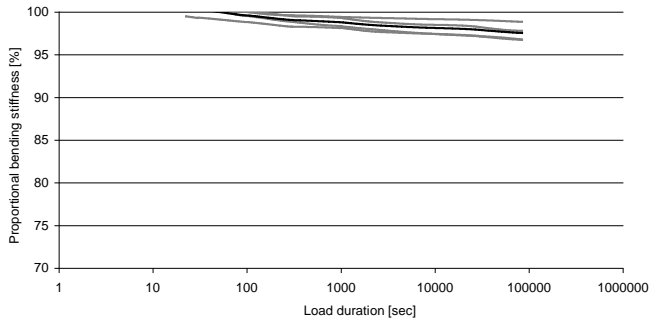
55 °C



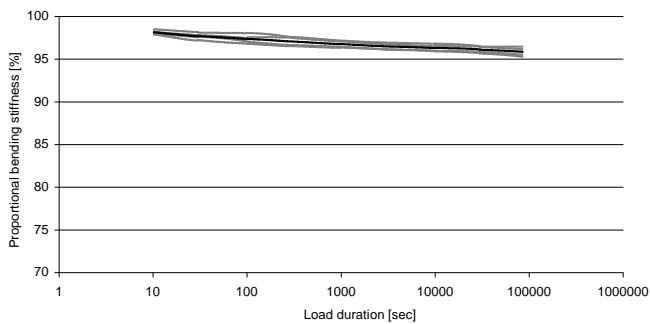
# Appendix K: Bending relaxation results series C

---

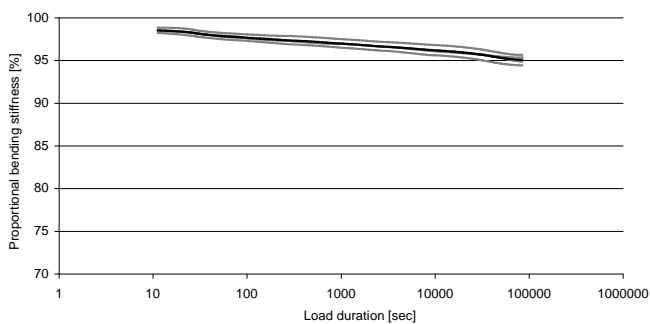
Results of bending relaxation experiments on specimen from series C (3000 mm long, 360 mm wide and a thickness of 2x 8 mm annealed glass and 1.52 mm SG)



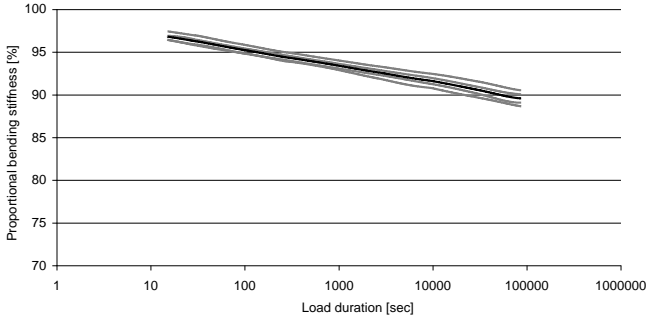
5 °C



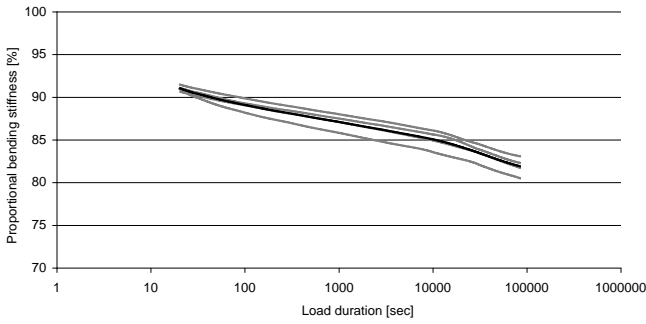
20 °C



35 °C



50 °C



65 °C

# Appendix L: Shear deformation in glass pane

---

When a two sided supported plate element is loaded with a bending force, generally only the bending deformations are taken account of. However, due to the internal shear forces in the plate, also a shear deformation occurs (see Fig. L.1). For relatively thin plates, these are normally negligible. To verify whether these are truly insignificant, the analytical shear deformations in the centre of the plate  $w_{shear,middle}$  were calculated for the experimental bending configurations, with Eq. (L.1). These are very low in comparison with the bending deformations of a monolithically glass plate (calculated with Eq. (L.2)). Their ratio, presented in Table L.1, indicates that in the worst case  $w_{shear}$  remains lower than 0.12 % of  $w_{bending}$ .

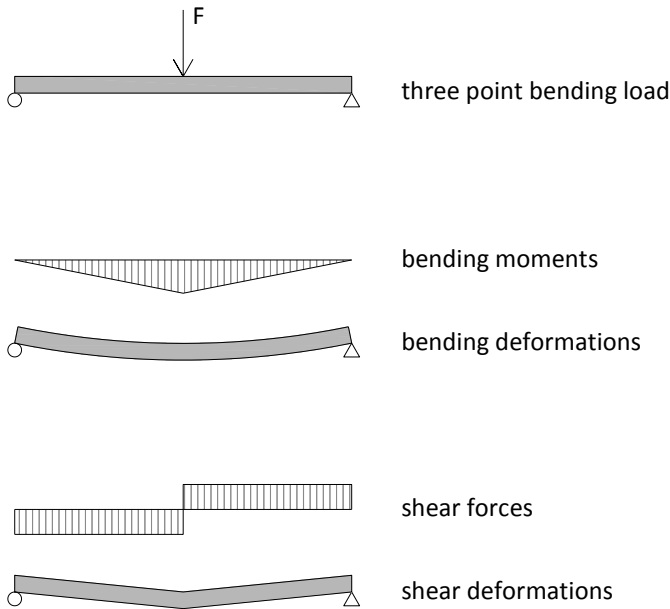


**Figure L.1: Principle of bending and shear deformation for a two sided supported plate**

$$w_{shear,middle} = 1.5 \frac{F}{2 \cdot W \cdot t_{glass} \cdot G_{glass}} \cdot \frac{L_{span}}{2} \quad (L.1)$$

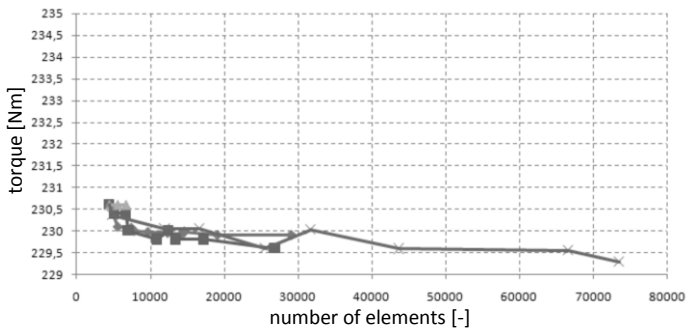
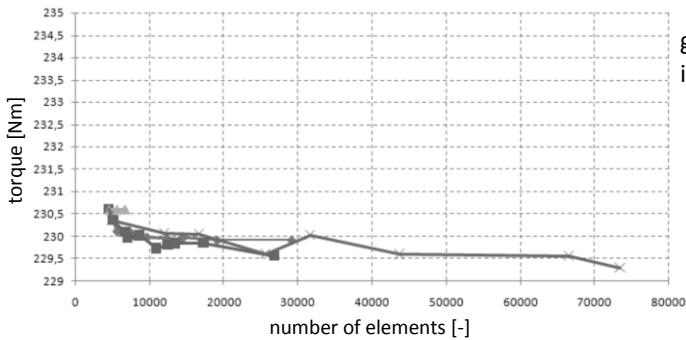
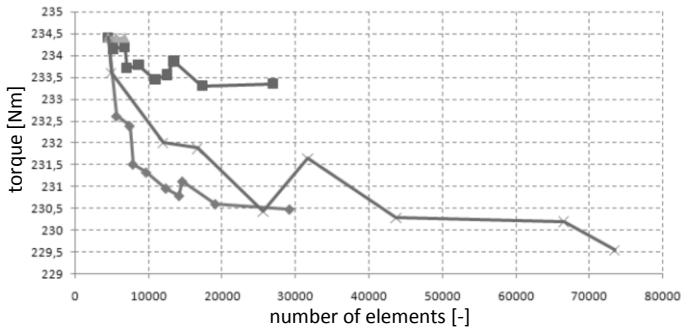
$$w_{bending,middle,upper} = \frac{F \cdot L_{span}^3}{4 \cdot E_{glass} \cdot W \cdot t_{total}^3} \quad (L.2)$$

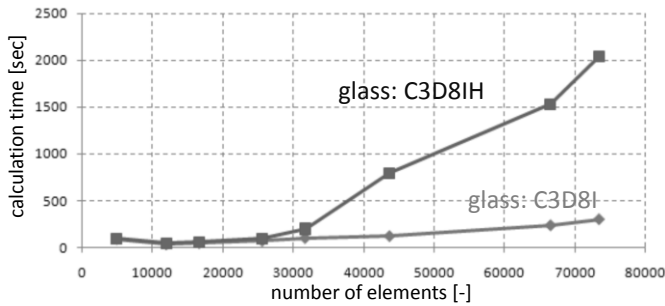
**Table L.1: Calculated shear and bending deformations for the bending test configurations**

<b>Test configuration</b>	<b><math>w_{shear,middle}</math> [mm]</b>	<b><math>w_{bending,middle,upper}</math> [mm]</b>	<b>ratio [%]</b>
Large bending	0.0025	17.820	0.014
Small bending	0.0007	0.6027	0.111

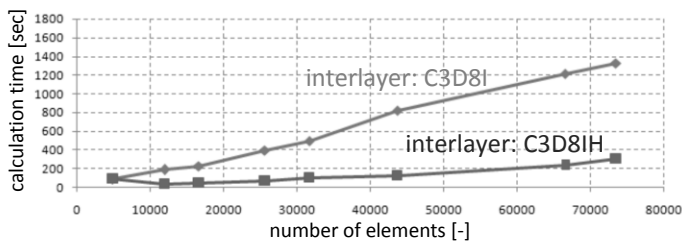
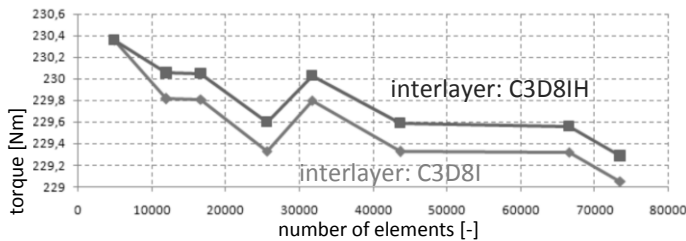
# Appendix M: FE mesh study

A FE mesh study was executed with a varying amount of elements and with different element types for both the glass and the interlayer sheets. Here, some of the results are presented for the FE model of the torsion test setup. The influence on the reaction moment, the maximum principal stress and the calculation time were verified.





Based on the above mentioned graphs, the C3D8I elements - which show a stable stiffness and limited calculation time - were preferred for the glass sheets. Hereafter, also the element type of the interlayer sheet was varied and the C3D8IH elements gave an acceptable result with a limited calculation time. Additionally, the variations on the stiffness of the FE model due to a changing mesh fineness remain modest, while this property was used in the numerical analysis of the experimental results.



Based on this study, which is only partially shown here, a mesh with almost 30000 elements as presented in § IV.2.1 was chosen to simulate the torsion test configuration. The complete mesh study is written down in [Nachergaele 2009].



# Appendix N: Interlayer stresses (FE)

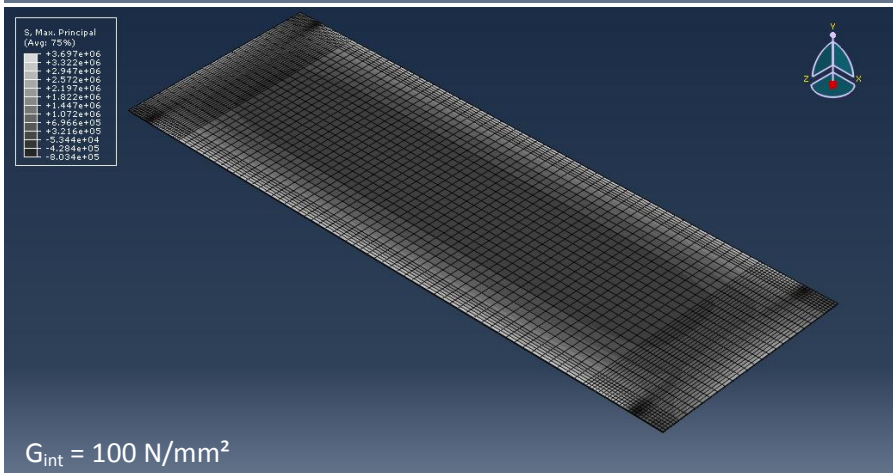
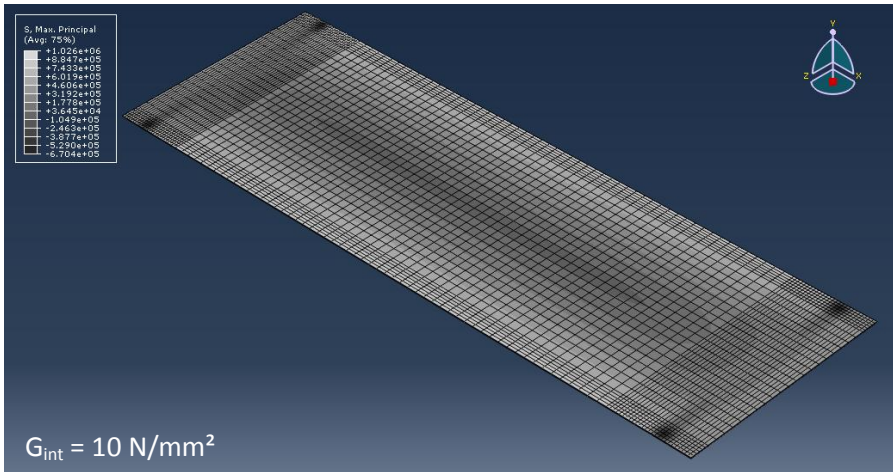
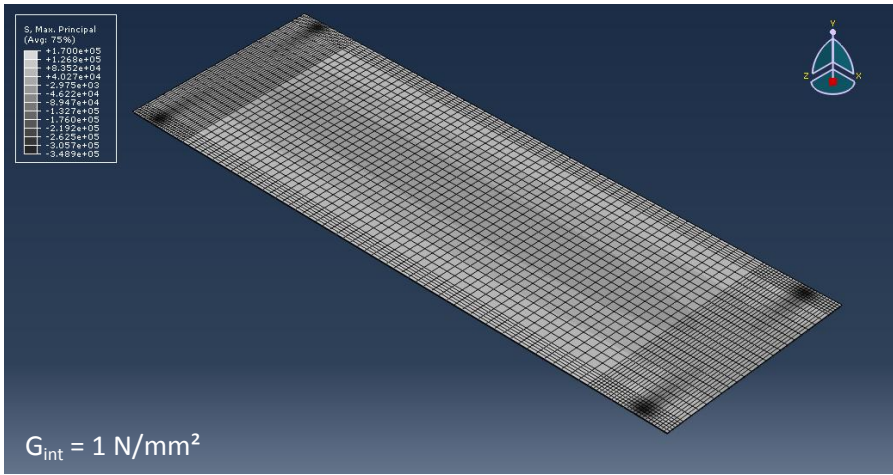
Because the proposed linear visco-elastic material model is generally only valid for relatively small strains, the numerically determined maximum principal stresses on the interlayer material are presented here. The maximum and minimum values are summarised in Table N.1. Even for the rather large torsional deformation, the stress levels remain relatively low.

The values shown here are illustrative, since the FE mesh was mainly constructed for a good stiffness simulation with an acceptable calculation time. Generally, for an accurate FE stress analysis, the mesh should be much denser.

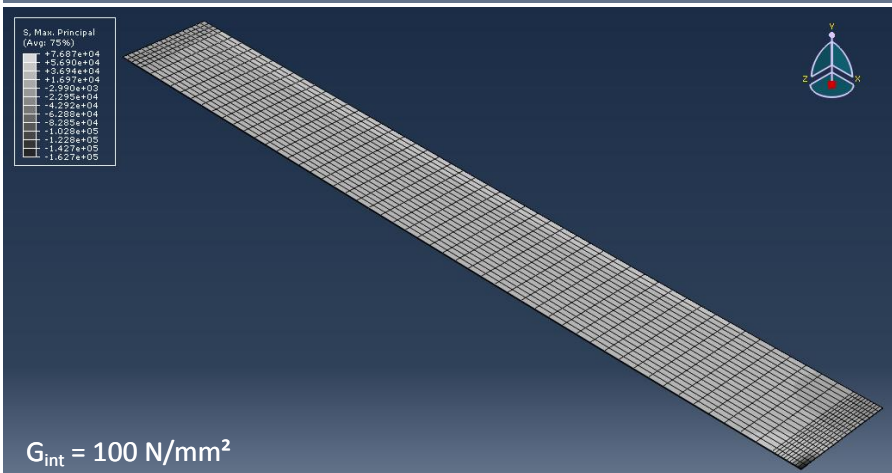
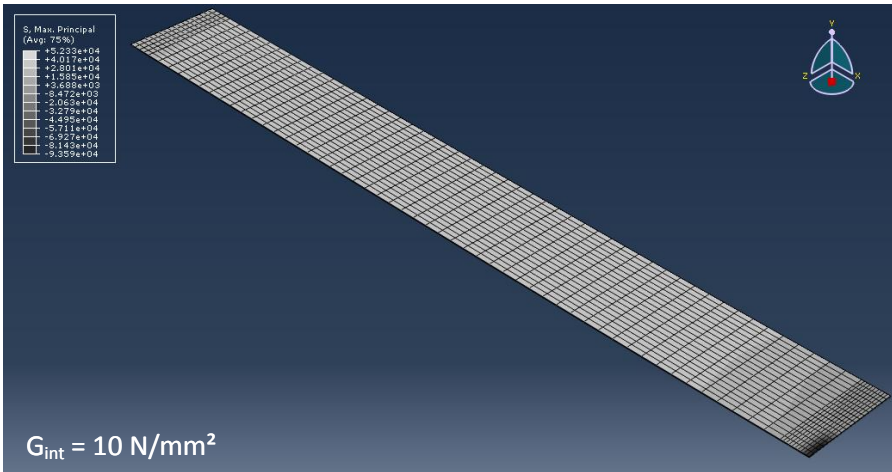
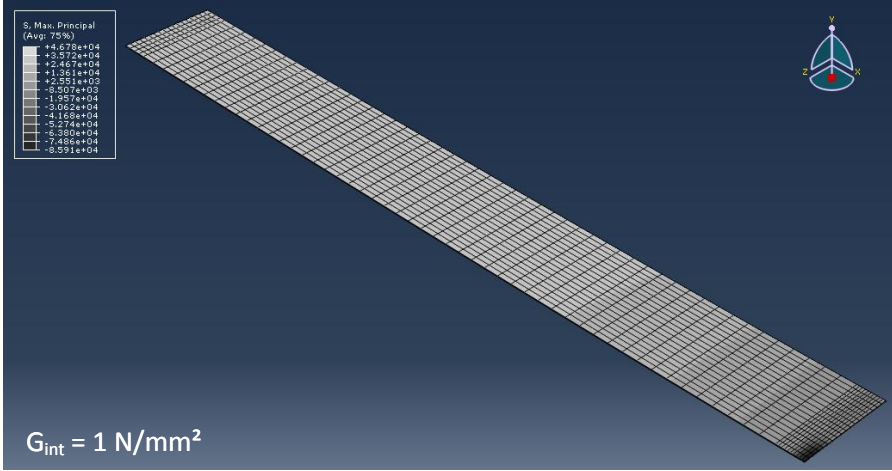
**Tabel N.1: Maximum and minimum principal stress in interlayer from FE model [N/mm<sup>2</sup>]**

	torsion		large bending		small bending	
	max	min	max	min	max	min
$G_{int} = 1 \text{ N/mm}^2$	0.1700	-0.3489	0.0468	-0.0859	0.0234	-0.0637
$G_{int} = 10 \text{ N/mm}^2$	1.0260	-0.6704	0.0523	-0.0936	0.0344	-0.0463
$G_{int} = 100 \text{ N/mm}^2$	3.6970	-0.8034	0.0769	-0.1627	0.0425	-0.0544

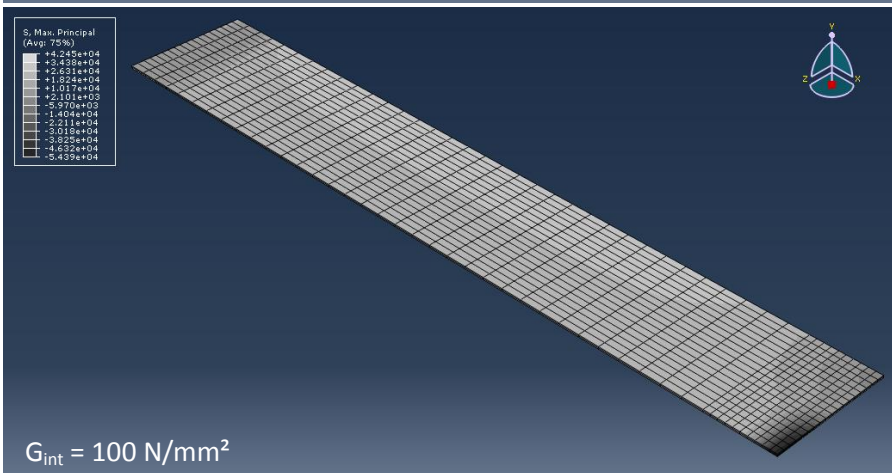
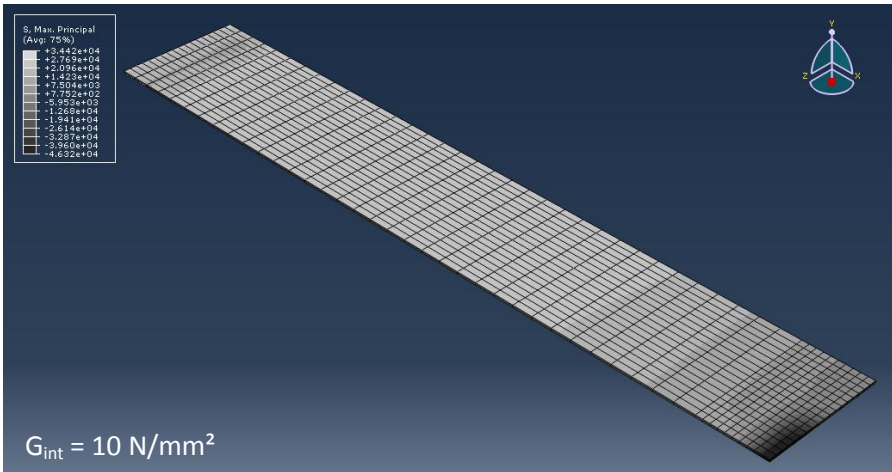
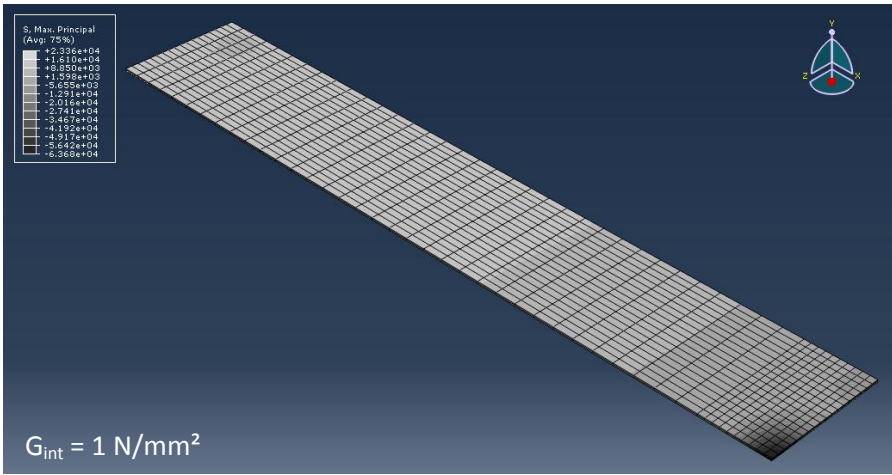
Torsion test setup (rotation of 6 ° over the longitudinal axis of the element)



Three-point bending test setup spanning 2950 mm (central load of 392 N)



Three-point bending test setup spanning 1050 mm (central load of 147 N)



# Appendix O: Numerically determined $G_{SG}$

---

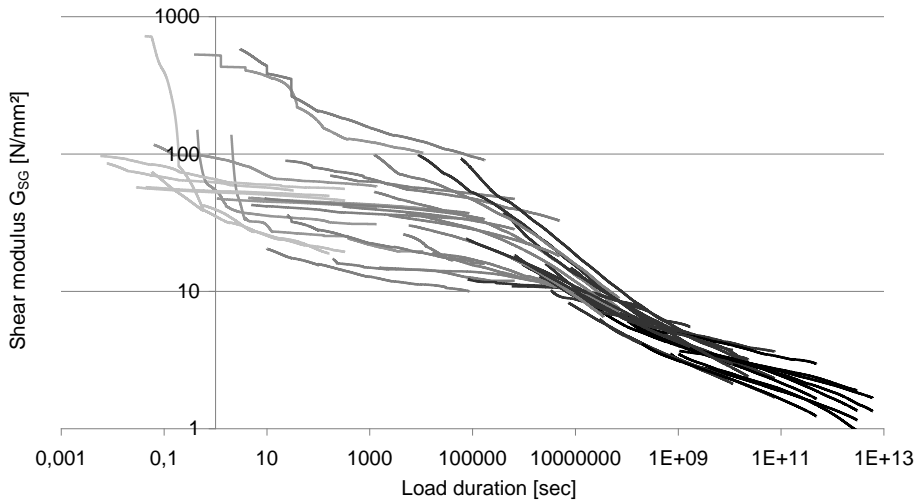


**Figure O.1: Numerically deduced values for  $G_{SG}$  from all experimental results: tests at low temperatures (light gray curves); tests at elevated temperatures (dark grey curves)**

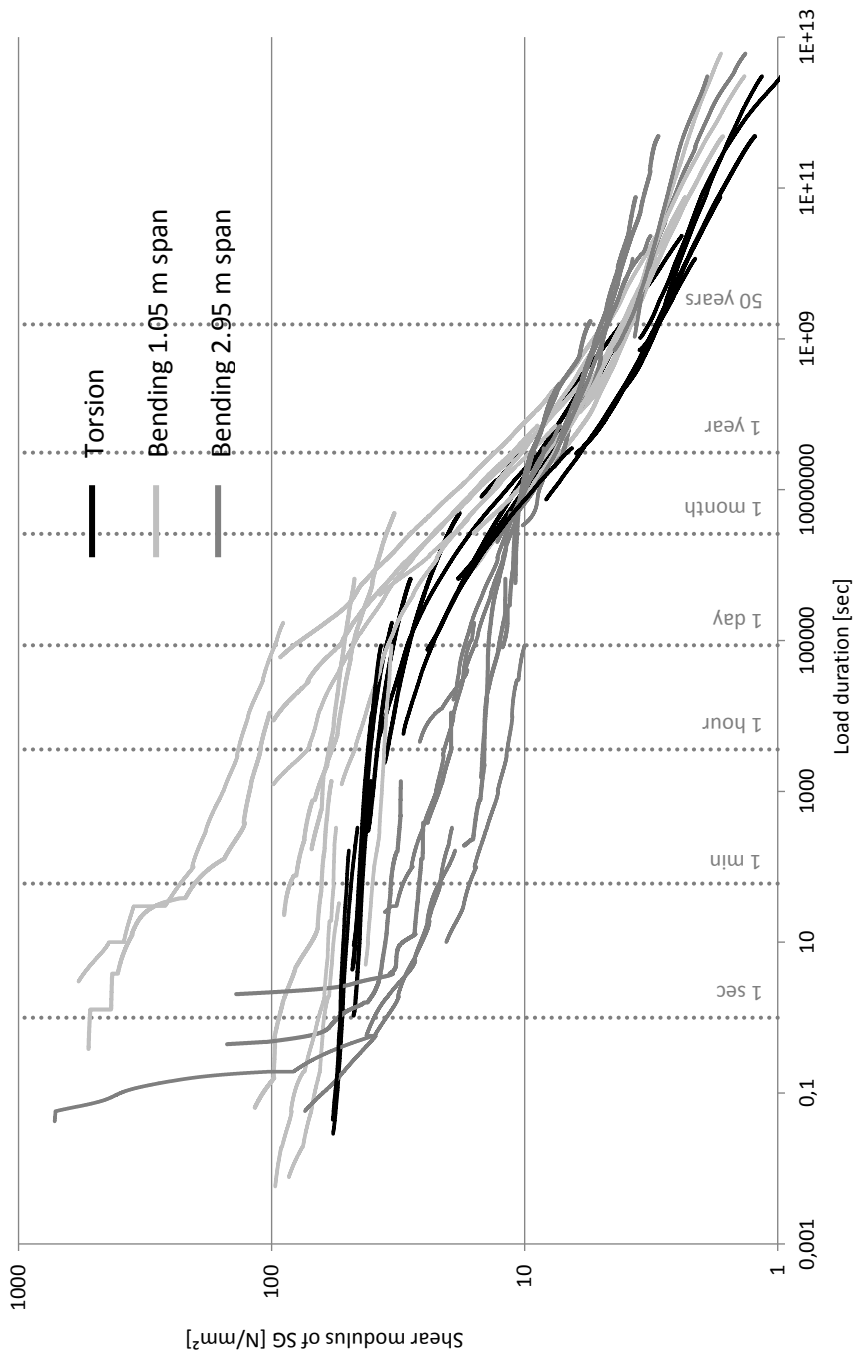


**Figure O.2: Numerically deduced values for  $G_{SG}$  from all experimental results: torsion tests (black curves); bending tests spanning 1050 mm (light gray curves); bending tests spanning 2950 mm (dark grey curves)**

# Appendix P: SG material model

Based on the proposed material model and the assumption of a bulk modulus  $K_{SG}$  of 2000 N/mm<sup>2</sup>, a number of values for the SG material properties are summarised in Tables P.1 and P.2.

*Table P.1: Values for  $E_{SG}$  for seven load durations at different temperature levels*

$E_{SG}$ [N/mm <sup>2</sup> ]	1 sec	3 sec	1 min	1 hour	1 day	1 month	10 years
5 °C	n/a	n/a	220.5	131.5	126.5	104.4	58.93
10 °C	n/a	n/a	150.2	130.0	110.4	88.24	39.61
15 °C	212.0	165.8	131.4	118.9	99.33	64.58	23.61
20 °C	149.2	133.8	129.9	106.0	79.16	45.75	16.30
25 °C	131.4	131.0	118.9	92.25	58.07	27.64	10.85
30 °C	130.0	126.3	106.3	69.10	39.83	18.34	8.375
35 °C	119.9	111.0	93.22	50.49	24.31	12.39	6.720
40 °C	107.0	101.0	70.76	32.41	16.97	9.493	5.320
45 °C	94.97	83.86	52.36	20.74	11.32	7.528	2.798
50 °C	73.70	62.81	34.85	14.94	8.904	5.848	n/a
55 °C	55.27	45.61	22.20	10.54	7.222	4.519	n/a
60 °C	38.43	28.66	16.10	8.248	5.650	n/a	n/a
65 °C	24.34	19.28	11.02	6.741	4.123	n/a	n/a

*Table P.2: Values for  $\nu_{SG}$  for seven load durations at different temperature levels*

$\nu$ [-]	1 sec	3 sec	1 min	1 hour	1 day	1 month	10 years
5 °C	n/a	n/a	0.482	0.489	0.489	0.491	0.495
10 °C	n/a	n/a	0.487	0.489	0.491	0.493	0.497
15 °C	0.482	0.486	0.489	0.490	0.492	0.495	0.498
20 °C	0.488	0.489	0.489	0.491	0.493	0.496	0.499
25 °C	0.489	0.489	0.490	0.492	0.495	0.498	0.499
30 °C	0.489	0.489	0.491	0.494	0.497	0.498	0.499
35 °C	0.490	0.491	0.492	0.496	0.498	0.499	0.499
40 °C	0.491	0.492	0.494	0.497	0.499	0.499	0.500
45 °C	0.492	0.493	0.496	0.498	0.499	0.499	0.500
50 °C	0.494	0.495	0.497	0.499	0.499	0.500	n/a
55 °C	0.495	0.496	0.498	0.499	0.499	0.500	n/a
60 °C	0.497	0.498	0.499	0.499	0.500	n/a	n/a
65 °C	0.498	0.498	0.499	0.499	0.500	n/a	n/a





# Appendix Q: SG versus PVB

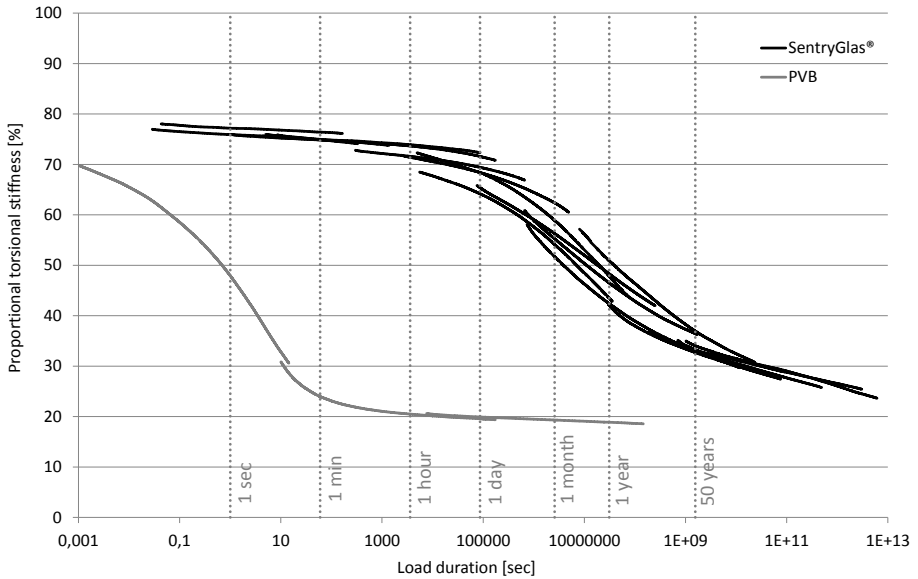


**Figure Q.1: Time-shifted proportional torsional stiffness of glass/SG and glass/PVB samples at  $T_{ref} = 20\text{ °C}$**

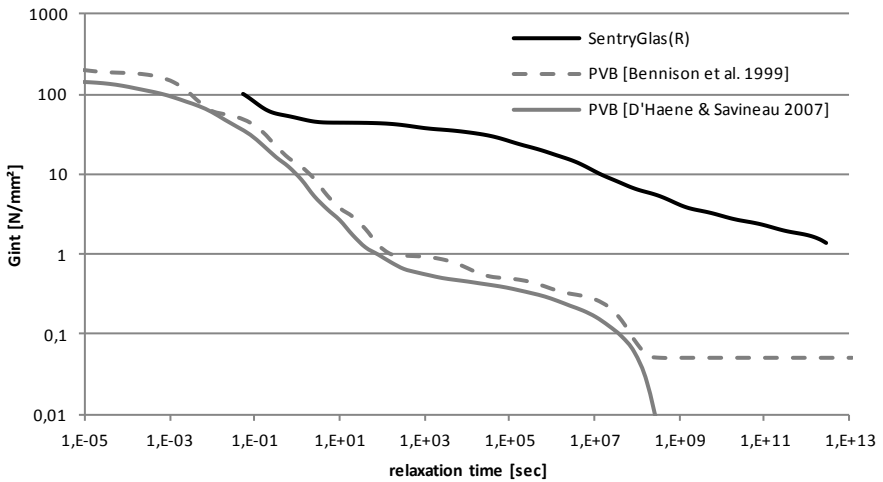


**Figure Q.2: Comparison between the proposed linear elastic material models for SG and two existing models for PVB at  $T_{ref} = 20\text{ °C}$**





